# Molecular and Cellular Determinants of Pattern Formation During Wound Repair in *Xenopus laevis*

By

Nicholas R. Davenport

A dissertation submitted in partial fulfillment of

the requirements for the degree of

Doctor of Philosophy

(Cellular and Molecular Biology)

at the

UNIVERSITY OF WISCONSIN−MADISON

2016

Date of final oral examination: 05/23/2016

The dissertation is approved by the following members of the Final Oral Committee:

William Bement, Professor, Zoology
Kurt Amann, Associate Professor, Zoology
Erik Dent, Associate Professor, Neuroscience
Timothy Gomez, Professor, Neuroscience
Thomas Martin, Professor, Biochemistry

## Table of Contents

**Acknowledgements**

Bill - Thank you.

I was incredibly fortunate to have my tenure in the lab overlap with that of Ann Miller, Josh Sandquist, Emily Vaughan, Brian Burkel, and Angela Kita. I could not have asked for a better set of teachers and science role-models. Angela, thank you for your friendship and support. I also have to thank the dynamic trio that are my fellow graduate students: Matt Larson, Alison Moe, and Adriana Golding. You're wonderful labmates, incredible scientists, and I wish you all the best in your future endeavors. Kevin Sonnemann is an invaluable part of the lab - as a technical resource, an oft-needed source of common sense, and as an all-around great person. Outside of lab, Kevin and his family have been incredibly warm and inviting to both Tara and I. The time we've spent with them has been one of the highlights of our time in Madison.

I was delighted by the network of friends I gained when I started graduate school. Our common link may have been science, but it grew far beyond that; you have become my extended family. I truly cherish the time we've spent together and appreciate all you've done for Tara and I and the joy you've brought to our lives. My family - both the Davenports and the Starks - you've always been there with love and support even if you've been unsure of what I've been up to all these years in lab. Sophie, it's taken some time to get used to your hands-on editing style, but I love you all the same. Coming home to your silly grin never ceases to warm my heart. (Just so we're clear, 'hands-on' refers to your habit of button-mashing/pulling on the monitor of my laptop as I frantically tried to save my progress before you wreck things.)

And finally, Tara, none of this would've happened without you. You've been my unwavering support system since before I started thinking about graduate school. Through all the

tough times, long hours, and late nights - you've been there for me. If that wasn't impressive enough, you've somehow managed to do all that while earning two graduate degrees, planning a wedding, moving across the country (twice!), and giving birth to an infant of unusual size. Simply put, you are amazing.

This work was primarily supported by National Institutes of Health grant GM52932 to William Bement with additional funding provided by NIH National Research Service Award GM07215 (administered by the Molecular Biosciences Training Grant, UW-Madison) to myself. Imaging instrumentation and technical support was provided by the Laboratory for Optical and Computational Instrumentation (Kevin Eliceiri, UW-Madison). Early imaging data was acquired on the Bio-Rad 1024 Confocal microscope, procured with funds from National Science Foundation grant 9724515 to James Pawley (Department of Zoology, UW-Madison). Funding for travel was generously provided by the Vilas Conference Travel Grant (Graduate School, UW-Madison) and John Jefferson Davis Travel Award (Department of Zoology, UW-Madison).

**Molecular and Cellular Determinants of Pattern Formation During Wound Repair in *Xenopus laevis***

Nicholas R. Davenport

Under the supervision of Professor William M. Bement

At the University of Wisconsin-Madison

The boundary between life and death for a single cell is razor-thin. Less than ten nanometers of a flexible, selectively permeable lipid bilayer separate the harsh extracellular environment from conditions favorable for biological processes. Although assaults to these fragile barriers are common, damage can be limited by evolutionarily-conserved mechanisms employed to repair plasma membrane defects. The wound response is shaped by a series of overlapping signaling gradients including calcium and membrane lipids. These gradients are used to construct complex patterns such as concentric zones of active Rho and Cdc42 which, in turn, drive the formation and ingression of corresponding rings of myosin-2 and F-actin, respectively. Organisms use many of these same patterns to close multicellular wounds. My work endeavors to identify and characterize factors that generate and refine the patterns seen at wounds. In Chapter 1, I summarized our current knowledge of the molecular players and mechanisms driving the wound response. I report that this field has seen growing interest as the connections between wound repair defects and human diseases have become more evident. In Chapter 2, I continued a candidate screen initiated by Vaughan *et al*. (2011) in search of regulators of Rho GTPase activity zones at wounds in *Xenopus laevis* oocytes. I examined the roles of two Rho GTPase inactivators, RhoGAP1 and RhoGAP8. I found that they localize

between the zones of active Rho and Cdc42 and are responsible for limiting outward spread of the Rho zone. In Chapter 3, I expand the characterization of RhoGAP1 and RhoGAP8 to determine their function in the intact epithelia of *Xenopus* embryos. I find that RhoGAP1 and RhoGAP8 both localize to multicellular wounds. Knockdown of RhoGAP1 causes an increase in cellular F-actin and leads to defects during gastrulation. In Chapter 4, I used a combination of traditional cell-labelling approaches and recent advances in confocal microscopy to study the dynamics of calcium, various membranous compartments, and selected membrane-associated proteins immediately after wounding at higher spatiotemporal resolution than previously possible. I find that upon wounding, calcium entered the cell and remained elevated for several minutes in a ring that encompassed both the Rho and Cdc42 activity zones. Membrane compartments of various sizes were observed undergoing complex fusion events to shape the lipidic environment around the wound. Combined, the results of this work add to a growing list of processes and participants needed to reestablish the integrity of the plasma membrane and underlying cytoskeleton. More importantly, these findings demonstrate additional mechanisms for shaping intracellular patterns and gradients generated during wound repair and may serve as a proxy for other forms of single cell pattern formation.

# Chapter 1

## Introduction

***Pattern Formation***

The biological world is replete with patterns; patterns that are used to define, duplicate, and specialize biological units. Some of these patterns are conspicuous like the repeated segments of annelids and arthropods, whereas others are more subtle, such as the spinal column of vertebrates. As disparate as these two examples may appear, they are joined by a common thread: for each bauplan there exists an underlying system to not only generate, but to also react to, a series of gradients that direct the morphological development of an organism. These gradients exert their effects at all levels of organismal scale, from the distribution of molecules within a single cell to the organization of tissues and organs.

At the heart of these patterns is the creation of asymmetries, whether it be the polarization of resting cells or differentiation within a homogenous population of cells. The development of patterns within a multicellular context is often controlled by the actions of morphogens, long-range signaling molecules that initiate transcriptional programs in affected cells to dictate specific cell fates or activities (Turing, 1952; Rogers and Schier, 2011). Morphogens are emitted from specific locations, diffuse amongst target tissues, and are eventually degraded (Crick, 1970). The initial rate of morphogen synthesis, interactions that affect diffusion coefficients, distance from source, and rate of clearance combine to affect the amount of a morphogen a cell encounters (Yang *et al.,* 1997; Yan and Lin, 2009).

Cellular responses to morphogens are not necessarily binary, i.e. based solely on the presence or absence of the signal. Cells can mount graded responses based on the concentration of morphogen (Driever and Nüsslein-Volhard, 1988b; Struhl *et al.,* 1989) and duration of exposure (Yan and Lin, 2009). Further, developing tissues can secrete inhibitors to limit the

spread of the morphogen signal (Jones and Smith, 1998). Combined, these mechanisms permit initially homogeneous tissues to be sculpted into distinct populations of cells along sharp gradients. Given that organisms are under the control of many morphogens at any given time (Rogers and Schier, 2011), it becomes apparent how integration of multiple signals can be used to direct complex morphological events leading to the formation of a diverse range of tissues and organs.

Many patterns seen in tissues originate from asymmetries in maternal contribution during oogenesis. Perhaps the most well-known examples of the maternal contribution effect is in the syncytial embryos of *Drosophila*. Maternally-derived mRNA gradients from opposite ends of the oocytes and embryos specify the anterior/posterior axis (Driever and Nüsslein-Volhard, 1988a; Lehmann and Nüsslein-Volhard, 1991). Interactions between the products of these two gradients (*bicoid* and *nanos*) and the zygotic genes they regulate begin to shape segmentation of the developing embryo (Driever and Nüsslein-Volhard, 1989; Hülskamp *et al.,* 1990). Asymmetric localization of maternal mRNA and yolk proteins in oocytes plays a similar role in the development of amphibian embryos (Rebagliati *et al.,* 1985; Heasman, 2006).

Just as signaling gradients can control multicellular pattern formation , a growing body of evidence suggests that signaling gradients may control pattern formation in single cells (Bement and von Dassow, 2014). Asymmetric distribution of signaling molecules is the basis of cell motility and chemotaxis (Yoo *et al.,* 2010). Patterns are also used to determine the position of the cytokinetic furrow during the final stage of cell division (Pollard, 2010). The activation of the small GTPase RhoA in a narrow band at the equatorial cortex of dividing cells dictates where actomyosin will accumulate and ingress to separate the daughter cells (Bement *et al.,* 2005). Cell

fate determination can be driven by asymmetric cell division, a process controlled by polarization of mother cells (Roubinet and Cabernard, 2014). For example, polarization of the PAR proteins in *Caenorhabditis elegans* promotes a series of asymmetric divisions needed to partition cell fate determinants into the correct precursor cells (Macara, 2004). Further, polar body emission, perhaps the most extreme example of cell division asymmetry, is preceded by localized Cdc42 activity at the site of protrusion (Ma *et al.,* 2006).

Another striking example of single-cell pattern formation is seen in the evolutionarily-conserved cellular wound response. From an initial influx of calcium, a complex series of patterns are generated proximal to the wound to direct repair of the plasma membrane and underlying cytoskeleton (Sonnemann and Bement, 2011; Moe *et al.,* 2015).

### *Wound Repair*

Life as we know it exists, in part, due to barriers. These barriers, whether they are fragile lipid bilayers or sheets of cells fortified by intercellular contacts, selectively create environments to promote specialized functions. If barriers are disrupted and homeostasis is lost, the very survival of an organism is in danger. Damage is an inevitable challenge to biological systems and presents itself in a variety of forms. Puncture wounds and lacerations cause damage at both the cellular and tissue level (McNeil and Ito, 1990). Several taxa of microorganisms produce pore-forming toxins, plasma membrane-spanning proteins that produce channels across which cellular components may freely flow (Los *et al.,* 2013). The plasma membrane can also be penetrated by intracellular parasites (Formaglio *et al.,* 2014). Cellular ion channels may also be damaged by proteolytic attack, leading to unrestricted diffusion into the cell (Turner *et al.,* 1993). Further,

traumatic brain injury damages the plasma membrane of neurons and causes axonal retraction (Pettus and Pavlishock, 1996; Shi *et al.,* 2000).

However, membrane damage need not be due to an external physical assault. Cells of the skin (McNeil and Ito, 1990), gut (McNeil and Ito, 1989), and muscle (McNeil and Khakee, 1992; Petrof *et al.,* 1993) incur plasma membrane damage under physiological conditions. At resting heart rates, shear forces from blood flow are sufficient to wound endothelial cells lining the aorta of rats (Yu and McNeil, 1992). Further, given that cells constrained to less than 50% of their original diameter by microfluidic devices sustain membrane damage (Sharei *et al.,* 2013), it is not difficult to imagine how amoeboid cells migrating between cells or through the extracellular matrix might encounter wound-inducing forces. Even trypsinization, a common, century-old procedure for resuspending adherent cells (Rous and Jones, 1916), may damage the plasma membrane (McNeil *et al.,* 1989).

Without the benefit of a wound repair mechanism, cells will die due to loss of cytoplasm and induction of deleterious signaling events (Orrenius *et al.,* 2003). This problem extends beyond the level of a single cell and can have profound effects on an entire organism. From the rates of cellular damage seen under physiological conditions (McNeil and Ito, 1989), attrition alone would outstrip the replicative capacity of surviving cells to maintain a tissue were there not a mechanism for fixing damaged cells. Further, degradative factors released by dying cells can cause secondary, deleterious effects in the surrounding tissues, only exacerbating the damage from the initial insult (Limaye *et al.,* 2003). Many disease states, including muscular dystrophies (Petrof *et al.,* 1993), diabetes (Howard *et al.,* 2011a), and vitamin deficiencies (Howard *et al.,* 2011b; Labazi *et al.,* 2015) lead to increased susceptibility to damage or have an attenuated

wound response. The disorganization of axonal cytoskeletons due to damage incurred during traumatic brain injury may lead to later neurodegenerative disorders (Johnson *et al.,* 2013).

The evolutionary conservation of the wound response serves to exemplify its importance. While the mechanism of repair may vary slightly between taxa and cell type based on available cellular components, there is some form of wound response along the entire phylogenetic tree. Responses have been observed in protists (Chambers, 1917; Szubinska, 1971), yeast (Kono *et al.,* 2012), plants (La Claire, 1989; Klima and Foissner, 2010), insects (Abreu-Blanco *et al.,* 2011), amphibians (Holtfreter, 1943; Bement and Capco, 1991), and rodents (Bansal *et al.,* 2003). Thus, there is likely a strong selective advantage to quickly reestablishing cellular homeostasis after injury.

The wound response is readily scalable to handle a variety of wound sizes. If defects in a lipid bilayer are small enough, lipid disorder at the wound edge can promote resealing (Chang and Reese, 1990; Hibino *et al.,* 1993). However, depending on the tension of the bilayer, even initially small defects can grow quite large (Sandre *et al.,* 1999). Since the plasma membrane is continually under tension due to its attachment to the cytoskeleton, only defects in the nanometer range can spontaneously reseal (Gozen and Dommersnes, 2014). Cells are able to remove pores, like those created by toxins secreted from bacterial or immune cells (Lioi *et al.,* 2012; Los *et al.,* 2013), either by extrusion into the extracellular environment or internalization for subsequent proteolytic degradation (Corrotte *et al.,* 2013; Jimenez *et al.,* 2014; Sheffer *et al.,* 2014).

Single cells have the capacity to cope with wounds that are many micrometers in size (e.g. Terasaki *et al.,* 1997). The wound response is even robust enough to close a bisected *Xenopus* oocyte (Bement and Capco, 1991). Further, if two or more wounds are made within

sufficient proximity to each other, the response will behave as though they are one, much larger wound (Mandato and Bement, 2001; Simon *et al.,* 2013). If more than one cell in a tissue is damaged, a multicellular response is initiated to close the defect. In embryonic tissues, this response proceeds in a manner that is similar to the extrusion of apoptotic or necrotic cells from an epithelial sheet (Andrade and Rosenblatt, 2011; Herrgen *et al.,* 2014), and shares many of the same components and processes as the single cell wound response (Clark *et al.,* 2009; Sonnemann and Bement, 2011).

### *Signaling, the Cytoskeleton, and Single Cell Wound Repair*

Early embryologists noted the capacity of echinoderm and amphibian embryos to mount responses to plasma membrane disruption (Chambers, 1917; Holtfreter, 1943), but could only conjecture as to the events and players involved in this phenomenon. Work over the past several decades has begun to unveil the complex sequence of molecular interactions required to repair damage incurred to the plasma membrane. The wound repair response is now known to involve contributions from an influx of extracellular calcium, fusion of membranous compartments, and rearrangement of cytoskeletal elements.

#### *Calcium Influx*

Calcium has long been known as an important factor in eliciting a cellular wound response (Heilbrunn, 1930). Cells use calcium as a prominent second messenger, and as such, keep intracellular calcium concentrations low (~ 100 nM) to enhance sensitivity to these signals and prevent spurious signaling events. Excess calcium is actively transported into intracellular stores (endoplasmic reticulum and mitochondria) or outside of the cell, where calcium

concentrations can be in the millimolar range (Orrenius *et al.,* 2003). Given this concentration gradient, large amounts of calcium have the potential to enter cells through even the smallest disruptions in the plasma membrane.

The permeability of the plasma membrane to calcium upon damage presents an interesting paradox: excessive calcium influx causes cell death (Geeraerts *et al.,* 2011), whereas cells wounded in the absence of calcium fail to repair (Heilbrunn, 1930; Benink and Bement, 2005). Thus, initial entry of calcium into damaged cells must initiate a wound repair "program" used to squelch unabated calcium entry. The ultimate fate of the calcium that passes through the wound is unknown, but may be transported back through the plasma membrane or into intracellular stores. Given the low mobility of $Ca^{2+}$ in the cytoplasm, low levels of calcium influx are unlikely to diffuse broadly across the cell if the wound is repaired in a timely manner (Allbritton *et al.,* 1992).

### *Membrane Resealing*

The earliest studies of wound repair noted the ability of cells to quickly reestablish a membranous layer between the cytoplasm and extracellular environment (Chambers, 1917). Many years later, electron microscopy was used to examine this membranous layer in greater detail and revealed extensive remodeling of the plasma membrane proximal to the wound and the presence of multilamellar structures of unknown origin at the wound center (Gingell, 1970; Szubinska, 1971; Bluemink, 1972). Extensive effort over the past two decades has begun to elucidate the identities of some the membranous compartments and processes involved in this resealing event.

The membrane responsible for sealing the defect, often referred to as the patch or patching membrane, comes from the cytoplasm rather than from the plasma membrane (McNeil *et al.,* 2000; 2003). Vesicles accumulate at the site of membrane disruption soon after wounding (Miyake and McNeil, 1995) and are thought to combine via membrane fusion to stop material from passing across the plasma membrane (Eddleman *et al.,* 1997; McNeil *et al.,* 2000). While here is an assumption that membrane resealing occurs within seconds (Andrews *et al.,* 2014), this assumption may not be completely warranted as it appears to depend greatly on cell type and how resealing is measured. Echinoderms repair membrane disruptions within seconds (Terasaki *et al.,* 1997; Fein and Terasaki, 2005), whereas the axons of squid and earthworms may take up to an hour to heal (Krause *et al.,* 1994).

The accumulation of vesicles at wounds acts as an increasingly selective molecular sieve; large molecules, such as high molecular weight dextrans, are excluded first (Eddleman *et al.,* 2001) followed later by exclusion of smaller dextrans and ions (Krause *et al.,* 1994; Eddleman *et al.,* 1997). Even in cells considered to repair rapidly, such as the oocytes of starfish (Fein and Terasaki, 2005) and *Xenopus* (Luxardi *et al.,* 2014) permit the passage of ions across the plasma membrane long after dyes are excluded from the cytoplasm. Thus, measuring the exclusion of dye-labeled markers or current across a membrane can give different closure rates. The rate of sealing may also be related to the extracellular calcium concentration; echinoderms are often wounded in 10 mM $Ca^{2+}$ and show reduced repair when $Ca^{2+}$ is reduced to that seen in media for other cell types (Steinhardt *et al.,* 1994).

Exocytosis of intracellular compartments is required for wound repair (Steinhardt *et al.,* 1994; Miyake and McNeil, 1995). Exocytosis causes a relaxation in membrane tension (Togo *et*

*al.*, 2000) which could aid in resealing the plasma membrane (Sandre *et al.,* 1999; Gozen and Dommersnes, 2014). Lysosomes, via calcium-dependent activation of synaptotagmin VII, were identified as being the wound-induced exocytic compartment (Reddy *et al.,* 2001), but are unlikely to be the only source (Shen *et al.,* 2005). Cortical and yolk granules also appear to undergo exocytosis or fuse in response to wounding (Bi *et al.,* 1995; McNeil *et al.,* 2000). Enlargeosomes (Cocucci *et al.,* 2004) and peroxisomes (Jedd and Chua, 2000) have also been seen accumulating at wounds. Proteomic analysis of wounded cells discovered mitochondrial (Sharma *et al.,* 2012) and ER-associated (Mellgren, 2010) proteins exposed on the cell surface. Despite the simplified textbook model of cell morphology, both of these organelles are in close association with the plasma membrane (Gingell 1970; Giordano *et al.,* 2013). Thus, it is likely that any membrane-bound compartment close to the wound can contribute to resealing.

An increase in endocytosis can also be seen following wounding (Eddleman *et al.,* 1997) and could serve to remove damaged membranes. This is also seen after lysosomal exocytosis in response to pore-forming toxins (Indone *et al.,* 2008). The lysosome releases acid sphingomyelinase, an enzyme that converts sphingomyelin present on the outer leaflet of the plasma membrane into ceramide (Andrews *et al.,* 2014). Due to the small head group of ceramide, this conversion leads to a local inward curvature of the plasma membrane, promotion of caveolar endocytosis, and removal of the pore from the plasma membrane (Corrotte *et al.,* 2013). Interestingly, some non-enveloped viruses facilitate infection by perforating cell membranes with pore-forming toxins to induce lysosomal exocytosis and enter the cell when the damaged membrane is endocytosed (Miller *et al.,* 2012; Luisoni *et al.,* 2015). The ESCRT

pathway can also be used to shed damaged membrane away from the cell following damage (Jimenez *et al.,* 2014; Sheffer *et al.,* 2014).

Much of our knowledge concerning how intracellular compartments combine to repair the plasma membrane comes from studies of muscle repair. Vesicles containing dysferlin, a transmembrane protein with multiple $Ca^{2+}$-binding domains, are reported to accumulate at wounds in muscles and promote the aggregation of vesicles (McDade *et al.,* 2014; McDade and Michele, 2014). Additionally, MG53 (also known as TRIM72) can associate with dysferlin (Cai *et al.,* 2009a; 2009b). MG53-containing vesicles are shuttled to the site of repair (Lin *et al.,* 2012) where MG53 dimerizes in the oxidizing environment (Hwang *et al.,* 2011), thereby tethering membranous compartments together at the wound.

Annexins bind to acidic phospholipids in the presence of calcium and are required for wound repair (McNeil *et al.,* 2006; Swaggart *et al.,* 2014). They quickly localize to wounds and may associate with the actomyosin cytoskeleton (Gerke and Moss, 2002) and dysferlin (Lennon *et al.,* 2003). Wounds may recruit multiple annexin isoforms depending on the amount of calcium influx, providing a possible means to tailor a cellular response proportional to wound size (Potez *et al.,* 2011). The S100 proteins, with calcium-dependent scaffolding capabilities, associate with annexins at wounds (Rezvanpour *et al.,* 2011; Jaiswal *et al.,* 2014). Since S100 proteins can dimerize, they may promote membrane fusion by linking annexin-bound compartments (Gerke and Moss, 2002).

Regardless of the components utilized during repair, the patching membrane is only a temporary solution to regaining cellular homeostasis. This is particularly important in tissues that see repeated stresses, such as muscle fibers. At a minimum, the patch lacks connections to

cytoskeleton afforded by ERM (ezrin, radixin, moesin) proteins that connect F-actin to plasma membrane PIP2 (phosphatidylinositol 4,5-bisphosphate) and the cytoplasmic domains of transmembrane proteins (Bretscher *et al.,* 2002). Since the patch consists of membrane from a variety of intracellular sources, its lipid composition will be different than that of the original plasma membrane (van Meer *et al.,* 2008). The patching membrane will thus likely have different thickness, strength (Needham and Nunn, 1990; Evans *et al.,* 2003), and the activity of transmembrane proteins will be altered (Anderson and Koeppe, 2007) due to the new lipidic environment.

### *Cytoskeletal Response*

#### Actomyosin

Actomyosin, the dynamic association of filamentous actin (F-actin) and the molecular motor myosin-2, plays an integral role in both maintaining cell shape and driving physical deformations such as cell division and motility (Carter, 1967; Schroeder, 1970). F-actin is a polymer; it is assembled from globular monomers (G-actin) to form helical linear filaments. Crosslinking proteins, such as α-actinin, can bundle filaments to modulate the strength of the actomyosin network (Stricker *et al.,* 2010). The high intracellular concentration of G-actin favors spontaneous filament assembly so polymerization is tightly regulated, either by sequestration of monomers or capping of existing filaments. Localized assembly of new F-actin to perform a specific task can be promoted by the Arp2/3 complex or formins. Arp2/3 aids in the creation of new filament branches off of existing F-actin at a characteristic 70° angle (Amann and Pollard, 2001), thereby creating a dendritic network cells utilize to drive protrusive extensions at the cell

edge or to retract endocytic compartments (Theriot and Mitchinson, 1991; Sokac *et al.,* 2003). Formins polymerize unbranched F-actin and protect growing filaments from capping filaments (Watanabe *et al.,* 1997; Pollard 2007). Both formins and Arp2/3 are subject to additional regulation (e.g., Rohatgi *et al.,* 2000), thereby further refining spatiotemporal regulation of actin polymerization.

The functional unit of myosin-2 is an heterohexamer consisting of two heavy chains with actin-activated ATPase activity, two essential light chains, and two regulatory light chains. The two heavy chains associate by tail regions consisting of helical coiled-coil domains. The light chains, one each of both light and essential, associate with the heavy chains at a "neck" region between the helical tails and globular head domains. Conformational changes in the head group throughout the ATPase cycle alter its affinity for F-actin and can transmit forces along to the heavy chain neck region. When acting in concert, the two heavy chains act to translocate myosin-2 along F-actin. Myosin-2 assembles into bipolar filaments that can pull antiparallel actin filaments towards each other in a manner similar to muscle contraction. Heavy chain isoforms localize differently and possess different biochemical characteristics (e.g., ATPase activity and actin binding affinity) that allow for myosin-2 to provide either tension- or contraction-mediated roles in specific locations (Sandquist and Means, 2008; Smutney *et al.,* 2009). In some circumstances, the ability of myosin-2 to cross-link F-actin may be more important than its ability to slide filaments past each other (e.g., Ma *et al.,* 2012). Regulation of myosin-2 activity is, in part, dictated by phosphorylation of two key residues in the regulatory light chains (Perrie *et al.,* 1973; Heissler and Sellers, 2016). The activity of the kinases and phosphatases responsible for the phosphorylation state of the light chains is also regulated,

thereby applying an additional layer of control on actomyosin contractility (Kimura *et al.,* 1996; Kureishi *et al.,* 1997).

Actomyosin is required for the closure of single-cell wounds (Merriam and Christianson, 1983; Mandato and Bement, 2001; Abreu-Blanco *et al.,* 2011). Myosin-2 accumulates at wounds prior to F-actin and is not dependent on cortical flow or the presence of F-actin. Myosin-2 localizes to the wound edge, whereas the majority of wound-associated F-actin resides in a ring displaced from the wound edge. Accumulation of F-actin at wounds is due to recruitment of pre-existing fibers by cortical flow and *de novo* polymerization (Mandato and Bement, 2001). There are two distinct populations of F-actin at wounds: a stable pool actin at wound edge and a more dynamic population within the ring (Burkel *et al.,* 2007). Despite the requirement of actomyosin for wound repair, contraction (i.e., sliding of actin filaments by myosin-2 motor activity) of the cytoskeletal array *per se* is not required for wound closure. Disruption of myosin contractility reduces the rate of and organization of the cytoskeletal array, but does not halt its ingression (Burkel *et al.,* 2012).

**Microtubules**

Microtubules are critical in providing a structural role in a diverse assortment of processes including maintaining cell shape, segregating chromosomes, and providing avenues for transport of organelles and cargo (Alfaro-Aco and Petry, 2015). Heterodimers of α- and β-tubulin polymerize end-to-end to form long protofilaments which, in turn, associate along their lateral surfaces to form a hollow, cylindrical microtubule. The length of microtubules is dynamic; the rates of intrinsic GTP hydrolysis and addition of α/β-tubulin to the growing end dictate whether a

particular microtubule is growing or shrinking (Mitchinson and Kirschner, 1984). Many microtubule-associated proteins (MAPs) have the ability to fine-tune to microtubule dynamics to drive specialized cellular functions by binding to, and often modifying, the α/β-tubulin heterodimers (Alfaro-Aco and Petry, 2015). Two classes of motor proteins, kinesins and dyneins, move cargo along microtubules and slide microtubules past each other, as seen in cell division (Gennerich and Vale, 2009). Additionally, select proteins are able to cross-link microtubules to the actomyosin cytoskeleton (Rodriguez *et al.,* 2003).

The microtubule cytoskeleton has also been shown to contribute to the single-cell wound response. Wounding of both PtK2 cells (Togo, 2006) and *Xenopus* oocytes (Mandato and Bement, 2001; 2003) causes disruption and subsequent reorganization of the microtubule cytoskeleton around the site of damage. Microtubules are transported to the wound via F-actin mediated cortical flow to form a radial array or generated by *de novo* polymerization at the wound edge (Mandato and Bement, 2003).

**Rho GTPases**

The Rho family of small GTPases (Rho, Cdc42, and Rac) are key regulators of cytoskeletal structure and dynamics (Jaffe and Hall, 2005). They are involved in critical cellular behaviors including migration, cell division, and wound repair (Stacia *et al.,* 1991; Kishi *et al.,* 1993; Benink and Bement, 2005). These proteins assert their biological role when bound to the plasma membrane (Adamson *et al.,* 1992). Integration into this lipidic environment is aided by a series of post-translational modifications (Katayama *et al.,* 1991) and electrostatic interactions with acidic phospholipids by a carboxy-terminal polybasic region (Williams, 2003). The Rho

GTPases are often a described as switches, cycling between an active, GTP-bound, and an inactive, GDP-bound state. GTPase inactivation occurs via hydrolysis of GTP to GDP, whereas conversion back to the active state requires exchange of GTP for GDP (Jaffe and Hall, 2005). When in the active, GTP-bound form, the Rho GTPases assume a conformation favorable for binding to, and thereby activating, a variety of effector proteins capable of eliciting changes in the cytoskeleton (Bishop and Hall, 2000). These downstream cytoskeletal effects include increased actomyosin contractility due to signaling from ROCK, a Rho effector (Kimura *et al.,* 1996; Kureishi *et al.,* 1997). Rho can also activate formins to increase polymerization of linear, unbranched actin filaments (Watanabe *et al.,* 1997; Pollard, 2007). Active Cdc42, through activation of the N-WASP/Arp2/3 pathway, can catalyze the formation of branched actin filaments (Rohatgi *et al.,* 1999).

In isolation, the Rho GTPases are poorly suited to direct useful cytoskeletal rearrangements due to intrinsically slow rates of both nucleotide hydrolysis and nucleotide exchange (Zhang and Zheng, 1998). Cells are able to accelerate the GTPase cycle to a physiologically useful rate by the activities of four classes of GTPase regulators. GTPase Activating Proteins (GAPs) promote GTPase inactivation by electrostatically stabilizing a transition state during the hydrolysis of GTP to GDP (Graham *et al.,* 1999). Guanine Nucleotide Exchange Factors (GEFs) promote activation of GTPases by catalyzing release of GDP from the nucleotide binding pocket of GTPases (Vetter and Wittinghofer, 2001). Given the 4:1 ratio of intracellular GTP to GDP (Kleineke *et al.,* 1979), mass action dictates unloading of the GDP will preferentially lead to GTPase activation. Guanosine nucleotide dissociation inhibitors (GDIs) reduce GTPase activity by sequestering GTPases from the plasma membrane and inhibiting the

activation/inactivation cycle (Dovas and Couchman, 2005). The interaction of GDIs is important for cytoplasmic solubility of GTPases due to hydrophobicity of the isoprenyl tail (Boulter *et al.,* 2010). The GDI/GTPase complex is bound at high affinity (Nomanbhoy and Cerione, 1996), so dissociation of the GTPase and subsequent return to the plasma membrane requires the action of GDI displacement factors (GDFs) (Dovas and Couchman, 2005).

Cells ensure the fidelity of biomechanical processes by directing cytoskeletal rearrangements with high spatiotemporal precision. These rearrangements proceed in concert with corresponding activation/inactivation of the Rho GTPases. There are several mechanisms by which Rho GTPase regulators can direct localized GTPase activity. Whereas GDIs can sequester all three GTPases (Boulter *et al.,* 2010), GEFs and GAPs can have more specific activities, often with preference towards only one of the GTPases (Zhang *et al.,* 1998) and may be based on interactions with plasma membrane lipids (Ligeti and Settleman, 2006).

Beyond the conserved GAP and GEF (DH/PH) domains of these proteins, most GEFs and GAPs possess additional domains that direct their activities towards specific locations within cells. These additional domains include those that detect the composition and curvature of membranes, allow for association with the actin cytoskeleton, mediate additional protein-protein interactions, and respond to second messengers such $Ca^{2+}$ and cyclic nucleotides (Moon and Zheng, 2003; Rossman *et al.,* 2005). Further, autoinhibition may play a role in regulating GEF/ GAP activity by preventing interaction with GTPases (Moskwa *et al.,* 2004; Aghazadeh *et al.,* 2009). There is significant evidence of post-translational modification in GAPs and GEFs that can lead to changes in activity towards GTPases (Aghazadeh *et al.,* 2009; Minoshima *et al.,* 2003). Acetylation (Kulhmann *et al.,* 2015) and phosphorylation (Dovas *et al.,* 2010) of

RhoGDIα by GDFs affects the interaction of the GDI/RhoA complex, thereby providing additional avenues of regulating Rho GTPase activity.

By using the GTPase binding domains (GBDs) of Rho and Cdc42 effectors (rhotekin and N-WASP, respectively) fused to fluorescent proteins, it is possible to observe the dynamic activation of Rho GTPases in a range of cellular processes (Benink and Bement, 2005; Bement *et al.,* 2005; Clay and Halloran, 2013). In oocytes and embryos of *Xenopus* (Benink and Bement, 2005; Clark *et al.,* 2009), disruption of the plasma membrane induces activation of Rho and Cdc42. The Rho GTPases form concentric "zones" around the wound, with active Rho at the wound edge circumscribed by a ring of active Cdc42. Their locations with respect to the wound edge are consistent with promoting contraction of the actomyosin ring (i.e., active Rho at the wound edge to promote activation of myosin-2, circumscribed by a ring of active Cdc42 to promote formation of F-actin). Wound-induced GTPase activation, a calcium-dependent process, occurs diffusely approximately twenty seconds after wounding before becoming sharply defined zones that remain segregated as they move inward to close the wound. A similar mechanism of repair utilizing Rho GTPase activation has been described in the syncytial embryos of *Drosophila* (Abreu-Blanco *et al.,* 2014), suggesting evolutionary conservation of the process.

A growing body of evidence suggests there is considerable crosstalk between the Rho GTPases and the associated cytoskeletal elements in the wound array. Contraction of actomyosin organizes, but is not required for, inward movement of active Rho and Cdc42 during wound closure (Burkel *et al.,* 2012). However, proper dynamics of F-actin at wounds is critical for activity of the GTPases; disruption of F-actin polymerization disrupts the organization and inward movement of the GTPase zones (Benink and Bement, 2005), whereas stabilization of F-

actin with jasplakinolide causes outward movement of F-actin, myosin-2, and the Rho GTPases, away from the wound (Burkel *et al.,* 2012). Pharmacological perturbations also indicate that microtubules play a role in the organization of both Rho GTPase activity zones and actomyosin at wounds, with microtubule stabilization enhancing GTPase segregation (Bement *et al.,* 1999; Benink and Bement, 2005). Exactly how microtubules exert these effects is unclear, but they may be delivering cargos to the wound (Togo, 2006; McDade and Michele, 2014) or providing a structural role by associating with actomyosin (Rodriguez *et al.,* 2003).

There is also crosstalk between the different Rho family GTPases at wounds. Inhibition of Cdc42 activity at wounds by expression of a dominant negative Cdc42 abolished Rho activity whereas a constitutively active Cdc42 increased the width of the Rho zone, but eliminated the Cdc42 zone (Benink and Bement, 2005). Similar perturbations in GTPase activities resulted in altered zone width and intensities in *Drosophila* (Abreu-Blanco *et al.,* 2014). However, off-target effects should be taken into consideration when analyzing the crosstalk of Rho GTPases. That is, the amount of RhoGDI compared to total Rho GTPases is stoichiometrically balanced (Wühr *et al.,* 2014). Any overexpression of Rho GTPases, whether it be wild-type or dominant-negative, reduces the amount of RhoGDI available for endogenous Rho GTPases. Since cytoplasmic stability and transport of Rho GTPases is dependent on RhoGDI, overexpression of one GTPase may have unintended consequences on the stability, and thus activity of the other GTPases (Boulter *et al.,* 2010).

Another instance of Rho GTPase crosstalk was discovered in a candidate screen initiated to identify regulators of GTPase signalling at wounds (Vaughan *et al.,* 2011). Of more than a dozen candidate regulators tested, only Abr, containing both GEF and GAP domains, was

confirmed to control Rho GTPase activity at wounds. Abr localizes to the zone of active Rho where its GEF domain promotes Rho activity. The GAP domain of Abr maintains GTPase segregation at wounds by inactivating any Cdc42 present in the zone of active Rho. Thus, Rho activity influences, albeit indirectly via Abr recruitment, both the activity and location of the Cdc42 zone at wounds.

These results conflicted with previous models where GTPases were activated at a particular location en masse, allowed to perform their functions, and were inactivated when the task was completed. This idea is incongruous with a zone of GTPase activity moving along a stationary plasma membrane during contraction-independent wound repair, nor can these models explain the dynamic repositioning of Rho activity at the cytokinetic furrow (Bement *et al.,* 2005; Miller and Bement, 2009). Photoactivation experiments indicated movement of Rho and Cdc42 at wounds is driven by signaling treadmills, i.e. preferential activation of a GTPase at the leading edge of a zone and inactivation at the trailing edge (Burkel *et al.,* 2012). Contractile forces at wounds serve to reinforce the activation bias, thereby organizing GTPase activity and promote quick, efficient ingression of wounds.

### *Lipids as Signaling Molecules*

Membrane bilayers are not merely physical barriers to separate cargos and chemical reactions from each other and the extracellular environment; they also act as vital substrates for intracellular signaling. Eukaryotic cells are capable of synthesizing in excess of 1000 different types of lipid (Sud *et al.* 2014), thereby providing nearly endless possibilities for creating unique

signals to elicit specific cellular functions. The numerous protein domains devoted to interacting with lipids further underscores the importance of lipid signaling (Stahelin, 2009).

While the plasma membrane is not a major site of lipid synthesis, alterations of existing lipids can create lipid microdomains that can be recognized by signaling proteins (Di Paolo and De Camilli, 2006; van Meer *et al.,* 2008). Hydrolysis of lipids can produce second messengers that have long range effects (Berridge, 1984). Asymmetric shuttling of lipids between leaflets can also influence several cellular behaviors, including polarized growth (Saito *et al.,* 2007a) and recognition of apoptotic cells by macrophages (Fadok *et al.,* 1992). Bilayer asymmetry is catalyzed by several classes of ATPases that translocate lipids between membrane leaflets (Graham, 2004). Despite the contributions of lipids in a variety processes that require the cytoskeleton (e.g., Rohatgi *et al.,* 2000), little attention has been paid to the contribution of lipid signaling during wound repair.

### *Lipid Signaling at Wounds*

Wounding provokes striking changes in the composition and distribution of lipids on the inner leaflet of the plasma membrane (Vaughan *et al.,* 2014). From an initially homogeneous population of lipids at the membrane, wounding creates distinct zones of phosphatidic acid (PA), diacylglycerol (DAG), phosphatidylserine (PS), PIP2 (phosphatidylinositol 4,5-bisphosphate) and PIP3 (phosphatidylinositol 3,4,5-trisphosphate). PA and DAG are synthesized rapidly at the wounds from lipid precursors whereas PS, PIP2, and PIP3 accumulate at wounds later as a result of cortical flow. Wound-induced synthesis of DAG is required for Rho and Cdc42 activity. The other lipids examined (PA, PS, PIP2, and PIP2) are key determinants of protein localization in

other contexts (Stahelin, 2009), so may play a role in the wound response in an Rho GTPase-independent manner. Further, since Vaughan *et al.* (2014) only examined a fraction of the possible lipid species (Sud *et al.,* 2014), additional complexity of lipid domains at wounds is likely. The requirement for lipid signaling during wound repair is supported by evidence suggesting excessive lipid peroxidation can inhibit healing (Howard *et al.,* 2011b; Labazi *et al.,* 2015).

The synthesis of DAG at wounds in *Xenopus* promotes localization of two protein kinases, PKCβ and PKCη. PKCβ, a conventional PKC, binds to DAG in a calcium-dependent manner whereas the affinity of PKCη, a novel PKC, for DAG is independent of calcium (Oancea and Meyer, 1998; Ochoa *et al.,* 2001). At wounds, PKCβ positively regulates Rho and Cdc42 activity, whereas PKCη negatively regulates GTPases. Unexpectedly, in some cases PKCη overexpression leads to an inversion of the GTPase activity zones, i.e. a zone of active Cdc42 circumscribed by the zone of active Rho.

Modeling suggests PKCβ enhances positive feedback of GTPase signaling throughout the Rho and Cdc42 zones after wounding (Holmes *et al.,* 2015). This may occur specifically at the level of GEFs for a particular GTPase, as in the case of Abr-mediated activation of Rho (Vaughan *et al.,* 2011; Simon *et al.,* 2013), or more generally by removing inhibition of both GTPases by phosphorylating RhoGDI (Dovas *et al.,* 2010). PKCη is believed to be responsible for promoting inactivation of the GTPases, likely by interactions with GAPs. Since PKCη localization, and therefore activity, is biased towards the Rho zone, it is likely keeping Abr-enhanced Rho activation in check while simultaneously reinforcing Abr-mediated exclusion of Cdc42 activity from the Rho zone. The GTPase zone inversion phenotype seen in some cells

overexpressing PKCη can be explained by stochastically heightened Rho activity extending beyond its normal range. This extension puts Rho activity outside the range of PKCη influence and allows for positive feedback of Rho activation. To date, the molecular targets of PKCβ and PKCη in the context of wound repair have yet to be identified.

### *Embryonic Wound Repair*

The multicellular wound response in embryos is strikingly similar to single-cell repair. The cells adjacent to the wound polarize to produce an hybrid actomyosin array facing the wound (Bement *et al.,* 1999; Davidson *et al.,* 2002) that is stabilized by adherens junctions (Abreau-Blanco *et al.,* 2013). Cells at the leading edge of wounds also exhibit lamellipodial crawling towards the center of the wound (Abreau-Blanco *et al.,* 2013; Li *et al.*, 2013). Accompanying the actomyosin purse string at the wound edge are corresponding zones of active Rho and Cdc42 (Clark *et al.,* 2009; Abreu-Blanco *et al.,* 2012). Strikingly, if a wound is made close enough to a cell-cell junction, the Rho GTPases will also be activated in the adjacent cell to produce a hybrid purse string to close the wound. Further, in early *Xenopus* blastomeres, intracellular calcium is elevated in cells adjacent to the injury despite not incurring damage themselves (Clark *et al.,* 2009). In further developed embryos, wounding induces a wave of calcium elevation in cells distal to the wound that may aid in coordinating migration to reestablish epithelial integrity (Shindo *et al.,* 2010; Soto *et al.,* 2013).

***Introduction to This Dissertation***

My work seeks to answer a fundamental question in cell biology: How, from a seemingly homogenous cytoplasm and plasma membrane, is a cell able to direct the localization and activity of certain components to perform tasks with spatiotemporal precision? Implicit in these localized activities are the creation of patterns from asymmetric distribution of signaling molecules. Until the underlying signals have identified, it is difficult to explain the subsequent pattern formation and cellular response. While modeling can infer the presence of the molecular participants (e.g., Simon *et al.,* 2013), empirical identification and characterization is required for confirmation. Wound healing in *Xenopus laevis* is a powerful model for studying pattern formation; the ability to generate repeatable wounds and their associated molecular patterns in both single cells and epithelia provides insight into cellular processes in other vertebrate systems. However, we lack the entire picture of events and participants required to close wounds. This work attempts to address those deficiencies.

Specifically, my work attempts to identify factors responsible for shaping the Rho GTPase activity zones at wounds, determine the intracellular compartments and events used to repair the damaged plasma membrane, and further examine the dynamics of calcium throughout the healing process. In the second chapter, I identify RhoGAP1 and RhoGAP8 as factors responsible for maintaining the width of the Rho zone. In the third chapter, I examine the roles of RhoGAP1 and RhoGAP8 in the intact epithelia of *Xenopus* embryos. In the fourth chapter, I confirm a ring of calcium persists at wounds for several minutes after damage. Further, I characterize the events that shape membranous compartments that accumulate at wounds and provide what appears to be the first direct visual confirmation of the patching hypothesis.

# Chapter 2

Maintenance of Subcellular Rho GTPase Patterning During Single-Cell Repair

**Abstract**

The ability to respond to physical damage is an essential and evolutionarily conserved feature of single cells. Wounding induces the formation of subcellular protein localization and activity domains that coordinate the cytoskeletal rearrangements needed to reestablish the integrity of the plasma membrane and underlying cortex. The Rho family GTPases, Rho and Cdc42, are activated in concentric activity zones at wounds where they direct the actions of their respective effectors. The remarkable segregation exhibited by the Rho GTPase activity zones throughout wound repair implies they are sculpted by spatially patterned GTPase regulators. Here, I identify two GAPs, RhoGAP1 and RhoGAP8, as potential regulators of Rho GTPase activity during wound repair. I show that, in addition to having activity towards both Rho and Cdc42, RhoGAP1 and RhoGAP8 localize between the zones of active Rho and Cdc42 in wounded *Xenopus laevis* oocytes. Further, modest overexpression of RhoGAP1 can reduce the width of the Rho zone without altering zone activity. Combined, these results suggest RhoGAP1 and RhoGAP8 act as an enzymatic barrier to reinforce Rho GTPase activity zone segregation during wound repair.

**Introduction**

Single cells display the remarkable capacity to alter their shape to perform a diverse array of tasks. In many cases, as in cell division, it is necessary for these activities to be performed with high spatiotemporal accuracy and precision (Santaguida and Amon, 2015). Inherent in these morphological changes are cell polarization events in response to various internal or external signaling cues. In a manner similar to long-range morphogenic signaling during embryonic development, single cells are able to integrate initially broad signaling gradients into progressively tighter, spatially-localized domains within a shared cytoplasm (Bement and von Dassow, 2014). Precise patterning of intracellular components ensures efficient application of forces, and as a result, timely completion of tasks (e.g., Miller and Bement, 2009).

A striking example of single cell pattern formation is seen during the evolutionarily-conserved wound repair response (Sonnemann and Bement, 2011). From an initially broad gradient of calcium (Clark *et al.,* 2009; this work, Chapter 4), damaged cells are able to assemble an actomyosin contractile array at the wound edge that ingresses to close the defect (Bement *et al.,* 1999; Abreu-Blanco *et al.,* 2011). Subcellular patterning is evident within the contractile array; the majority of wound-associated myosin-2 and a pool of stable F-actin at the wound edge (Mandato and Bement, 2001) are surrounded by a ring of dynamic F-actin (Burkel *et al.,* 2007). Further, the Rho GTPases, upstream regulators of both F-actin polymerization and myosin-2 activity (Jaffe and Hall, 2005), are activated in corresponding zones upon wounding, with a zone of active Cdc42 circumscribing a zone of active Rho at the wound edge (Benink and Bement, 2005; Abreu-Blanco *et al.,* 2014). Inhibition of actomyosin contraction (either directly, or indirectly by altering upstream GTPase activity) attenuates the repair response (Benink and

Bement, 2005; Burkel *et al.*, 2012), thereby exemplifying the importance of proper pattering for successful wound closure. More broadly, the necessity for self-repair is evident, as cell damage occurs under physiological conditions (McNeil and Ito, 1990) and deficiencies in repair mechanisms or increased susceptibility to damage are associated with a variety of pathologies, such as muscular dystrophies (Bansal *et al*., 2003) and diabetes (Howard *et al.*, 2011a).

The precision with which Rho and Cdc42 are activated and maintained in distinct, subcellular activity zones throughout cellular repair suggests the involvement of multiple Rho GTPase regulators at wounds (Bement *et al.*, 2006). Cells regulate GTPase activity, in part, through the actions of guanine nucleotide exchange factors (GEFs) and GTPase activating proteins (GAPs) (Moon and Zheng, 2003; Rossman *et al.,* 2005). Given the abundance of GEFs and GAPs (in excess of 100 total in vertebrates) and the diversity of additional protein domains present therein (Tcherkezian and Lamarche-Vane, 2007; Rossman *et al.,* 2005), cells possess an incredible potential to spatially regulate Rho GTPase activity in response to a variety of signaling cues. A candidate screen to identify GEFs and GAPs involved in cell repair in *Xenopus laevis* oocytes revealed that Abr, a protein with both a GAP and a GEF domain, is a regulator of Rho GTPase activity at wounds (Vaughan *et al.,* 2011). Specifically, Abr localizes to the zone of active Rho, where it promotes Rho activation via its GEF domain. Further, the GAP domain of Abr, which has activity towards Cdc42, keeps the Rho zone free of active Cdc42, thereby reinforcing zone segregation (Vaughan *et al.*, 2011; Simon *et al.*, 2013).

However, these results only partially explain GTPase behavior at wounds. For example, while Abr dictates the location of the Cdc42 zone leading edge (Vaughan *et al.*, 2011), no complementary mechanism to control the outward extent of active Rho has been identified.

Nonetheless, analysis of Rho zone dynamics (Burkel *et al*., 2012) indicated its activity is subject to a signal treadmill, i.e. Rho is preferentially activated at the leading edge the zone, whereas it is inactivated at the trailing edge of the zone. Together, these results suggest involvement of additional GTPase regulators to modulate Rho GTPase dynamics at wounds.

Here, I identify RhoGAP1 and its homologue, RhoGAP8 (also known as BPGAP1), as participants in cell repair in *X. laevis* oocytes. I show that *X. laevis* RhoGAP1 and RhoGAP8 possess *in vivo* and *in vitro* activity towards both Rho and Cdc42, localize to wounds between the zones of active Rho and Cdc42, and are able to modulate the width of the zone of active Rho. Together, these results suggest RhoGAP1 and RhoGAP8 are involved in defining the outer extent of the Rho zone and may represent key players in driving Rho GTPase signal treadmilling at wounds.

## Results

### *RhoGAP1 and RhoGAP8 are identified as potential regulators of wound repair*

To continue the candidate screen initiated by Vaughan *et al.* (2011) to identify regulators of Rho GTPase activity at wounds, we focused our efforts on characterizing two RhoGAPs, RhoGAP1 and RhoGAP8 (Figure 1A). Both RhoGAPs contain a N-terminal Sec14-like domain (based on similarity to the yeast phospholipid transfer protein, Sec14p [Aravind *et al.*, 1999]), a central proline-rich region (PRR), and a C-terminal RhoGAP domain with a canonical catalytic arginine (Leonard *et al.,* 1998). They were of particular interest due to reported interactions of the Sec14-like domains with both Rho (Zhou *et al.*, 2010) and phospholipids (reviewed in Saito *et al.*, 2007b), while the PRR was shown to be able to bind to SH3 domains (Barfod *et al.*, 1993),

thereby providing at least three potential GAP domain-independent means for localization to wounds. While RhoGAP1 and RhoGAP8 share similar domain structure and size (435 a.a. vs. 420 a.a.), the two have limited amino acid sequence conservation (Figure 1A).

To assess the ability of RhoGAP1 and RhoGAP8 to localize to wounds, and thereby potentially participate in wound repair, an eGFP tag was added to each (Figure 1A). Wounding induced the recruitment of both eGFP-RhoGAP1 and eGFP-RhoGAP8 to the site of damage (Figure 2B). The proteins were focused in a ring at the wound edge, corresponding to the general region occupied by active Rho and Cdc42 (Benink and Bement, 2005). Thus, both RhoGAPs were identified as potential wound regulators and subjects for further investigation.

There have been conflicting reports of the activity of RhoGAP1, both *in vivo* and *in vitro,* towards specific GTPases with some identifying RhoGAP1 as a GAP for Rho and others as a GAP for Rac and Cdc42 (Ridley *et al.*, 1993, Lancaster *et al.,* 1994; Zhang and Zheng, 1998; Moskwa *et al.*, 2005; Yang *et al.,* 2006). I therefore sought to characterize the activity of *X. laevis* RhoGAP1 and RhoGAP8. GST-tagged versions of each protein were purified from baculovirus-infected insect cells (Figure 1B) and their ability to stimulate hydrolysis of Rho and Cdc42 *in vitro* was assessed. Both GST-tagged RhoGAP1 and RhoGAP8 have activity against both Rho and Cdc42, with less activity towards Cdc42 (Figure 1D).

***RhoGAP1 Localizes Between the Zones of Active Rho and Active Cdc42***

To address the potential of RhoGAP1 to regulate the GTPase activity during wound repair, I compared the localization of eGFP-RhoGAP1 to that of the active GTPases at wounds. Rho and Cdc42 are broadly activated (as detected by eGFP-rGBD and mRFP-wGBD,

respectively; Benink and Bement, 2005) ~20 seconds after wounding before becoming rapidly refined to distinct activity "zones", with active Rho localized to the wound edge, circumscribed by a zone of active Cdc42. The GTPase activity zones maintain segregation as the wound array ingresses inward (Figure 2A, Movie 1).

When cells coexpressing eGFP-RhoGAP1 (Figure 2B) and mRFP-wGBD were wounded, eGFP-RhoGAP1 localized to the wound edge slightly interior to the zone of active Cdc42 (Figure 2C, Movie 2). Since the zone of active Cdc42 circumscribes the Rho zone (Figure 2A, Movie 1), it appeared eGFP-RhoGAP1 might be localizing between the two GTPase activity zones. To investigate this possibility, 3XeGFP-RhoGAP1 was co-injected with mCherry-2xrGBD, BFP-wGBD (probes for the active GTPases, see Methods) (Figure 2D). 3XeGFP-RhoGAP1 localized between the zone of active Rho and active Cdc42 (Figure 2, D and D'). This distinct localization pattern becomes more apparent using kymography of average fluorescence intensity around the wound with respect to time (Figure 2E). A line scan across the kymograph in Figure 3E (corresponding to 90 seconds post-wounding) reveals the peak of eGFP-RhoGAP1 between the zones of active Rho and Cdc42, with bias towards the peak of Rho activity (Figure 3E'). Analysis of 4D movies (e.g. Figure 2, C and E) suggested eGFP-RhoGAP1 was localized to wounds later than Cdc42 activation. The time required for these two events occur post-wounding was quantified and found to be significantly different ($t$ = 31.5 ± 1.3 s for Cdc42 activation, $t$ = 75.3 ± 3.3 s for eGFP-RhoGAP1 recruitment; $p < 0.001$). Further examination of active Cdc42 and eGFP-RhoGAP1 localization along the *xz*-axis (Figure 2G) revealed that in addition to being slightly interior to the zone of active Cdc42, eGFP-RhoGAP1 localizes below the Cdc42 zone. Together, the above activity and localization results suggest

RhoGAP1 is positioned to potentially maintain GTPase activity zone position within the wound array.

### *RhoGAP1 is Expressed in* Xenopus laevis *oocytes*

While the foregoing localization and *in vitro* activity results were promising, I sought to determine whether they were physiologically relevant. That is, since the source RhoGAP1 clone was obtained from stage 31 and 32 embryos (Pontius *et al.,* 2003), I could not be certain that *X. laevis* express RhoGAP1 at the oocyte stage. I synthesized cDNA from oocyte-derived RNA, which in turn, was used to amplify RhoGAP1 (Figure 3A, center) that matched the size of the source clone (Figure 3A, right). Sequencing of the oocyte-derived amplicon (data not shown) confirmed that RhoGAP1 is present in *X. laevis* at the transcript level.

Since translation of many transcripts is developmentally controlled (Newport and Kirschner, 1982), I sought to determine whether RhoGAP1 protein was present in oocytes. Due to the dearth of commercial antibodies available against *X. laevis* antigens, it was necessary to raise a polyclonal antibody against *X. laevis* RhoGAP1 (see Methods). In a western blot of oocyte lysates, the affinity purified α-RhoGAP1 polyclonal antibody recognized a ~50 kDa species (Figure 3B, lane 1), matching the predicted size of endogenous RhoGAP1. Further, the antibody recognized overexpressed full-length untagged and eGFP-tagged RhoGAP1 (Figure 3B; lanes 2 and 4, respectively). Expression of either untagged or eGFP-tagged RhoGAP8 went undetected by α-RhoGAP1, indicating that despite the domain conservation between RhoGAP1 and RhoGAP8 (Figure 1), there are enough differences between the two to allow immunogenic differentiation.

To determine whether endogenous RhoGAP1 localizes to wounds, oocytes were wounded, fixed, and then stained with the α-RhoGAP1 polyclonal antibody described above. Consistent with the results obtained with eGFP-RhoGAP1, endogenous RhoGAP1 localized to punctae at sites distal to the wound and in a ring around the wound edge (Figure 3C, left). This staining was specific in that it was not detected in a secondary antibody-alone control (Figure 3C, right). Together, these results suggest RhoGAP1 is not only present in oocytes, but also participates in the wound response.

***RhoGAP1 Localizes to Early and Recycling Endosomes***

The foregoing results (Figures 1B, 2C, 3C, and not shown) showed that in addition to the wound-induced localization of eGFP-RhoGAP1 to the wound edge, it also labeled small intracellular compartments. Previous reports of localization of RhoGAP1 to endosomes (Sirokmány *et al.,* 2006) in HeLa cells led me to assess whether the punctate structures labeled by eGFP-RhoGAP1 in *X. laevis* oocytes are also part of the endosomal pathway. Cells expressing eGFP-RhoGAP1 were incubated in extracellular fluorescent dextran to non-specifically label the entire endosomal pathway (Figure 4, A and A'). While dextran was present in eGFP-RhoGAP1-labelled structures (Figure 4A), closer examination revealed a heterogeneous population of labeled structures (Figure 4A'). That is, some dextran-positive compartments lack eGFP-RhoGAP labeling; this suggests that eGFP-RhoGAP1 is only recruited to a subset of endosomes.

To identify the endosomal compartment(s) labeled by RhoGAP1, I coexpressed eGFP-RhoGAP1 and mCherry-tagged Rab GTPases, markers of endosomal compartments (reviewed in Hutagalung and Novick, 2011). Both low- and high-magnification en face views (Figure 4, B and

B') of cells expressing mCherry-Rab7, a marker of late endosomes, and eGFP-RhoGAP1 show minimal colocalization. This is exemplified in views along the *xz*-axis, where mCherry-Rab7 and eGFP-RhoGAP1 occupy adjacent, but primarily exclusive regions in *z* (Figure 4B''). Conversely, coexpression of eGFP-RhoGAP1 and mCherry-Rab5 (Figure 4C), a marker for early endosomes, reveals extensive colocalization along *xy*- (Figure 4C') and *xz*-axes (Figure 4C''). eGFP-RhoGAP1 also labeled mCherry-Rab11-positive (recycling) endosomes (Figure 4D), although not as extensively as seen with Rab5-labelled endosomes (Figure 4, C' and D'). Views along the *xz*-axis of resting cells illustrate that eGFP-RhoGAP1 and mCherry-Rab11 only co-occur in a small region with respect to their individual distributions in *z* (Figure 4D'').

***RhoGAP8 Localizes in a Manner Similar to RhoGAP1***

To further characterize eGFP-RhoGAP8 localization to wounds (Figure 1B), its mRNA was injected along with that of mRFP-wGBD. eGFP-RhoGAP8 (Figure 5A) localizes to the leading edge of the Cdc42 zone (Figure 5B) with the peak of localization slightly interior to (with respect to the wound center) to the peak of Cdc42 activity (Figure 5B'); this localization pattern is similar to what is seen with eGFP-RhoGAP1 (Figure 2C). Wounds made in cells co-expressing eGFP-RhoGAP1 and mCherry-RhoGAP8 (Figure 5C) reveal a striking degree of colocalization of the two RhoGAPs (Figure 5C').

*X. laevis* RhoGAP8 is currently unannotated and was identified only by similarity to RhoGAP1. As such, I sought to confirm the presence of RhoGAP8 transcripts and protein in oocytes. RhoGAP8 matching the size of that derived from the source plasmid was amplified from oocyte cDNA (Figure 5D). As with the case of RhoGAP1, there were no commercial

antibodies against *X. laevis* RhoGAP8, necessitating the production of a RhoGAP8 polyclonal antibody (see Methods). Although α-RhoGAP8 does recognize a species near the predicted ~ 48 kDa in oocyte lysates, the antibody also detects several other bands, mainly above 75 kDa (Figure 5E, left). All attempts to remove the spurious reactivity from α-RhoGAP8 were unsuccessful (not shown). However, α-RhoGAP8 does recognize overexpression of untagged and eGFP-tagged RhoGAP8 (Figure 5E, right; lanes 4 and 6, respectively), but not similar expression of RhoGAP1 constructs (Figure 5E, right; lanes 3 and 5, respectively) suggesting the ~48 kDa band corresponds to endogenous RhoGAP8 and that α-RhoGAP8 does not cross-react with RhoGAP1.

The similarity of RhoGAP1 and RhoGAP8 with respect to localization (Figures 1B, 2B and C) and *in vitro* GAP activity (Figure 1D) leads me to treat them as one in the same. This does not preclude minute differences in RhoGAP1 and RhoGAP8 function at wounds, but to the best of my knowledge, they appear to play redundant roles in wound repair. Thus, the forthcoming results will focus exclusively on RhoGAP1.

***RhoGAP1 has Activity Towards the Rho GTPases at Wounds***

To assess the *in vivo* function of RhoGAP1, a full-length construct as well as two truncations (Figure 6A), the isolated N-terminus (a.a. 1-218, containing a Sec14-like domain) and C-terminus (a.a. 219-435, containing the proline-rich region and RhoGAP domain) were overexpressed in oocytes expressing eGFP-rGBD and mRFP-wGBD to reveal the Rho and Cdc42 activity zones, respectively (Figures 2A, 6B). Overexpression of full-length RhoGAP1 nearly eliminates the zone of active Rho (Figure 6C, left and right; Figure 6C', $p < 0.001$; Movie

3) while causing disorganization in the Cdc42 zone (Figure 6C, left and center; Movie 3). This combination of results is reminiscent of those reported with cells treated with C3 exotransferase (Benink and Bement, 2005; Burkel *et al*., 2012), a specific inhibitor of Rho (Stasia *et al*., 1991). However, while disorganized, the zone of active Cdc42 still persists, suggesting RhoGAP1 activity *in vivo* is mainly directed towards Rho.

Surprisingly, overexpression of the RhoGAP1 N-terminus also led to reduction of Rho zone intensity (Figure 6D, left and right; Figure 6D', $p < 0.05$). Further, like full-length RhoGAP1, the N-terminus does not affect Cdc42 activity (Figure 6D, left and center). The Sec14-like domain has been reported to bind RhoA (Zhou *et al.*, 2010), so the foregoing results may represent the N-terminus of RhoGAP1 interrupting normal interactions with binding partners (see Discussion).

Overexpression of the RhoGAP1 C-terminus has profound effects on Rho GTPase activity at wounds; both Rho and Cdc42 activity are greatly diminished (Figure 6, E and E'; $p < 0.001$). It should be noted that the isolated C-terminus of RhoGAP1 has strikingly potent GAP activity when compared to the full-length protein; the mRNA for the C-terminus was injected at 1-2% the concentration than that of the full length construct. Given that disparity, it is difficult to attribute the potency of the C-terminal fragment on differences in translation rates of different sized transcripts (~ 1.3 kb for full-length, ~ 0.65 kb for the C-terminus). The potency of the isolated C-terminus also lends support to the notion that the Sec14-like domain and GAP domain of RhoGAP1 interact, thereby keeping RhoGAP1 in an autoinhibited state (Moskwa *et al*., 2005; Zhou *et al.*, 2010).

***Determinants of RhoGAP1 Localization***

To determine how RhoGAP localizes to wounds, eGFP-tags were added to the constructs depicted in Figure 6A. The eGFP-tagged N-terminus of RhoGAP1 (eGFP-N') is able to localize to wounds (Figure 7B) at the leading edge of the zone of active Cdc42 (Figure 7B'), similar to full-length eGFP-RhoGAP1 (Figure 7, A and A'). However, eGFP-N' localizes to wounds more slowly than eGFP-RhoGAP1 (data not shown), suggesting the C-terminus also contributes to RhoGAP1 localization.

Closer examination of resting oocytes expressing eGFP-N' revealed a localization pattern (Figure 7C) strikingly distinct from that of the full-length construct (Figures 1-4). Instead of primarily cytoplasmic staining with the occasional punctate structure, as seen with full-length eGFP-RhoGAP1, eGFP- N' also extensively labels a population of large vesicles that, based on size and appearance, appear to be cortical granules (Campanella and Andreucetti, 1977; this work, Chapter 4). Given the reported ability of Sec14-like domains to bind to phospholipids (Saito *et al.*, 2007), it seems likely that the endogenous conformation of full-length RhoGAP1 may inhibit this interaction.

The behavior of eGFP- N' immediately after wounding (i.e. less than 30 s) further supports my assertion that it is labeling cortical granules. Labeled compartments begin to disappear from regions distal to the wound (Figure 7D, Movie 4) as early as 6 seconds post wounding and continued until a region ~40 μm in diameter was devoid of eGFP-N'-labelled compartments. Cortical granules are known to exocytose upon wounding (Bi *et al.,* 1995; this work, Chapter 4), so loss of labeling could reflect cortical granule fusion with the plasma membrane and subsequent change in lipid composition. However, the extent of loss is not

congruent with observations of wound-induced cortical granule exocytosis in *X. laevis* oocytes. That is, not all cortical granules near the wound edge exocytose, and those that do are often delayed (> 30 s post-wounding) with respect to the initial wounding event (this work, Chapter 4). Therefore, loss of eGFP-N' at sites proximal to the wound may reflect other, still unknown processes that alter the affinity of eGFP-N' for cortical granules.

The eGFP-tagged C-terminus of RhoGAP1 (eGFP-C') is also capable of localizing to wounds (Figure 7, E and E'). However, unlike full-length eGFP-RhoGAP1 (Figure 7, A and A') and eGFP-N' (Figure 7, B and B'), eGFP-C' does not localize between the two GTPase activity zones (Figure 7E). Instead, eGFP-C' localizes to the Cdc42 zone (Figure 7E'). Although, as with the case of the untagged C-terminus (Figure 6E), eGFP-C' appears to attenuate Rho GTPase activity, as evident by the appearance and behavior of the Cdc42 zone (Figure 7E, not shown). Therefore, eGFP-C' might localize differently if a proper Rho zone was present. Nevertheless, the foregoing results suggest that both the N- and C-termini of RhoGAP1 are, in part, responsible for its recruitment to the wound array.

The foregoing results indicated that RhoGAP1 might be recruited to wounds via association with endosomes that are transported, directly or indirectly, via associations with the wound-induced cytoskeletal array. Cortical flow, the pulling of material toward the wound by actomyosin contraction, has been implicated in localization of many repair components (Mandato and Bement, 2001; 2003; Vaughan *et al.*, 2014). Microtubules form radial arrays at the wound edge, where they regulate Rho GTPase activity zone organization by a mechanism that may involve transport of material to the wound (Mandato and Bement, 2001; Benink and Bement, 2005). Treatment of oocytes with nocodazole and latrunculin B, inhibitors of

microtubule and actin polymerization, respectively, fail to prevent localization of eGFP-RhoGAP1 to wounds (Figure 7F, center and right), revealing that RhoGAP1 localization to wounds is not solely based on microtubule-based transport or cortical flow.

***Moderate Overexpression of RhoGAP1 Narrows the Zone of Active Rho***

The phenotypes observed with RhoGAP1 overexpression (e.g., the reduction of Rho zone intensity and Cdc42 zone discontinuity) seen in Figure 6 (see also Movie 3), while striking and informative to *in vivo* GAP activity, are likely a result of RhoGAP1 asserting its effects ectopically and may be masking any specific, localized activities. That is, given the distinct localization of RhoGAP1 between the zones of active Rho and Cdc42, it seems possible that its activity must be needed in that specific location. Further, if the function of RhoGAP1 at wounds were to only non-specifically regulate Rho zone activity, its localization should be broadly distributed throughout the Rho zone.

To address whether there were subtleties in GTPase dynamics not observed with gross overexpression of RhoGAP1, I injected mRNA for untagged RhoGAP1 into oocytes (also expressing the probes for active Rho and Cdc42) at 1/10 the concentration I previously used (Figure 6). While Rho and Cdc42 in cells overexpressing RhoGAP1 (Figure 8B) were activated to the same degree as GTPase activity zones in control cells (Figure 8, A and C), the width of the Rho zone was reduced in overexpressing cells (Figure 8D, $p < 0.001$). These results support the hypothesis that RhoGAP1 acts as barrier to limit the outward extent of the Rho zone. Overexpression of RhoGAP1 would broaden the region occupied by RhoGAP1 between Rho and Cdc42 zone, allowing RhoGAP1 to ingress further into the zone of active Rho. The presence of

Rho inactivator at the trailing edge of the Rho zone has been posited to underlie a signaling treadmill wherein Rho is preferentially activated at the leading edge and inactivated at the trailing edge (Burkel *et al*., 2012).

**Figure 1.** *Xenopus laevis* RhoGAP1 and RhoGAP8 are identified as potential regulators of Rho GTPase activity at single cell wounds. **(A)** Domain structure and conservation between *Xenopus laevis* RhoGAP1 and RhoGAP8, shown with eGFP tags. Both contain a N-terminal Sec14-like domain, a central proline rich region, and a C-terminal GAP domain. **(B)** Wounded *X. laevis* oocytes expressing mRNA encoding the constructs described in (A), revealing recruitment of eGFP-tagged RhoGAP1 and RhoGAP8 to wounds. **(C)** Recombinant GST-tagged *X. laevis* RhoGAP1 and RhoGAP8 purified from baculovirus-infected *Sf*9 insect cells. **(D)** The ability of the recombinant proteins shown in (C) to stimulate GTP hydrolysis in Rho and Cdc42 was measured. Times in min:sec with t = 0:00 corresponding to moment of wounding. Scale bars, 10 μm.

# Figure 1

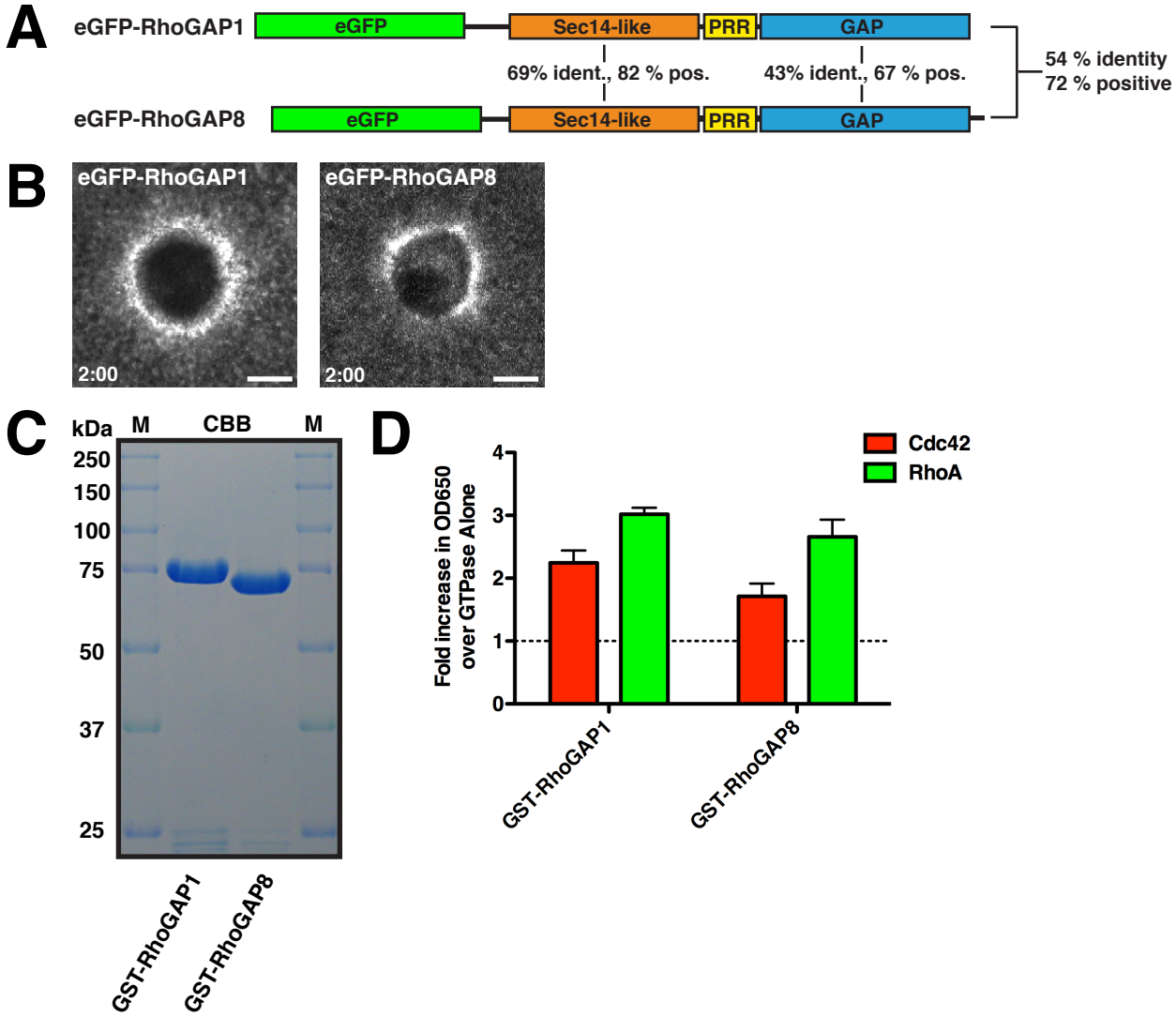
A
eGFP-RhoGAP1
eGFP
Sec14-like
PRR
GAP
69% ident., 82 % pos.
43% ident., 67 % pos.
54 % identity
72 % positive
eGFP-RhoGAP8
eGFP
Sec14-like
PRR
GAP
B
eGFP-RhoGAP1
2:00
eGFP-RhoGAP8
2:00
C
kDa
M
CBB
M
250
150
100
75
50
37
25
GST-RhoGAP1
GST-RhoGAP8
D
Cdc42
RhoA
Fold increase in OD650 over GTPase Alone
4
3
2
1
0
GST-RhoGAP1
GST-RhoGAP8

**Figure 2**. Fluorescently-tagged RhoGAP1 localizes between the zones of active Rho and Cdc42 at wounds. **(A)** A wounded oocyte expressing mRFP-wBGD and eGFP-rGBD, probes for active Cdc42 and active Rho, respectively. Rho and Cdc42 form spatially distinct wound-induced activity zones. See Movie 1. **(B)** Domain structure of (1X or 3X) eGFP-RhoGAP. **(C)** An oocyte coexpressing mRFP-wGBD and eGFP-RhoGAP1 was wounded to track RhoGAP1 recruitment to sites of damage. See Movie 2. **(D)** A wounded oocyte expressing BFP-wGBD, mCherry-2xrGBD, and 3XeGFP-RhoGAP1. **(D')** An enlargement of (D) revealing 3XeGFP-RhoGAP1 localization between the zones of active Rho and Cdc42. **(E)** An kymograph representing average position and intensity of BFP-wGBD, mCherry-2xrGBD, and 3XeGFP-RhoGAP1 during a wounding event. Center of the wound is indicated by the "W". **(E')** Line scan of kymograph in (E) corresponding to 1:30 post-wounding, showing the relative positions of active Rho, active Cdc42, and 3XeGFP-RhoGAP1. **(F)** Time required for Cdc42 activation and RhoGAP1 recruitment to wounds was quantified (n = 21 oocytes from three independent experiments, $p < 0.001$). **(G)** *xz*-view of a wound, showing the relative positions of mRFP-wGBD and eGFP-RhoGAP1 in *z.* Times in min:sec with t = 0:00 corresponding to moment of wounding. Scale bars: 10 μm.

# Figure 2

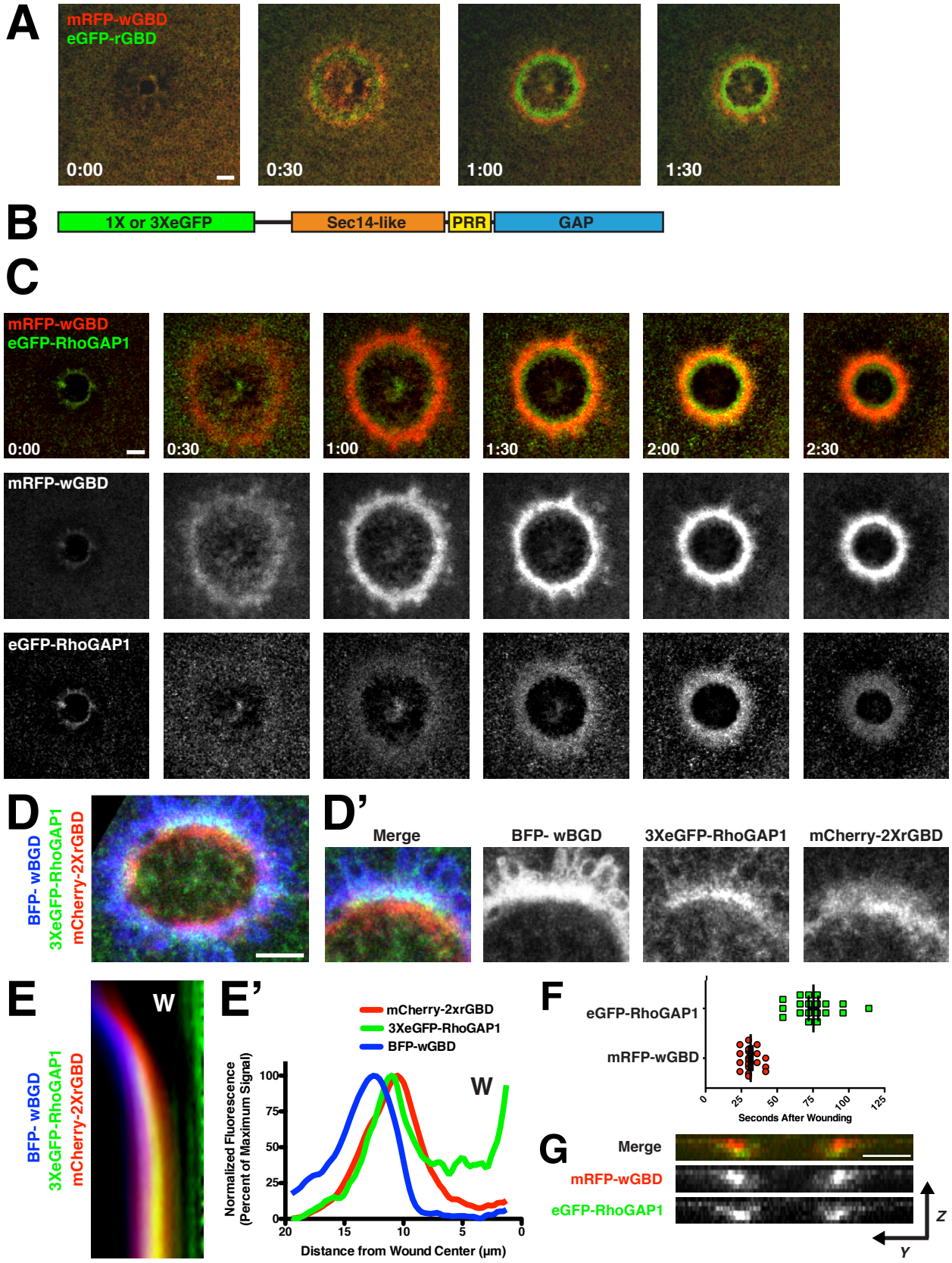
A
mRFP-wGBD
eGFP-rGBD
0:00
0:30
1:00
1:30
B
1X or 3XeGFP
Sec14-like
PRR
GAP
C
mRFP-wGBD
eGFP-RhoGAP1
0:00
0:30
1:00
1:30
2:00
2:30
mRFP-wGBD
eGFP-RhoGAP1
D
BFP- wBGD
3XeGFP-RhoGAP1
mCherry-2XrGBD
D'
Merge
BFP- wBGD
3XeGFP-RhoGAP1
mCherry-2XrGBD
E
W
BFP- wBGD
3XeGFP-RhoGAP1
mCherry-2XrGBD
E'
mCherry-2xrGBD
3XeGFP-RhoGAP1
BFP-wGBD
W
Normalized Fluorescence (Percent of Maximum Signal)
100
75
50
25
0
20
15
10
5
0
Distance from Wound Center (µm)
F
eGFP-RhoGAP1
mRFP-wGBD
0
25
50
75
100
125
Seconds After Wounding
G
Merge
mRFP-wGBD
eGFP-RhoGAP1
Z
Y

**Figure 3.** RhoGAP1, an endogenously expressed protein in *X. laevis* oocytes, localizes to wounds. **(A)** Amplification of RhoGAP8 from oocyte cDNA provides evidence for its presence at the transcript level in oocytes. **(B)** Western blot showing both presence of RhoGAP1 protein in oocytes (lane 1, uninjected) and that anti-RhoGAP1 does not recognize RhoGAP8 (lanes 3 and 5, RhoGAP8 overexpression and eGFP-RhoGAP8). **(C)** Oocytes were wounded and fixed prior to staining with antibodies against RhoGAP1. Endogenous RhoGAP1 localization to wounds is evident (left) when compared to a secondary-only control (right). Scale bars: 10 μm.

# Figure 3

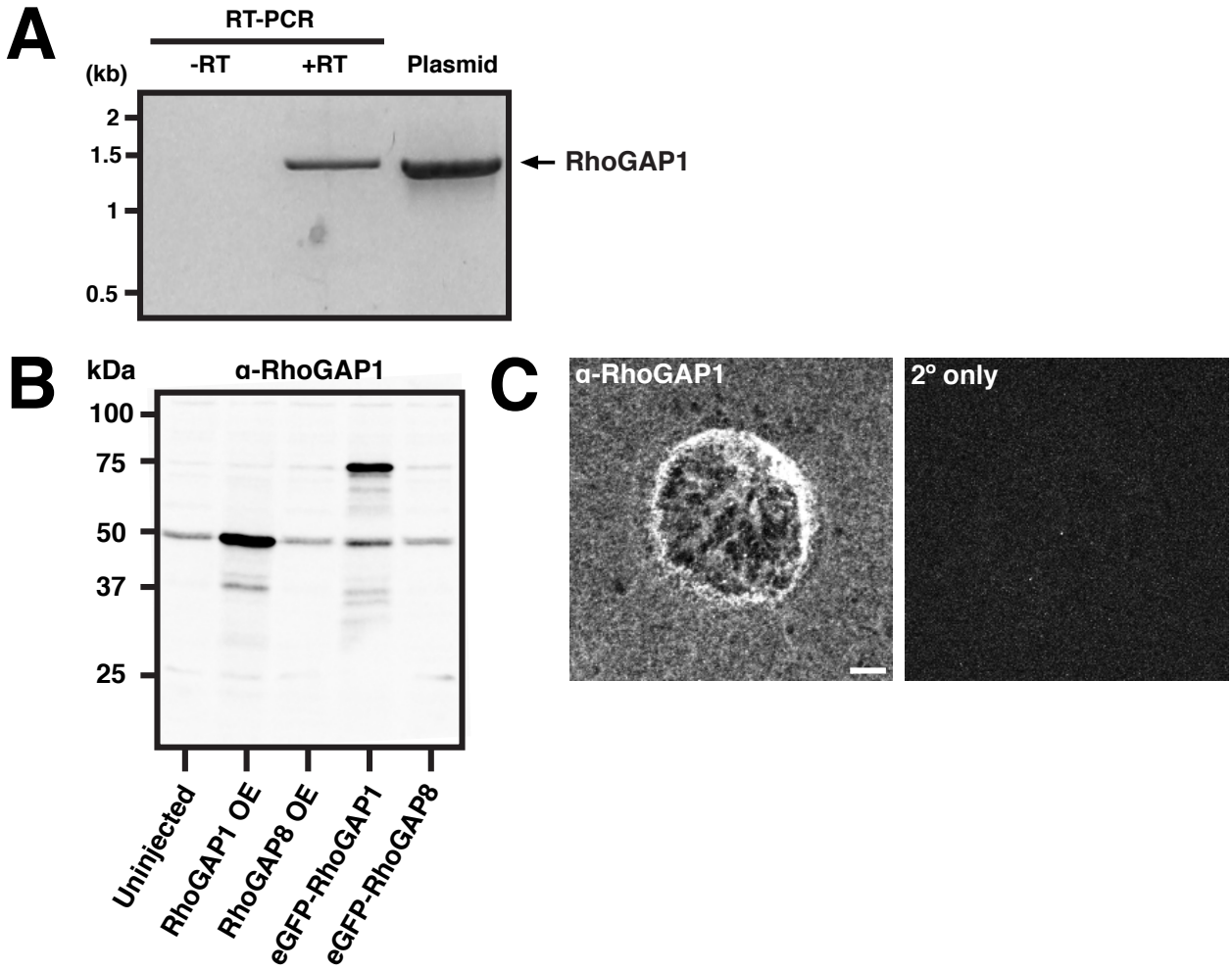
A
RT-PCR
-RT
+RT
Plasmid
(kb)
2
1.5
1
0.5
RhoGAP1
B
kDa
α-RhoGAP1
100
75
50
37
25
Uninjected
RhoGAP1 OE
RhoGAP8 OE
eGFP-RhoGAP1
eGFP-RhoGAP8
C
α-RhoGAP1
2° only

**Figure 4.** RhoGAP1 labels compartments of the endosomal pathway. **(A)** En face view of an oocyte expressing eGFP-RhoGAP1 that was incubated in extracellular dextran (Texas Red dextran) to highlight the endosomal pathway. **(A')** Enlargement of highlighted region indicated in (A), showing some endosomal compartments are labelled by eGFP-RhoGAP1. **(B)** An oocyte expressing eGFP-RhoGAP1 and mCherry-Rab7, a marker of late endosomes. **(B')** Enlargement of highlighted region indicated in (B). **(B")** *xz*-view of image shown in (B). **(C)** An oocyte expressing eGFP-RhoGAP1 and mCherry-Rab5, a marker of early endosomes. **(C')** Magnification of highlighted region indicated in (C). **(C")** *xz*-view of image shown in (C). **(D)** En face view of an oocyte expressing eGFP-RhoGAP1 and mCherry-Rab11, a marker of recycling endosomes. **(D')** Magnification of highlighted region indicated in (D). **(D")** *xz*-view of image shown in (D). Scale bars:10 μm.

# Figure 4

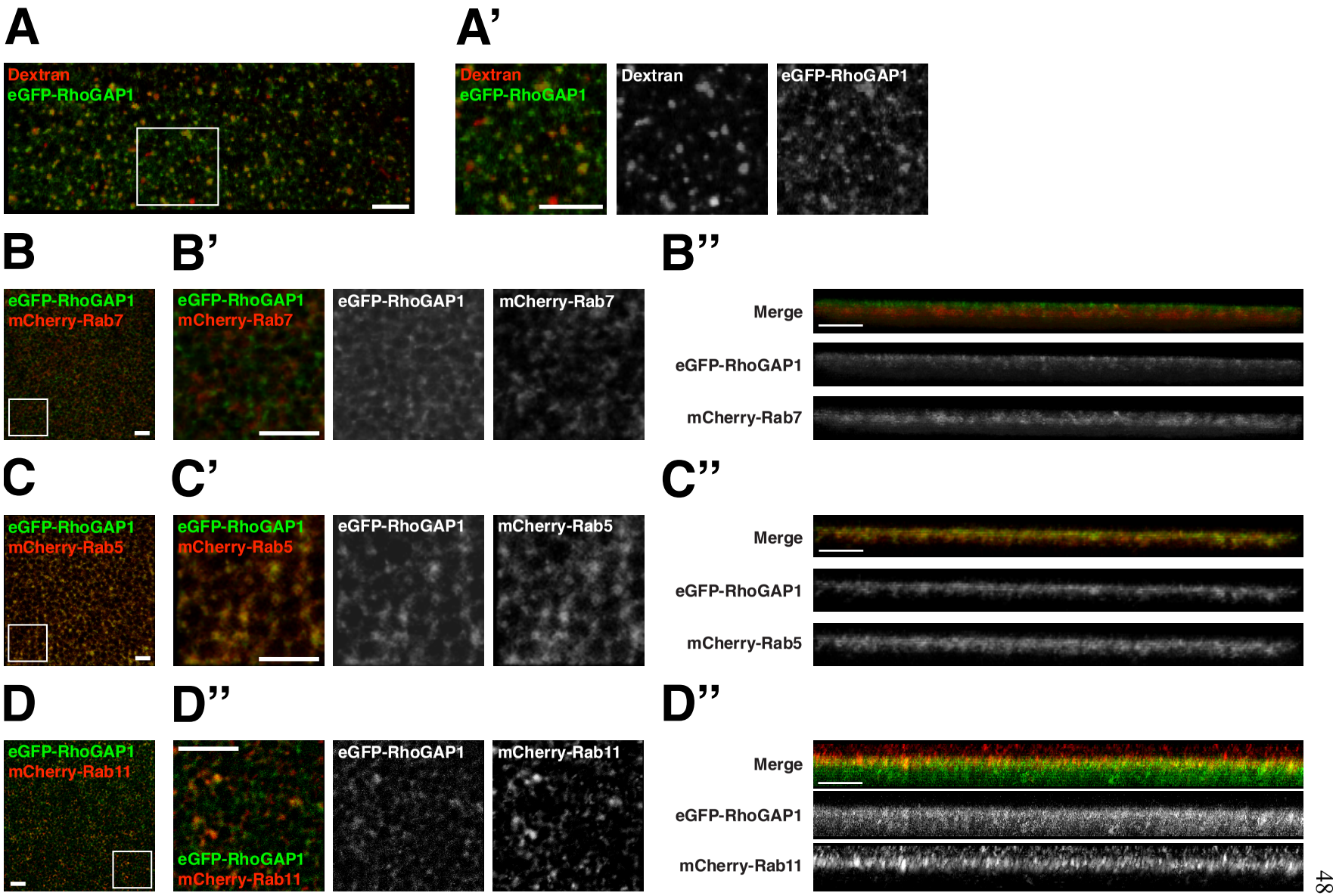
A
A'
Dextran
eGFP-RhoGAP1
Dextran
eGFP-RhoGAP1
Dextran
eGFP-RhoGAP1
B
B'
B''
eGFP-RhoGAP1
mCherry-Rab7
eGFP-RhoGAP1
mCherry-Rab7
eGFP-RhoGAP1
mCherry-Rab7
Merge
eGFP-RhoGAP1
mCherry-Rab7
C
C'
C''
eGFP-RhoGAP1
mCherry-Rab5
eGFP-RhoGAP1
mCherry-Rab5
eGFP-RhoGAP1
mCherry-Rab5
Merge
eGFP-RhoGAP1
mCherry-Rab5
D
D''
D''
eGFP-RhoGAP1
mCherry-Rab11
eGFP-RhoGAP1
mCherry-Rab11
eGFP-RhoGAP1
mCherry-Rab11
Merge
eGFP-RhoGAP1
mCherry-Rab11

**Figure 5.** RhoGAP8 localization to wounds mirrors that of RhoGAP1. **(A)** Domain structure of (1X or 3X) eGFP-RhoGAP. **(B)** An oocyte coexpressing mRFP-wGBD and eGFP-RhoGAP8 was wounded to track RhoGAP8 recruitment to sites of damage, revealing RhoGAP8 localization ahead of the zone of active Cdc42. **(B')** Line scan of (B) showing the relative positions of active Cdc42 and eGFP-RhoGAP8 with respect to the wound center, denoted by the "W". **(C)** Coexpression of mCherry-RhoGAP8 and eGFP-RhoGAP1 in a wounded oocyte shows similar localization at wounds. **(C')** Line scan of (C) showing the relative positions of mCherry-RhoGAP8 and eGFP-RhoGAP1 with respect to the wound center, denoted by the "W". **(D)** Amplification of RhoGAP8 from oocyte cDNA provides evidence for its presence at the transcript level in oocytes. **(E)** Western blots showing RhoGAP8 is expressed in *X. laevis* oocytes (left) and that the anti-RhoGAP8 antibody does not recognize RhoGAP1. Times in min:sec with t = 0:00 corresponding to moment of wounding. Scale bars: 10 μm.

# Figure 5

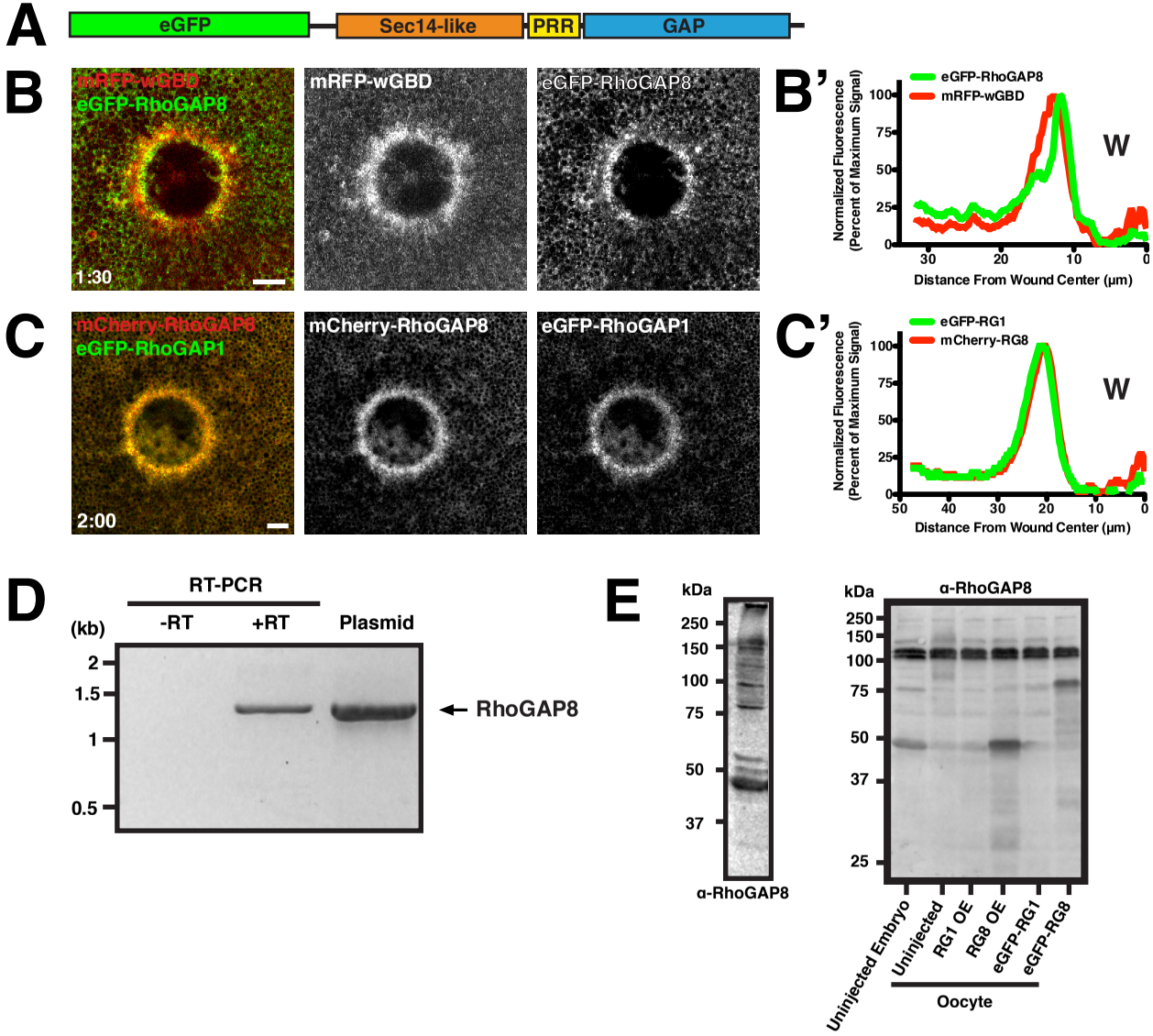
A
eGFP
Sec14-like
PRR
GAP
B
mRFP-wGBD
eGFP-RhoGAP8
1:30
mRFP-wGBD
eGFP-RhoGAP8
B'
eGFP-RhoGAP8
mRFP-wGBD
Normalized Fluorescence (Percent of Maximum Signal)
W
Distance From Wound Center (μm)
C
mCherry-RhoGAP8
eGFP-RhoGAP1
2:00
mCherry-RhoGAP8
eGFP-RhoGAP1
C'
eGFP-RG1
mCherry-RG8
Normalized Fluorescence (Percent of Maximum Signal)
W
Distance From Wound Center (μm)
D
RT-PCR
(kb)
-RT
+RT
Plasmid
RhoGAP8
E
kDa
α-RhoGAP8
kDa
α-RhoGAP8
Uninjected Embryo
Uninjected
RG1 OE
RG8 OE
eGFP-RG1
eGFP-RG8
Oocyte

**Figure 6.** Overexpression of RhoGAP1 attenuates Rho GTPase activity at wounds. **(A)** Domain structure of full length RhoGAP1 and two truncations, N' (a.a. 1-218, contains Sec14-like domain) and C' (a.a. 219-435, contains proline-rich region and a GAP domain). **(B)-(D)** Wounded oocytes expressing probes for active Rho (green) and active Cdc42 (red). **(B)** Rho GTPase activity zones at a wound under control conditions. **(C)** Overexpression of full-length RhoGAP1 reduces Rho, but not Cdc42, activity at wounds. See Movie 3. **(C')** Quantification of GTPase activity upon RhoGAP1 overexpression seen in (C)**.** $n = 22$ for control cells, $n = 20$ for cells overexpressing full-length RhoGAP1; from three independent experiments, $***p < 0.001$. **(D)** Overexpression of the RhoGAP1 N-terminus also reduces Rho, but not Cdc42, activity at wounds. **(D')** Quantification of GTPase activity upon overexpression of RhoGAP1 N', as seen in (D)**.** $n = 18$ for control cells, $n = 17$ for cells overexpressing RhoGAP1; from three independent experiments, $***p < 0.001$. **(E)** Overexpression of the RhoGAP1 C-terminus reduces activity of both Rho and Cdc42. **(E')** Quantification of GTPase activity upon overexpression of RhoGAP1 C', as seen in (E)**.** $n = 18$ for control cells, $n = 18$ for cells overexpressing RhoGAP1; from two independent experiments, $***p < 0.001$. Times in min:sec with t = 0:00 corresponding to moment of wounding. Scale bars, 10 μm.

# Figure 6

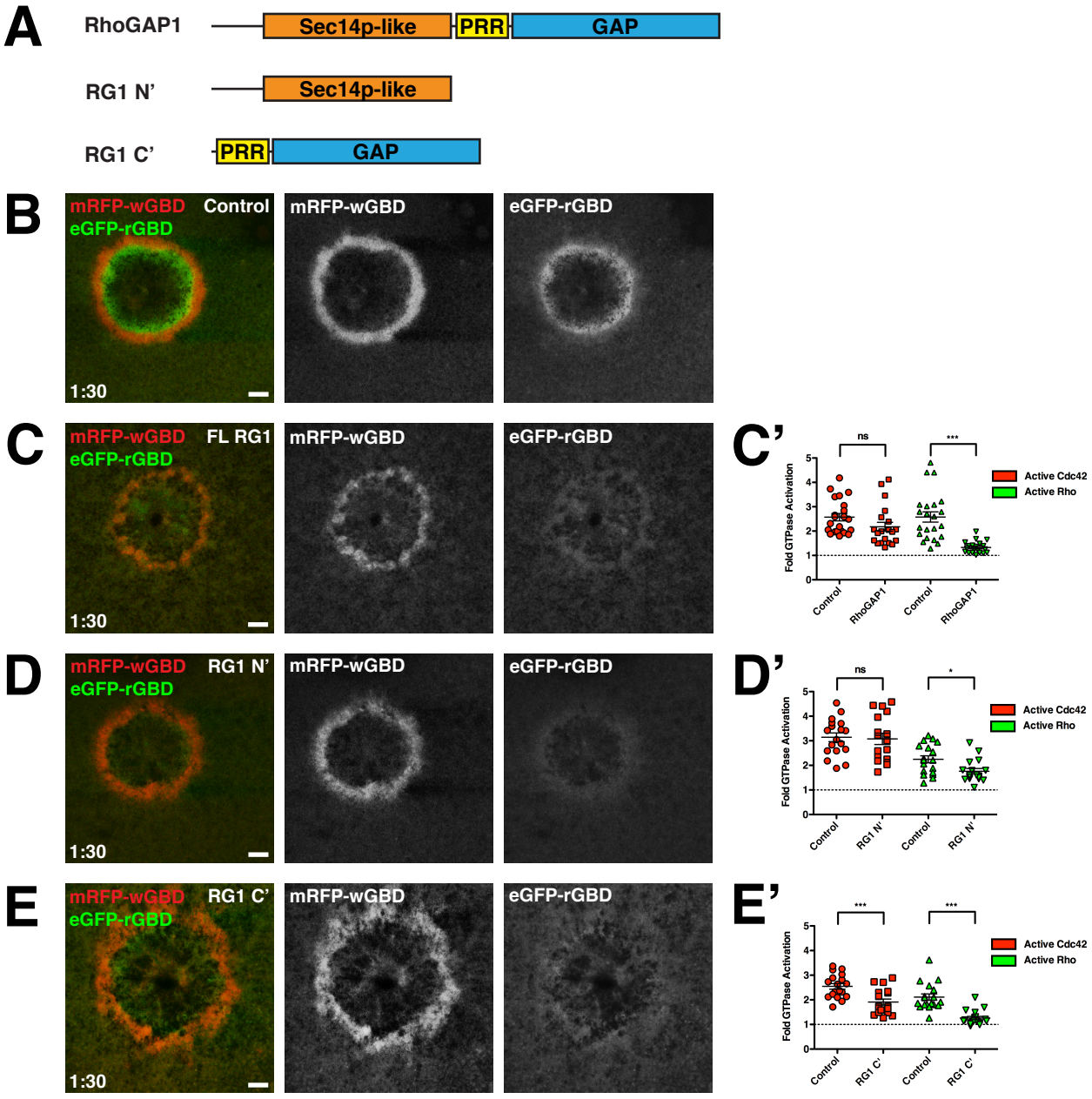
A
RhoGAP1
Sec14p-like
PRR
GAP
RG1 N'
Sec14p-like
RG1 C'
PRR
GAP
B
mRFP-wGBD
eGFP-rGBD
Control
1:30
mRFP-wGBD
eGFP-rGBD
C
mRFP-wGBD
eGFP-rGBD
FL RG1
1:30
mRFP-wGBD
eGFP-rGBD
C'
ns
***
Active Cdc42
Active Rho
Fold GTPase Activation
Control
RhoGAP1
Control
RhoGAP1
D
mRFP-wGBD
eGFP-rGBD
RG1 N'
1:30
mRFP-wGBD
eGFP-rGBD
D'
ns
*
Active Cdc42
Active Rho
Fold GTPase Activation
Control
RG1 N'
Control
RG1 N'
E
mRFP-wGBD
eGFP-rGBD
RG1 C'
1:30
mRFP-wGBD
eGFP-rGBD
E'
***
***
Active Cdc42
Active Rho
Fold GTPase Activation
Control
RG1 C'
Control
RG1 C'

**Figure 7**. Localization of RhoGAP1 to the wound array is directed by both its N- and C-termini and is not dependent on contributions from cytoskeletal-based motility. **(A)** A wounded oocyte coexpressing mRFP-wGBD and eGFP-RhoGAP1. **(A')** Line scan of (A) showing the relative positions of active Cdc42 and eGFP-RhoGAP1 with respect to the wound center, denoted by the "W". **(B)** A wounded oocyte coexpressing mRFP-wGBD and the eGFP-tagged N-terminus of RhoGAP1. **(B')** Line scan of (B) showing the relative positions of active Cdc42 and eGFP-RhoGAP1 N-terminus with respect to the wound center, denoted by the "W". **(C)** High magnification view of resting localization of the eGFP-tagged N-terminus of RhoGAP1, where it labels compartments of various sizes. **(D)** An oocyte expressing eGFP-RhoGAP1 N' was wounded, revealing loss of compartment labeling. See Movie 4. **(E)** A wounded oocyte coexpressing mRFP-wGBD and eGFP-RhoGAP1 N'. **(E')** Line scan of (E) showing the relative positions of active Cdc42 and eGFP-RhoGAP1 N' with respect to the wound center, denoted by the "W". **(F)** Cells expressing eGFP-RhoGAP1 were wounded after treatment with latrunculin B (center) or nocodazole (right) to assess the contributions of cortical flow and microtubule-based transport, respectively, to RhoGAP1 localization. Times in min:sec with t = 0:00 corresponding to moment of wounding. Scale bars: 10 μm; except (C), 2.5 μm.

# Figure 7

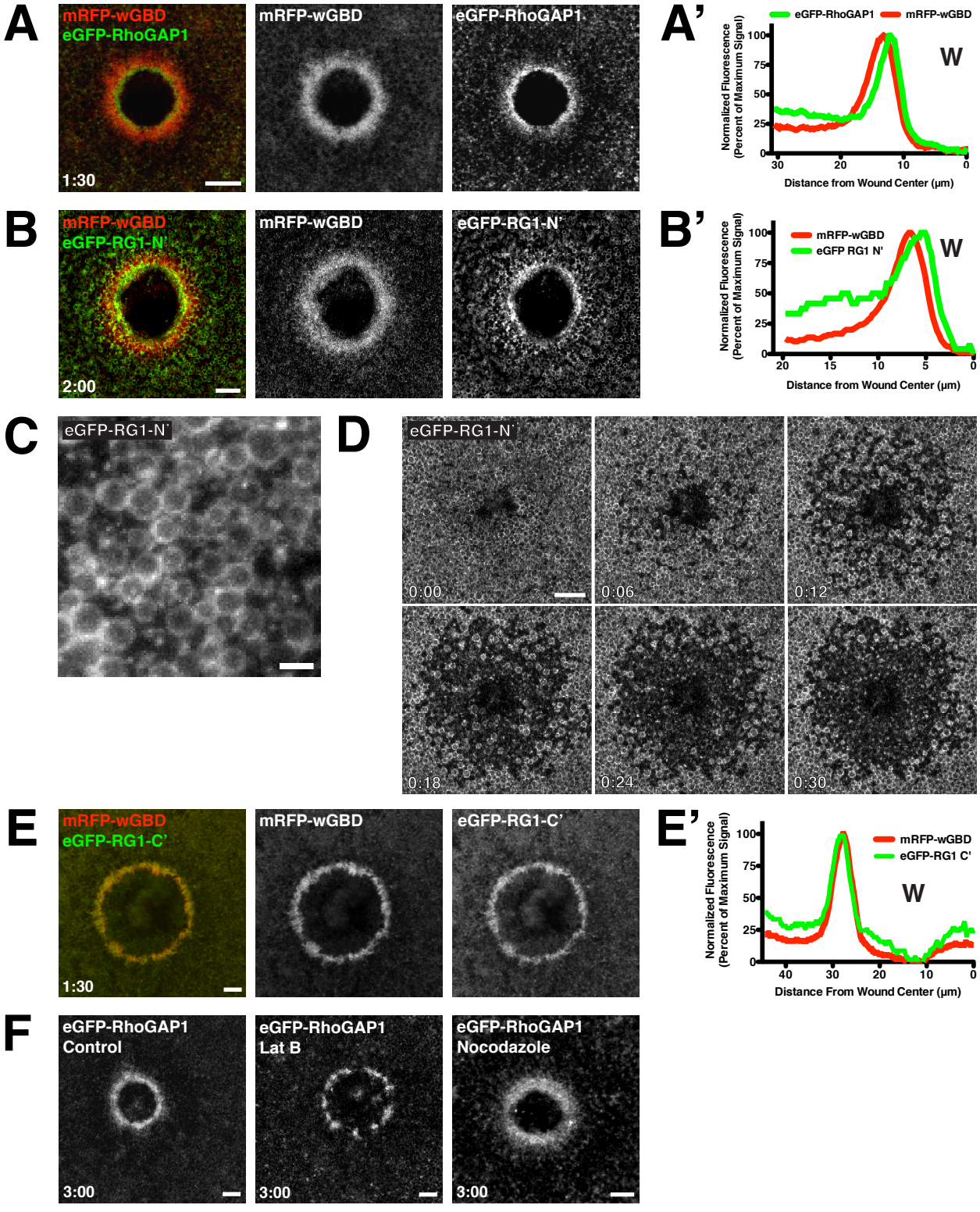
A
mRFP-wGBD
eGFP-RhoGAP1
1:30
mRFP-wGBD
eGFP-RhoGAP1
A'
eGFP-RhoGAP1
mRFP-wGBD
W
Normalized Fluorescence (Percent of Maximum Signal)
Distance from Wound Center (μm)
B
mRFP-wGBD
eGFP-RG1-N'
2:00
mRFP-wGBD
eGFP-RG1-N'
B'
mRFP-wGBD
eGFP RG1 N'
W
Normalized Fluorescence (Percent of Maximum Signal)
Distance from Wound Center (μm)
C
eGFP-RG1-N'
D
eGFP-RG1-N'
0:00
0:06
0:12
0:18
0:24
0:30
E
mRFP-wGBD
eGFP-RG1-C'
1:30
mRFP-wGBD
eGFP-RG1-C'
E'
mRFP-wGBD
eGFP-RG1 C'
W
Normalized Fluorescence (Percent of Maximum Signal)
Distance From Wound Center (μm)
F
eGFP-RhoGAP1
Control
3:00
eGFP-RhoGAP1
Lat B
3:00
eGFP-RhoGAP1
Nocodazole
3:00

**Figure 8**. Moderate Overexpression of RhoGAP1 Reduces Rho Zone Width. **(A)** A wounded oocyte expressing mRFP-wBGD and eGFP-rGBD, probes for active Cdc42 and active Rho, respectively. **(B)** A wounded oocyte expressing the probes for active Rho and Cdc42 (as in A) with moderate overexpression (1/10 the mRNA used in Figure 6) of RhoGAP1. **(C)** Quantification of GTPase zone intensity from control (A) and RhoGAP1 overexpressing (B) cells. **(D)** Quantification of GTPase zone width from control (A) and RhoGAP1 overexpressing (B) cells. Cdc42 zone width remains unaffected, whereas the zone Rho undergoes significant narrowing. For both (B) and (C), $n = 16$ for control cells, $n = 13$ for cells overexpressing RhoGAP1; from three independent experiments, $***p < 0.001$. Times in min:sec with t = 0:00 corresponding to moment of wounding. Scale bars, 10 μm.

# Figure 8

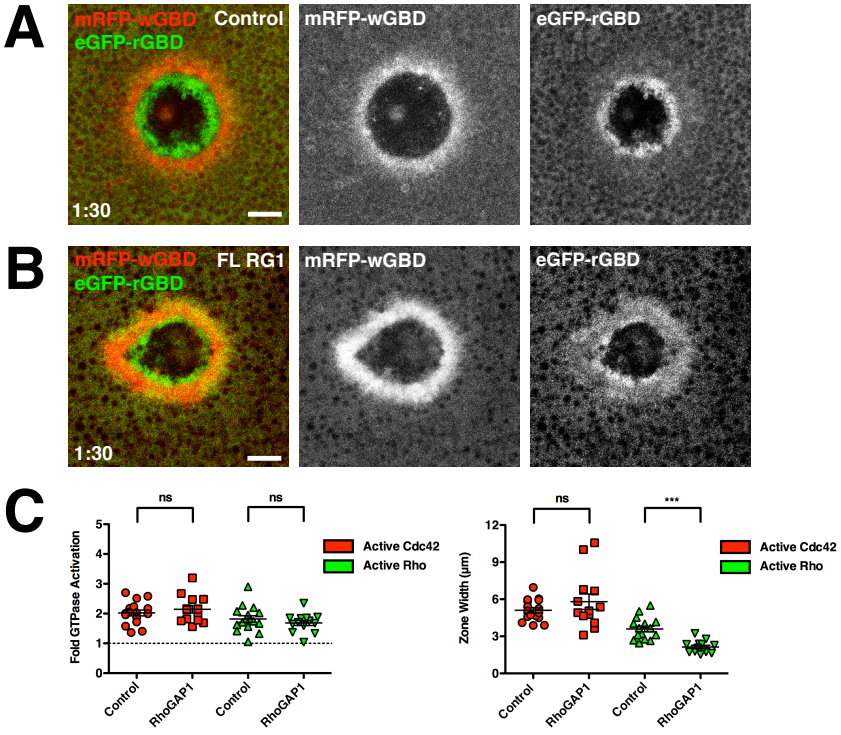
A
mRFP-wGBD
eGFP-rGBD
Control
1:30
mRFP-wGBD
eGFP-rGBD
B
mRFP-wGBD
eGFP-rGBD
FL RG1
1:30
mRFP-wGBD
eGFP-rGBD
C
Fold GTPase Activation
ns
ns
Active Cdc42
Active Rho
Control
RhoGAP1
Control
RhoGAP1
Zone Width (μm)
ns
***
Active Cdc42
Active Rho
Control
RhoGAP1
Control
RhoGAP1

**Movie Legends**

**Movie 1.** A wounded *Xenopus laevis* oocyte expressing eGFP-rGBD (green, probe for active Rho) and mRFP-wGBD (red, probe for active Cdc42)**.** From Figure 2A.

**Movie 2.** A wounded oocyte expressing mRFP-wGBD (red, probe for active Cdc42; also, center grayscale sequence) and eGFP-RhoGAP1 (green; also, right grayscale sequence)**.** From Figure 2C.

**Movie 3.** A wounded oocyte overexpressing RhoGAP1 co-injected with mRFP-wGBD (red, probe for active Cdc42; also, center grayscale sequence) and eGFP-rGBD (green, probe for active Rho; also, right grayscale sequence)**.** From Figure 6C.

**Movie 4.** A wounded oocyte expressing the eGFP-tagged N-terminus of RhoGAP1. From Figure 7D.

**Discussion**

*"When I see a bird that walks like a duck and swims like a duck and quacks like a duck, I call that bird a duck."* - James Whitcomb Riley

The results presented in this chapter describe a novel role for two RhoGAPs, RhoGAP1 and RhoGAP8, in promoting GTPase activity zone segregation during single-cell wound repair. RhoGAP1 and RhoGAP8 localize to wounds between the zones of active Rho and Cdc42, where they exert their activity against Rho, thereby constraining Rho activity at the wound edge. Consistent with this hypothesis, moderate overexpression of RhoGAP1 reduces Rho zone width. Together, these results build on recent advances in our understanding of single-cell pattern formation and its role in directing plasma membrane repair.

What is responsible for the distinct localization of RhoGAP1 and RhoGAP8 at wounds? Given the late timing (>30 seconds after GTPase activation; Figure 2F) and dispensability of the GAP domain for localization (Figure 7B), RhoGAP1 likely does not depend on Rho or Cdc42 activity per se for recruitment to wounds. This is in stark contrast to Abr, which requires, in addition to active Rho, the presence of both its GEF and GAP domains for proper localization and is recruited to wounds coincident with Rho activation (Vaughan *et al*., 2011). The generation and/or concentration of several lipid species at the wound edge (Vaughan *et al.,* 2014; this work, Chapter 4) and the reported ability of Sec14-like domains to associate with phospholipids (Saito *et al.*, 2007) suggest a potential mechanism for RhoGAP1 localization. While the location (i.e. between the zones of active Rho and Cdc42) of at least three wound-induced lipid domains could account for the localization pattern of RhoGAP1, the time at which they are recruited to wounds is not coincident with that of RhoGAP1 (Vaughan *et al.*, 2014); however, the lipids examined by

Vaughan *et al.* (2014) only represent a small fraction known species (Sud *et al.,* 2007), therefore other, yet unexamined lipids may be recruiting RhoGAP1 to wounds. Further, the striking cortical granule localization exhibited by the isolated RhoGAP1 N-terminus implies that a portion of the protein which can impart localization is normally masked, in agreement with reports that RhoGAP1 can exist in an autoinhibited state (Moskwa *et al.,* 2005; Zhou *et al.,* 2010). The mechanisms governing relaxation of this autoinhibition are currently unclear. Evidence of posttranslational modification at several sites within the Sec14-like domain of RhoGAP1 (Grimsrud, Carson, *et al.*, 2012) and the known involvement of protein kinases at the wound array (Vaughan *et al.,* 2014; Simon *et al.,* 2015) could provide an avenue through which to temporally regulate RhoGAP1 localization and function.

Endosomal localization of appears to be a conserved feature of RhoGAP1 (Sirokmány *et al.*, 2006, Clay and Halloran, 2013; de Madrid *et al.*, 2015). Subcellular location and function of endosomes are defined by specific Rab GTPases, their associated effector proteins, compartment lipid composition (Hutagalung and Novick, 2011). Given the foregoing results demonstrating localization of RhoGAP1 with Rab5 and Rab11 in resting oocytes, it is also likely that RhoGAP1 is also labelling Rab4, an additional regulator of the early/recycling endosomal pathway (Sönnichsen *et al.*, 2000) and known interactant of the *Drosophila* RhoGAP1 homologue (RhoGAP68f; de Madrid *et al.*, 2015). What role does RhoGAP1 play on endosomes? It is possible that RhoGAP1 localization is a vestige of its role in regulating Rho GTPase activity during endocytosis (Sirokmány *et al.*, 2006; Yu and Bement, 2007). Further, endosomal localization could serve as a subcortical pool of RhoGAP1 to be released as needed when damage occurs. This seems compelling based on the loss of compartment labeling by the isolated

N-terminus upon wounding (Figure 7C) and that RhoGAP1 is delivered, in part, to the intracellular bridge between dividing cells by Rab11-positive endosomes, where it aids in reducing F-actin so abscission can occur (Schiel *et al.*, 2012).

The putative activity of RhoGAP1 and RhoGAP8 at wounds is congruent with the GTPase flux model; instead of Rho GTPases being activated prior to a task and inactivated at the completion of task, the GTPases are continually cycling between active and inactive states (Bement *et al.*, 2006). In isolation, localized increases in GTPase activity are insufficient to produce tightly localized activity zones; rather, localized inactivation is required to limit diffusion of active GTPases away from the site of activation (Bement *et al.*, 2006). In our model of wound repair, Rho is activated by Abr throughout the Rho zone (Vaughan *et al.,* 2011) and preferentially inactivated at the trailing edge of the zone by the localized activities of RhoGAP1 and RhoGAP8. These presumptive activities agree with measurements of turnover of active Rho within the activity zone (Burkel *et al.,* 2012). While never directly compared, the time of RhoGAP1 recruitment to wounds (~75 s, Figure 2F) corresponds to the onset of Rho zone signal treadmilling. That is, in the first minute after wounding, turnover within the Rho zone lacks any spatial bias. However, beginning in the second minute after wounding, turnover occurs at a high rate towards the trailing edge of the zone, suggesting late contribution from a Rho inactivator. Finally, the region immediately exterior (with respect to the wound center) to the Rho zone is devoid of activity, even in cells with ectopic Rho activity (Vaughan *et al.,* 2011; my observations, not shown), suggesting the presence of a localized inactivator such as RhoGAP1.

Additionally, this model of GTPase activity zone regulation by RhoGAP1 and RhoGAP8 is remarkably similar to what is seen the cytokinetic ring. A stripe of active Rho along the

equatorial cortex dictates where the actomyosin ring will assemble and ingress to divide the two daughter cells (Takaishi *et al.,* 1995; Bement *et al.,* 2005). While localized Rho activity is dependent on a GEF, Ect2 (Tatsumoto *et al.*, 1999), it also requires the activity of a localized GAP, MgcRacGAP (Somers and Saint, 2003). Loss of MgcRacGAP in *X. laevis* embryonic epithelia widens the zone active Rho and causes oscillatory lateral displacement of Rho activity along the cortex (Miller and Bement, 2009; Breznau *et al.,* 2015). Further supporting the need for localized GAP activity for proper GTPase dynamics, loss of RhoGAP1 disrupts localized Rho activity and inhibits epithelial-to-mesenchymal transition in zebrafish (Clay and Halloran, 2013). Interesting, overexpression of MgcRacGAP reduces the width of the Rho zone (Miller and Bement, 2009), mirroring what is seen at wounds with RhoGAP1 overexpression (Figure 8, B and D).

Yet, even with the foregoing results, I cannot conclusively state that RhoGAP1 and RhoGAP8 are required for zone segregation. Ideally, I would examine loss-of-function phenotypes. Indeed, I made many attempts to do this. Surprisingly, overexpression of a mutant RhoGAP1 with a mutation in the GAP domain catalytic arginine (R283A, to abolish GAP activity) phenocopied wild-type RhoGAP1 overexpression (i.e. reduction of Rho activity, disorganization of the Cdc42 zone; not shown). The activity of the N-terminus against Rho (Figure 6) could be masking any dominant negative effect or a secondary arginine within the GAP domain active site could help RhoGAP1 retain activity against Rho (Leonard *et al.*, 1998). This unexpected activity of the N-terminus may be explained its ability to bind to both active and inactive forms of Rho (Zhou *et al.,* 2010), Therefore, it could be interfering with binding of Rho to either GEFs (i.e. Abr) or probes used to detect active Rho (eGFP-rGBD). An intriguing

possibility is that homo- or heterodimerization of RhoGAP1 (Low *et al.,* 2000; Shang *et al.,* 2003) could release autoinhibition of the endogenous protein, thereby increasing GAP activity. This last point has particular implications for any overexpression experiment, whether it be wild type or a putative dominant negative.

I also attempted RNAi (Lund *et al.*, 2011) to knockdown RhoGAP1 in oocytes. While this method was successful in reducing RhoGAP1 mRNA levels (data not shown), it was not able to appreciably reduce RhoGAP1 protein, likely due to inherently low protein turnover in resting oocytes and substantial maternal protein contributions (Peshkin *et al.*, 2015). Further, injection of concentrated α-RhoGAP1 into oocytes failed to elicit an effect; however, without *in vitro* analysis of this manipulation on GAP activity, conclusions as to the efficacy of this treatment or its potential results should be tempered. Finally, I attempted to locally eliminate RhoGAP1 using chromophore-assisted laser inhibition (Bulina *et al.,* 2006), but the laser power required for the procedure is sufficient to cause additional membrane damage. Future efforts will focus on analyzing mutations in Rho binding motifs (Zhou *et al.,* 2010) and dimerization domains (Low *et al.,* 2000) for dominant negative effects.

Even in light of previous work describing the actions of Abr (Vaughan *et al*., 2011), the discovery of RhoGAPs at the boundary between the Rho and Cdc42 activity zones is insufficient to fully explain wound-induced Rho GTPase pattern formation. At least two pieces of the puzzle remain to be solved: a small, “priming” pool of Rho activity is required to recruit Abr to the wound edge (Vaughan *et al*., 2011) and, to date, no regulators have been identified to explain activation of Cdc42 or its subsequent loss at the trailing edge of the zone (Burkel *et al*., 2012; Simon *et al*., 2013). With respect to the former, nucleotide exchange can be stimulated in Rho

GTPases in a GEF-independent manner under oxidizing conditions (Heo and Campbell, 2005). It is unclear whether cells experience sufficient oxidation from inrush of extracellular materials to trigger Rho activation, but seems to be a compelling line of inquiry. In regards to Cdc42 activation/inactivation, it would be most efficient to direct efforts towards characterizing Cdc42 GEFs that associate, either directly or indirectly, with F-actin (Orchard *et al.,* 2012). That is, the Cdc42 zone dynamics appear to be regulated at the level of activation (Burkel *et al.*, 2012), implying the outward extent of the Cdc42 zone may be dictated in a GAP-independent manner. Instead, it could be regulated by turnover of F-actin within the contractile ring, since stabilizing actin results in a broad zone of active Cdc42 (Burkel *et al.,* 2012). In this model, disassembly of the actin network at the trailing edge of the zone would cause GEF dissociation and subsequently define the outer extent of the positive feedback loop of Cdc42 activation (Simon *et al.,* 2013). Finally, in light of the colocalization of RhoGAP1 and RhoGAP8 at wounds (Figure 5C) and the general robustness of wound repair to perturbations (see Chapter 5), there are likely functional redundancies in the system.

Can the results presented here inform other studies of RhoGAP1 and RhoGAP8 function *in vivo*? RhoGAP1 has been implicated in regulating Rho GTPase activity in several forms of directed cell migration (Wang *et al.,* 2006, 2007; Yang *et al.,* 2007; Ahn *et al.*, 2012; Clay and Halloran, 2013). While most of the above studies examined the function of RhoGAP1 by measuring the bulk behavior (i.e. motility and total GTPase activity) of groups of cells, Clay and Halloran (2013) examined the effects of RhoGAP1 depletion on spatiotemporally-controlled Rho activity within single cells during epithelial-to-mesenchymal transition (EMT) in zebrafish. While total Rho activation during EMT was unaffected by loss of RhoGAP1, the distribution of

Rho activity was broadened and the ability of neural crest cells to leave the epithelium was hindered (Clay and Halloran, 2013). Thus, as with my results regarding single-cell wounds in *X. laevis* oocytes, it appears that EMT requires RhoGAP1 not for its ability regulate Rho activity per se, but rather to confine Rho activity to a particular region of a cell to promote productive actomyosin contraction.

## Methods

### *Plasmids*

*Xenopus laevis* RhoGAP1 and RhoGAP8 (accession numbers BC044312, BC072159) were obtained from Open Biosystems (IMAGE Clones 4681372, 4970462). RhoGAP1 was subcloned into pCS2+ using EcoRI/XbaI and into eGFP-, 3xGFP-, and GST-pCS2 using BglII and EcoRI. The N-terminus (a.a. 1-218) and C-terminus (a.a. 219-435) of RhoGAP1 were amplified via PCR and inserted into pCS2 using ClaI/EcoRI and ClaI/XbaI, respectively. Both N- and C-termini of RhoGAP1 were inserted into eGFP-pCS2 using BglII and EcoRI. RhoGAP8 was inserted into eGFP-, mCherry-, and GST-pCS2 using BspEI and XhoI. The probes for active GTPases, mRFP-wGBD and eGFP-rGBD, were generated as previously described (Sokac *et al.,* 2003; Benink and Bement, 2005). BFP-wGBD was constructed by excising mRFP from mRFP-wGBD using BamHI and BspEI and replacing it with BFP. mCherry-2xrGBD was constructed by adding an additional rGBD between the BspEI and XhoI sites of mCherry-rGBD. 3XeGFP-rGBD was generated by excising the rGBD from eGFP-rGBD with XhoI and XbaI and ligating into the corresponding sites into 3xeGFP-pCS2+. 6xHis- and GST- tagged version of RhoGAP1 and RhoGAP8 were generated for bacterial expression by excising full-length RhoGAPs from

their respective eGFP-tagged constructs using BglII and EcoRI and inserting it into the BamHI and EcoRI sites of pET28A and pGEX6P-1, respectively.

A FLAG sequence was added by PCR to the N-terminus of RhoGAP8, and the resultant FLAG-RhoGAP8 construct was subcloned into pFastBac1 using NotI and XhoI. 6xHis- and GST- tagged version of RhoGAP1 and RhoGAP8 were generated for expression in insect cells by amplifying the RhoGAPs from their respective pET28A and pGEX constructs and inserting them into the NotI and XhoI sites of pFastBac1. *Homo sapiens* Rab5 and Rab11 (accessions BC001267 and BC013348) and *Canis lupis* Rab7a (accession M35522) were obtained from Jon Audhya (University of Wisconsin-Madison) and subcloned into BFP-, eGFP-, and mCherry-pCS2 using BspEI and XhoI.

***Oocyte Acquisition and Preparation***

Ovarian tissue was procured from *Xenopus laevis* females via surgical procedures approved by the University of Wisconsin-Madison Institutional Animal Care and Use Committee. Tissue was stored in 1X Modified Barth's Solution (88 mM NaCl, 1 mM KCl, 2.4 mM $NaHCO_3$, 0.82 mM $MgSO_4$, 0.33 mM $NaNO_3$, 0.41 mM $CaCl_2$, 10 mM HEPES, pH 7.4; supplemented with 100 µg/mL gentamycin sulfate, 6 µg/mL tetracycline, 25 µg/mL ampicillin) at 16-18°C. Follicle cells were removed from oocytes by enzymatic digestion ([8 mg/mL Type I collagenase; Life Technologies] in 1X Barth's for 1 hour at 16-18°C on 60 rpm rotating plate) followed by manual dissociation with fine forceps. Defolliculated oocytes were stored in 1X Barth's (changed daily) until use.

***mRNA Preparation and Oocyte Microinjection***

Messenger RNAs were transcribed *in vitro* using the mMessage mMachine SP6 Transcription Kit (Life Technologies) followed by purification using the RNeasy Mini Kit (Qiagen) per manufacturer's instructions. 3XeGFP-rGBD mRNA was polyadenylated using the Poly(A) Polymerase Tailing Kit (Epicentre). Transcript size was verified on 1% agarose/ formaldehyde denaturing gels versus Millennium Marker (Life Technologies) molecular weight standard. Oocytes were injected while in 1X Barth's with a 40 nL injection volume. Cells were allowed to recover at least 30 minutes between injections. Probes for active GTPases were each injected a final needle concentration of 0.1-0.2 mg/mL. Untagged RhoGAP1 was injected 1.5-2.0 mg/mL (high concentration, Figure 6) or 0.15 mg/mL (low concentration, Figure 8). The N- and C-termini were injected at 0.75 mg/mL and 0.015-0.030 mg/mL, respectively. All fluorescently-tagged RhoGAP1/8 and Rab constructs were used at 0.25 mg/mL. Injected oocytes were stored in 1X Barth's at 16-18°C and mRNAs allowed to express for 24 hours prior to imaging. Fluorescent dextrans were added to the media, at 10-100 μM final concentration, 10-60 minutes prior to wounding. Nocodazole (20 μM) and latrunculin B (5 μM) were added to cell media at least 30 minutes prior to imaging.

***Amplification of RhoGAP1 and RhoGAP8 from cDNA***

Oocytes were lysed by manual disruption in homogenization buffer (0.3 M NaCl, 2% SDS, 50 mM Tris pH 7.5, 1 mM EDTA) using a Dounce homogenizer. Lysates were clarified by centrifugation, treated with DNaseI, and RNA was isolated by phenol/chloroform extraction.

cDNA was synthesized with M-MuLV Reverse Transcriptase (New England Biolabs) using an oligo-d(T) primer and 1 μg of template RNA. RhoGAP1 and RhoGAP8 were amplified by PCR using primers flanking their respective coding sequences.

***Fixation/Immunofluorescence***

Embryos were fixed overnight at room temperature in microtubule fixative solution (80 mM K-PIPES, 5 mM EGTA, 1 mM $MgCl_2$, 3.7% PFA, 0.25% glutaraldehyde, 0.2% Triton X-100, pH 7.4 ). Fixed embryos were dehydrated in a PBS:MeOH series and incubated overnight in 100% MeOH at -20°C. Cells were rehydrated with a MeOH:PBS series, quenched with 100 mM $NaBH_4$ in PBS for 4 hours, rinsed again with PBS, bisected and blocked overnight in TBSN + BSA (1X TBS, 0.1% NP-40, 5 mg/mL BSA) at 4°C. Anti-RhoGAP1 rabbit polyclonal antibodies were added (1:100 dilution) to samples and incubated overnight at 4°C. Cells were washed with TBSN + BSA overnight at 4°C, followed by an overnight incubation with secondary antibody (1:5000 Alexa Fluor 568 anti-rabbit secondary, Thermo Fisher Scientific). Unbound secondary was removed with an additional overnight round of washing with TBSN + BSA. Prior to imaging, embryos were dehydrated in a TBSN:MeOH series before clearing with Murry's Clear solution (2:1 benzyl alcohol, benzyl benzoate).

***Purification of Recombinant Proteins From Insect Cells***

RhoGAP1 and RhoGAP8 constructs in pFastBac1 were transformed into DH10Bac competent *E. coli* (Thermo Fisher Scientific) and positive clones selected by blue/white screening. Recombinant bacmids were isolated and subsequently transfected into *Sf9* cells using

Cellfectin II reagent (Thermo Fisher Scientific). Highly expressing clones were selected and virus amplified for two additional generations. *Sf9* cells (2.2 x $10^7$ per plate) were infected with high titer baculovirus and incubated for 72 hours at 27°C. Infected cells were collected by centrifugation (5 minutes at 500 x g) and stored at -80°C until protein purification.

Baculovirus-infected *Sf9* cell pellets expressing FLAG-RhoGAP8 were resuspended in 5 volumes of solubilization buffer (1X PBS pH 7.5, 1% v/v Triton X-100, 0.5 µg/mL Leupeptin, 0.5 µg/mL Aprotinin, 0.5 µg/mL Pepstatin A, 40 µg/mL PMSF, 100 µg/mL Benzamidine, 0.5 µg/mL E64) and incubated at 4°C for 1 hour with gentle end-over-end mixing. Lysates were clarified by centrifugation at 21,100 x g for 15 min. The supernatant was incubated in batch format with anti-FLAG-M2 agarose beads (Sigma) for 1 hour at 4°C prior to adding to a column. The column was washed with 3 x 10 column volumes of wash buffer (1X PBS pH 7.5, 40 µg/mL PMSF, 100 µg/mL benzamidine) and recombinant protein was eluted with 1M arginine, pH 4.4 into an equal volume of collection buffer (2X PBS pH 12.5, 80 µg/mL PMSF, 200 µg/mL benzamidine). Elution fractions were separated by SDS-PAGE (10% gel) followed by Coomassie Brilliant Blue staining. Desired fractions were pooled and concentrated using 10K MWCO Amicon Ultra-15 filters (Millipore). The buffer was exchanged in-filter to remove residual arginine to final conditions compatible with downstream applications (1X PBS, pH 7.5). The purity and concentration of the recombinant proteins were determined by SDS-PAGE and BCA Assay (Pierce), respectively. Aliquots were snap-frozen in liquid nitrogen prior to storage at -80°C.

Purification of GST-tagged RhoGAP1 and RhoGAP8 was performed as described above, with four notable exceptions: 1X TBS was utilized in place of PBS for lysis and wash steps,

glutathione-sepharose was used for purification, protein was eluted in a phosphate free buffer (50 mM Tris pH 8.0, 10 mM glutathione), and the eluate was exchanged in-filter with Hymann Buffer (50 mM HEPES pH 7.6, 100 mM KCl, 1 mM $MgCl_2$, 1 mM EDTA, 10% glycerol). Purification of 6xHis-RhoGAP8 from insect cells utilized Ni-NTA agarose (Qiagen) and a phosphate buffer (50 mM mM $NaH_2PO_4$, 300 mM NaCl, pH 8.0) supplemented with imidazole (10 mM for lysis, 20 mM for wash, 200 mM for elution).

***Purification of Recombinant Proteins from Bacteria***

RhoGAP1 and RhoGAP8 constructs in pGEX and pET28A were transformed into BL21-CodonPlus (DE3)-RIPL competent cells (Agilent). Overnight cultures were added to fresh LB (1:100) and grown until $OD_{600} \approx 0.5$ at 37°C. Expression was induced with 0.1 mM IPTG for 4 hours at 37°C. Cells were collected by centrifugation (10 min at 5000 x g) and stored at -80°C until protein purification. Purification of 6xHis- and GST-tagged proteins was performed as with insect-derived proteins, with only slight procedural modifications: lysozyme, DNaseI, and more intense centrifugation (20,000 x g for 30 minutes) were utilized to aid in cell disruption and lysate clarification.

***Antibody Production and Purification***

Antisera were obtained from rabbits (Covance) injected with either GST-RhoGAP1 or FLAG-RhoGAP8. Antibodies were purified using affinity chromatography against His-tagged variants of the respective antigens. 6xHis-RhoGAPs were dialyzed in coupling buffer (0.1M $NaHCO_3$, 0.5 M NaCl, pH 8.3) prior to addition to CNBr-Sepharose 4B (Sigma Aldrich). The

affinity resin washed with excess coupling buffer, blocked with 0.1 M Tris pH 8.0, and washed with alternating high salt washes (0.1 M NaOAc, 0.5 M NaCl, pH 4.0; 0.1 M Tris, 0.5 M NaCl, pH 8.8). Rabbit antiserum was diluted 1:1 with 20 mM Tris pH 7.5, passed through a 0.2 μm filter, and passed over the affinity column 5 times. Bound antibody was washed with 20 columns each of 20 mM Tris pH 7.5 and 20 mM Tris pH 7.5, 0.5 M NaCl prior to elution with 100 mM glycine pH 2.5. Elution fractions were collected into 1 M Tris pH 8.8 to neutralize solutions. Antibody concentration within each fraction was determined by BCA assay (Pierce). Desired fractions were pooled, concentrated using 30K MWCO Amicon Ultra-15 filters (Millipore), and stored at 4°C, supplemented with 0.02% sodium azide, until use.

***Cell Lysis and Western Blotting***

Oocytes were lysed by manual disruption in 10 mM imidazole, 50 mM KCl, 2.5 mM $MgCl_2$, 1 mM EGTA, 10 mM EDTA pH 7.8, 1 mM DTT, 0.5% (v/v) Triton X-100 with protease inhibitors (10 μM E-64, 4 mM pefabloc, 60 μg/ml chymostatin, 5 μg/ml leupeptin, 1 μg/ml pepstatin, 3.75 μg/ml aprotinin, 50 μM calpeptin, 50 μM ALLN). Lysates were centrifuged at 14,000 x g for 5 minutes followed by removal of the cytoplasmic fraction. Upon an additional centrifugation, clarified lysate was mixed with 6X Laemmli Buffer and stored at -80°C. Lysates were separated by SDS-PAGE (10% gels) and transferred onto nitrocellulose. Blots were blocked with 5% (w/v) milk in PBS for 1 hour at room temperature, incubated with primary antibody (1:500 rabbit α-RhoGAP1 or 1:500 rabbit α-RhoGAP8) overnight at 4°C, washed twice with excess 5% milk in PBS, and incubated with near-IR secondary antibodies (1:10,000 Alexa Fluor 680-conjugated α-rabbit IgG; Thermo Fisher Scientific) for 1 hour at room temperature.

Membranes were washed 4 times with PBST (1X PBS pH 7.5, 0.1% [v/v] Tween-20) prior to analysis with an Odyssey Fc Imaging System (LI-COR Biosystems).

***Image Acquisition and Data Analysis***

Confocal microscopy was performed using a Nikon Eclipse Ti inverted microscope with 60X oil objective (1.4 NA) and Prairie View confocal system (Bruker) or Axiovert 100M (Zeiss) inverted microscope with Lasersharp Confocal 1024 module (Bio-Rad) with a 63X oil objective (1.4 NA). Cells were wounded with illumination from a 488 nm uncaging laser (Bruker) or 440 nm dye laser setup pumped by a MicroPoint 337 nm nitrogen laser (Andor). Imaging data were processed using Fiji (Schindelin *et al.*, 2012) and Volocity (Perkin-Elmer). Line scans were made in Fiji by performing a radial reslice around the wound center and making an average intensity projection of the resultant stack. The fluorescence intensity along the line extending from the wound center was plotted in Prism 5 (GraphPad). Each channel was normalized such that the maximum and minimum fluorescence intensity values for that channel became 100% and 0%, respectively. GTPase activity was quantified in Fiji by determining ratio of mean gray value of activity zones to that of a region distal to the wound. Displayed activity zone widths represent the average length of eight lines drawn around each wound. Statistical analyses (two-tailed, unpaired t-tests) were performed in Prism 5, with statistical significance indicated according to the following: *, $p < 0.05$; **, $p < 0.01$; and ***, $p < 0.001$. Bars represent mean ± SEM.

***GTPase Activity Assays***

The catalytic activity of GST-tagged RhoGAP1/8 was assessed using the RhoGAP Activity Assay Kit (Cytoskeleton, Inc.) per manufacturer's instructions using GST-tagged RhoGAP1/8 at a final concentration of 2.6 μM. Phosphate release during the assay was measured by reading absorbance at 650 nm with a Spectromax Plus 384 microplate reader (Molecular Devices). The fold-increase in GTPase activity was calculated by comparing the amount of phosphate generated (as indicated by increased $OD_{650}$ of the detection reagent) in the +GAP wells versus that generated in the GTPase-alone wells.

# Chapter 3

Regulation of Rho GTPase Activity During Multicellular Wound Repair

**Abstract**

Tissues are continually challenged by both internal and external forces. Multicellular organisms display a remarkable capacity to repair otherwise life-threatening defects within damaged tissues. The conserved damage response integrates protrusive activity of cells at the leading edge of wounds in addition to collective cell migration towards the site of damage. These polarization events are thought to be regulated, in part, by the activity of the Rho family GTPases. Yet, precisely how the Rho GTPases themselves are directed to where they are needed is currently unclear. Here, we show two Rho GTPase regulators, RhoGAP1 and RhoGAP8, are recruited to the leading edge of wounds made in the epithelia of *Xenopus laevis* embryos, an area known to be a site of GTPase activation. Reduction of RhoGAP1 causes an increase in F-actin and leads to gastrulation failures. Further, translocation of RhoGAP1 and RhoGAP8 away from junctions of cells distal to the site of large wounds is coincident with corresponding increases in junctional F-actin and Rho activity. Together, these results suggest that RhoGAP1 and RhoGAP8 are involved in spatiotemporally regulating Rho GTPase activity in embryos, thereby allowing coordinated contractile events that allow for productive morphological changes, such as those utilized in multicellular wound repair.

**Introduction**

Multicellular organisms form barriers between themselves and their environment to maintain homeostasis and prevent infection from pathogens; these barriers can range from a single layer of cells (e.g., Xu and Chisholm, 2012) to highly specialized organs consisting of stratified layers of tissue (Gurtner *et al.,* 2008). Despite the morphological diversity of metazoan epithelia, they all share the capacity for repair (Martin and Lewis, 1992; Bement *et al.*, 1993; Bement *et al.*, 1999; Abreu-Blanco *et al.*, 2012; Xu and Chisholm, 2012). That is, mechanisms exist to repair defects inflicted under both physiological and pathological conditions (McNeil and Khakee, 1992). In humans, defects in multicellular wound repair are associated with a variety of disease states (reviewed in Sen *et al.,* 2009) and may represent life-threatening complications if left untreated (Ramsey *et al.,* 1999).

Despite the implications of multicellular wound repair for human health, much remains to be discovered about the underlying mechanisms driving resolution of tissue defects (Gurtner *et al.*, 2008; Sonnemann and Bement, 2011). In particular, although adult organisms possess a remarkable capacity to repair large wounds, healing is relatively slow and subject to the formation of scars; embryos and fetuses, on the other hand, are capable of quickly resolving defects and can do so without forming a scar (Ferguson and O'Kane, 2004). Elucidation of the cellular and molecular mechanisms underlying these differential responses represents a major focus of modern regenerative medicine (Borena *et al.,* 2015).

Many factors control the mechanisms utilized during multicellular wound repair, yet all responses appear to share two common characteristics: the formation of signaling gradients and subsequent cell polarization (Sonnemann and Bement, 2011). In complex systems, such as

mammalian skin, various growth factors are secreted to recruit specialized cells to perform functions ranging from pathogen clearance to remodeling of the extracellular matrix (Singer and Clark, 1999). In other contexts, such as simple epithelia, long range signaling by ions or nucleotides released from damaged cells may be sufficient to induce a response (e.g., Herrgen *et al*., 2014). Further, alterations in tension along a wounded epithelium may also contribute to damage-induced signaling (Takada *et al.,* 2014).

An additional conserved feature of multicellular wound repair is the polarization of "actomyosin", dynamically associated filamentous actin (F-actin) and the molecular motor myosin-2. An exceptional degree of cooperativity is exhibited between adjacent cells at the edge of wounds; despite being discontinuous (i.e. interrupted by cell-cell junctions), the actomyosin at the leading edge of wounds can behave as a single "purse-string" that contracts inward to close the wound (Martin and Lewis, 1992; Bement *et al.,* 1993). The purse-string is strengthened by enhanced cell-cell junctions to ensure efficient application of force and retain epithelial integrity (Safferling *et al.,* 2013). The purse-string model for wound repair is strikingly similar to the mechanisms utilized by *C. elegans* and *D. melanogaster* to close epithelial holes during embryonic development (Williams-Masson *et al.,* 1999; Jacinto *et al.,* 2002). Larger wounds may require the collective movement of tissue over underlying basement membranes or cell layers; these rearrangements often induce cells at the leading edge of the ingressing wound to extend actomyosin-rich protrusions at their leading edge (Bement *et al.,* 1993, Abreu-Blanco *et al.*, 2013, 2014).

The Rho family of GTPases are multifaceted regulators of actomyosin assembly and contraction (Jaffe and Hall, 2005) and have been implicated in directing the cytoskeletal

rearrangements needed to close multicellular wounds (Brock *et al.*, 1996; Clark *et al.,* 2009; Baek *et al*., 2010; Abreu-Blanco *et al.*, 2013, 2014). The Rho GTPases locally exert their activity due to contributions of guanine nucleotide exchange factors (GEFs) and GTPase activating proteins (GAPs), which are responsible for activating and inactivating Rho GTPases, respectively (Moon and Zheng, 2003; Rossman *et al.,* 2005). While the actions of GEFs and GAPs have been described in many other contexts (e.g., Vaughan *et al.*, 2011; Breznau *et al*., 2015), their involvement in regulating Rho GTPase activity during multicellular wound repair have yet to be characterized.

RhoGAP1 and RhoGAP8, two homologous RhoGAPs (Johnstone *et al.,* 2004), have been identified as regulators of single-cell wound repair (this work, Chapter 2) and directed cell migration (Wang *et al.,* 2006, 2007; Yang *et al.,* 2007; Ahn *et al.*, 2012; Clay and Halloran, 2013). In this study, I examined their roles in multicellular wound repair within the intact epithelia of *Xenopus laevis* embryos. I found that RhoGAP1 and RhoGAP8 are recruited to the leading edge of cells at the periphery of multicellular wounds, and that loss of RhoGAP1 results in both an increase in cytoplasmic F-actin and gastrulation defects. Together, these results suggest RhoGAP1 and RhoGAP8 are responsible for spatially regulating Rho GTPase activity to perform complex cellular movements. Further, I identified wound-induced long-range signaling gradients that may help pattern larger, tissue-wide responses to damage.

## Results

### *Localization of RhoGAP1 and RhoGAP8 in Intact Epithelia*

Based on my previous results characterizing RhoGAP1 and RhoGAP8 in *X. laevis* oocytes (Chapter 2), I sought to determine whether they were involved in multicellular wound repair. Using a polyclonal antibody against *X. laevis* RhoGAP1 (see Methods, also Chapter 2), I detected endogenous RhoGAP1 protein in embryos (Figure 1A). Further, the antibody was used to examine the localization of endogenous RhoGAP1. In *X. laevis* embryonic epithelial cells, RhoGAP1 was found to be punctate (Figure 1A), similar to its localization in other contexts/ systems (Sirokmány *et al.*, 2006; Clay and Halloran, 2013; de Madrid *et al.*, 2015; this work, Chapter 2), yet was often concentrated along the cell periphery, staining both cell-cell junctions (Figure 1B, center images) and apical surfaces (Figure 1B, left). No appreciable signal was detected in the secondary-only control (Figure 1B, right).

To monitor the dynamics of RhoGAP1 within an intact epithelium, mRNA for 3XeGFP-RhoGAP1 (Figure 1B) was injected into *X. laevis* embryos. A 3XeGFP-tag was utilized to achieve sufficient signal-to-noise to monitor protein localization without causing an overexpression phenotype. 3XeGFP-RhoGAP1 localization was punctate (Figure 1D), congruent with localization of endogenous RhoGAP1 (Figure 1B). However, in contrast to the results obtained with immunofluorescence, live imaging showed that 3XeGFP-RhoGAP1 was often concentrated in cell vertices (see Discussion). Further, many cells possessed 3XeGFP-RhoGAP1-labeled compartments that moved rapidly throughout the cell (Figure 1D'; Movie 1). For example, Figure 1D shows a labeled compartment that was tracked for over 3 minutes (Figure 1D', yellow line; Movie 1); the persistence of movement in one direction suggests the

movement is directed along microtubules. This rapid movement of RhoGAP1-labeled compartments was not seen in oocytes (Chapter 2), nor has it been described in any other system (e.g. Sirokmány *et al.*, 2006; Clay and Halloran, 2013; de Madrid *et al.*, 2015). Similar results were obtained when observing the localization of 3XeGFP-RhoGAP8 (Figure 1E), i.e. it localized to cell-cell boundaries and vertices (highlighted by mCherry-UtrCH, a probe for F-actin; Burkel *et al.,* 2007).

The punctate localization of 3XeGFP-RhoGAP1 is consistent with reports of its recruitment to endosomes (Sirokmány *et al.*, 2006; de Madrid *et al.*, 2015; this work, Chapter 2). To test this possibility, I examined embryos co-expressing 3XeGFP-RhoGAP1 and fluorescently-tagged Rab GTPase constructs, markers of the endosomal pathway (reviewed in Hutagalung and Novick, 2011). 3XeGFP-RhoGAP1 labeled Rab5-positive endosomes (early endosomes; Figure 2A), but failed to colocalize with Rab7-positive endosomes (late endosomes; Figure 2B). Closer examination of cells expressing 3xeGFP-RhoGAP1 and BFP-Rab5 (Figure 2C) revealed many 3XeGFP-RhoGAP1-positive compartments (arrowheads) did not appear to be early endosomes (i.e. they lacked BFP-Rab5 labeling). Rab11, a marker of recycling endosomes, was found to label many 3XeGFP-RhoGAP1-positive compartments (arrowheads). Together, the results suggest RhoGAP1 labels the same compartments (i.e. early and recycling endosomes) in both oocytes and embryos of *X. laevis*.

***RhoGAP1 and RhoGAP8 are Recruited to Multicellular Purse Strings***

To assess the role of RhoGAP1 and RhoGAP8 in multicellular wound repair, small laser-induced wounds were made in embryonic epithelial cells. In an embryo expressing 3XeGFP-

RhoGAP1 (Figure 3A), wounding of a single cell (denoted by the "W") induced the accumulation of 3XeGFP-RhoGAP1 at the side facing the damage in adjacent cells (arrow). The localization of 3XeGFP-RhoGAP1 at the wound resembles the actomyosin purse string used to close wounds (Martin and Lewis, 1992; Bement *et al.*, 1993; 1999; Clark *et al*., 2009) or extrude apoptotic cells (Rosenblatt *et al.*, 2001) in simple epithelia.

RhoGAP8 also appears to be involved in multicellular wound repair, as revealed by wounds made in embryos (Figure 3B; Movie 2) expressing 3XeGFP-RhoGAP8 and mCherry-CAAX (a plasma membrane marker; Yu and Bement, 2007). 3XeGFP-RhoGAP8 was robustly recruited to the leading edge of ingressing cells (arrowheads). Additionally, the width of the cell-cell junctions facing the wound edge do not change appreciably prior to recruitment of 3XeGFP-RhoGAP8 (Figure 3B; Movie 2), suggesting the accumulation of 3XeGFP-RhoGAP8 at the wound represents *de novo* recruitment rather than concentration of protein already associated with, or directly adjacent to, the plasma membrane. A kymograph (Figure 3B') generated from the line depicted in Figure 3B ($t$ = 0:00) revealed additional features of the wound response; namely, the wound edge retracts (as evident by leftward junctional movement; likely due to cortical tension), wound closure involves elongation of cells at the wound edge, and 3XeGFP-RhoGAP8 recruitment (arrow) occurs prior to ingression of the cell edge. Together, the above results demonstrating recruitment of 3XeGFP-tagged RhoGAP1 and RhoGAP8 to multicellular wound suggests their involvement in regulating Rho GTPase-mediated assembly of an actomyosin purse string.

***Loss of RhoGAP1 Leads to Increased Intracellular F-actin and Gastrulation Defects***

I sought to determine the roles of RhoGAP1 and RhoGAP8 in multicellular wound repair by examining loss-of-function phenotypes. Until recently, attempts to utilize RNAi in *Xenopus* had been largely unsuccessful. However, Lund *et al.* (2011) discovered that *Xenopus* eggs and early embryos lack a functional version of a critical component of the RNAi pathway, Argonaut 2 (Ago2). While exogenous expression of human Ago2 is sufficient to permit RNAi in *Xenopus* (i.e. degrade endogenous mRNAs; Lund *et al.*, 2011), its ability to subsequently deplete protein had never been demonstrated. I tested the ability of siRNA to knockdown endogenous RhoGAP1 by injecting Ago2 mRNA in addition to a non-specific (NS) siRNA or a pool of siRNAs targeting RhoGAP1 (see Methods) into embryos. Western blots of embryo lysates using the RhoGAP1 antibody demonstrated that siRNA is indeed capable of depleting endogenous RhoGAP1 by 24 hours post-fertilization (Figure 4A). To examine whether RhoGAP1 depletion lead to any gross phenotypes, Ago2/siRNA-injected cells were fixed and stained with Alexa Fluor 488-phalloidin, a probe for F-actin (Barak and Yocum, 1981). Both low- and high-magnification views of RhoGAP1 knockdown embryos (Figure 4B) reveal increased cytoplasmic F-actin when compared to control (NS) embryos. An increase in F-actin is consistent with loss of Rho GTPase regulators, as both Rho and Cdc42 are upstream regulators of actin polymerization (e.g., Watanabe *et al.,* 1997; Rohatgi *et al.,* 1999). In addition to increases in F-actin, RhoGAP1 knockdown consistently caused gastrulation defects (data not shown).

To confirm the above results from siRNA-mediated knockdown of RhoGAP1, I injected a translation-blocking morpholino designed to target RhoGAP1 mRNA. The RhoGAP1-targeting morpholino reduced expression of RhoGAP1 in a dose-dependent manner (Figure 4C). Similar

to RNA-mediated knockdown, the morpholino caused gastrulation defects (Figure 4D); in comparison to uninjected embryos (Figure 4D, left) or those injected with a control morpholino (Figure 4D, center), embryos injected with the RhoGAP1 morpholino failed to successfully close their blastopores, allowing loss of yolk-rich, unpigmented cells out of the embryo to be trapped between the embryo and the vitelline envelope (arrow). Similarly, loss of the *D. melanogaster* RhoGAP1 homolog, RhoGAP68F, has also been shown to cause gastrulation defects (Sanny *et al.*, 2006).

***Wounding Alters RhoGAP1 Localization in Cells Distal to the Site of Damage***

The foregoing results with respect to the wound response (Figure 3) represent relatively small wounds, typically encompassing only a couple of cells. While I intended to create small wounds, laser wounding occasionally produced large defects, likely dependent on local conditions (e.g. pigment granule density and/or tension of the epithelium). While the healing of these wounds was generally difficult to assess due to material exuded from the wound interfering with imaging (Figure 3B; not shown), occasionally such wounds revealed a novel behavior of RhoGAP1. Figure 5 shows one such example: In an embryo expressing 3XeGFP-RhoGAP1 and mCherry-UtrCH, a larger than desired wound was created. Surprisingly, I observed an increased cytoplasmic signal of 3xGFP-RhoGAP1 in cells distal to the site of damage (arrowhead, Figure 5A). A higher magnification view of the boxed region in Figure 5A revealed a dynamic redistribution of 3XeGFP-RhoGAP1 (Figure 5B; Movie 3). Specifically, 3XeGFP-RhoGAP1 signal pre-wounding ($t$ = 0:00) was concentrated at cell-cell junctions (arrowhead; see also Figure 1) with the occasional labeling of cytoplasmic structures, likely endosomes (Figure 2;

also, Chapter 2). However, as early as 30 s after wounding, 3XeGFP-RhoGAP1 redistributes to the cytoplasm and cell-cell junctions are devoid signal by *t* = 1:00 , before returning to a punctate, cytoplasmic localization, in spite of the fact that these cells are many micrometers away from the wound site and do not appear to be damaged in any way. Coincident with RhoGAP1 redistribution was an increase in junctional F-actin. This same signal redistribution was seen with RhoGAP8 and is not merely an artifact due of changes in focal plane (data not shown). Further, small wounds fail to elicit this striking redistribution (Figure 3), suggesting despite their similarities, wounds of different size invoke measurably different responses (see also Clark *et al.,* 2009).

***Large Wounds Produce Long-Range Signals***

To determine whether the increases in junctional F-actin in cells distal to the site of large wounds were coincident with long range, upstream signaling events, embryos were injected with a eGFP-rGBD, a probe for active Rho (Benink and Bement, 2005). Upon wounding, cell-cell junctions of cells distal to the site of injury (denoted by the "W") show Rho activation, as evident by an increase in eGFP-rGBD signal. Enlargement of the boxed area in Figure 6A, showing enrichment of Active Rho on cell-cell junctions (Figure 6A'). Activation is delayed (*t* = 0:30) from the initial wounding event, remains elevated for 1 minute, before receding back to basal levels (*t* =2:30 and not shown).

In *X. laevis* early blastomeres, junctional increases of GTPase activity are associated with corresponding increases of intracellular calcium (Clark *et al.*, 2009). To assess this possibility later in development, embryos were injected with GCaMP5G, a circularly-permuted eGFP

construct which exhibits increased fluorescence when in bound to calcium ions (Akerboom *et al.,* 2012). Upon wounding, intracellular calcium was elevated in cells proximal to wounds (Figure 6B, *t* = 0:03; Movie 4), before spreading to neighboring cells in a wave propagating away from the site of damage. Except for in the cells directly adjacent to the wounds, calcium elevation was transient, i.e. intracellular concentrations declined back to near pre-wounding levels fairly rapidly (Figure 6B, *t* = 1:12 - 1:35; Movie 4). This form of long-range calcium signaling is not seen in early blastomeres (Clark *et al.*, 2009); thus, changes in cell-cell interactions or expressed signaling receptors during development alter the response to long-range signals.

**Figure 1.** RhoGAP1 and RhoGAP8 label dynamic, punctate structures in *Xenopus laevis* embryonic epithelial cells. **(A)** Immunoblotting *X. laevis* embryo lysates with a RhoGAP1 polyclonal antibody confirms RhoGAP1 expression. **(B)** Antibody staining of fixed embryos reveals RhoGAP1 localization is punctate (absent in secondary-only control, far right image) and enriched along apical and junctional surfaces. **(C)** Domain structure of 3XeGFP-RhoGAP1, containing a N-terminal Sec14-like domain, a central proline rich region, and a C-terminal GAP domain. **(D)** A still from a 4D movie of an embryo expressing 3XeGFP-RhoGAP1, confirming punctate localization seen by immunofluorescence. **(D')** Enlargement of area highlighted by box in (D). A single 3xGFP-RhoGAP1-labelled vesicle moves (track highlighted in yellow) across a cell over the course of several minutes. See Movie 1. **(E)** Domain structure of 3XxeGFP-RhoGAP8, similar to that of RhoGAP1. **(F)** An embryo expressing 3XeGFP-RhoGAP8 and mCherry-Utr, a probe for F-actin. 3XeGFP-RhoGAP8 localization has a punctate localization similar to that of RhoGAP1. Times in min:sec. Scale bars: (B)(D)(E) 10 μm, (D') 2.5 μm.

# Figure 1

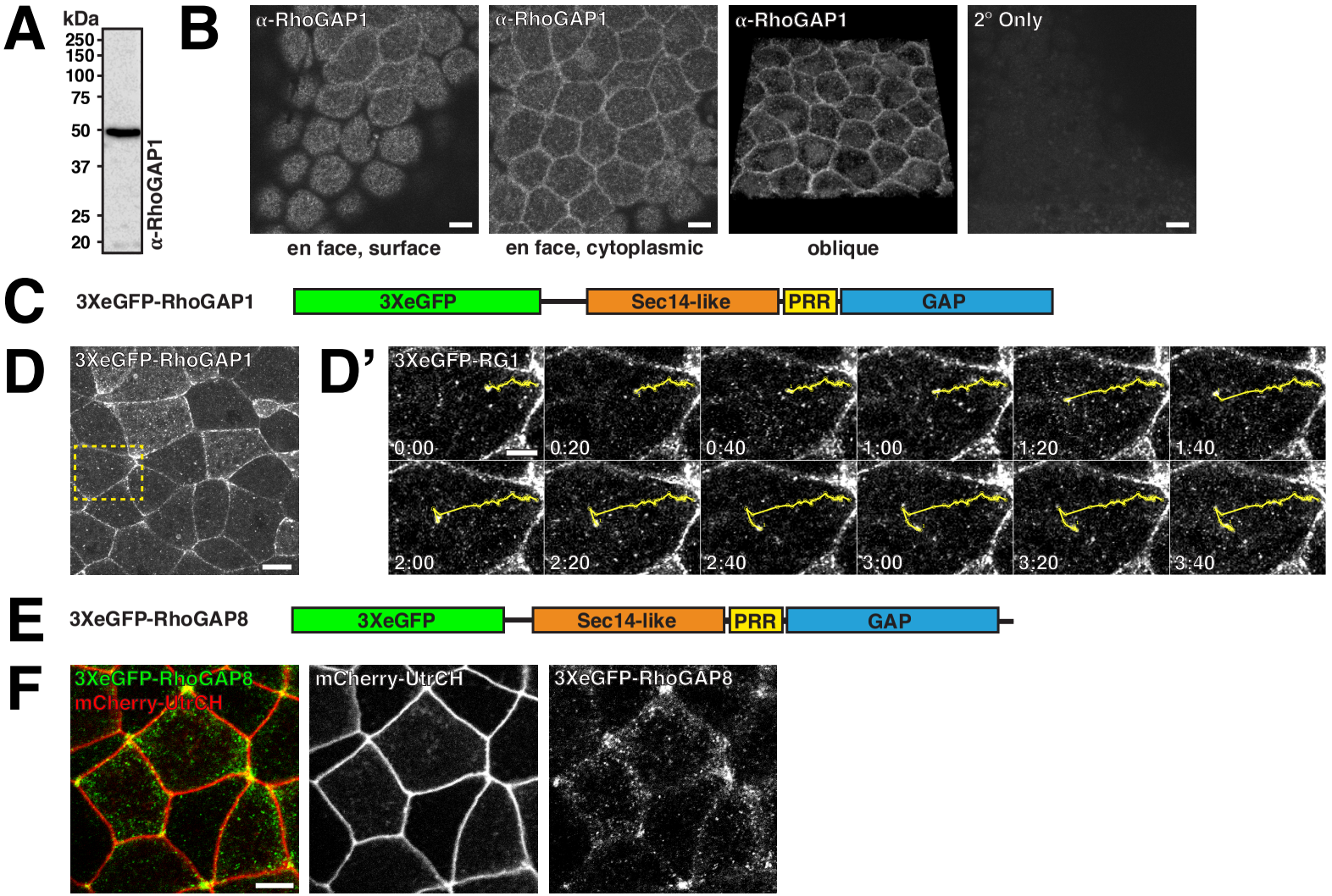
A
kDa
250
150
100
75
50
37
25
20
α-RhoGAP1
B
α-RhoGAP1
α-RhoGAP1
α-RhoGAP1
2° Only
en face, surface
en face, cytoplasmic
oblique
C
3XeGFP-RhoGAP1
3XeGFP
Sec14-like
PRR
GAP
D
3XeGFP-RhoGAP1
D'
3XeGFP-RG1
0:00
0:20
0:40
1:00
1:20
1:40
2:00
2:20
2:40
3:00
3:20
3:40
E
3XeGFP-RhoGAP8
3XeGFP
Sec14-like
PRR
GAP
F
3XeGFP-RhoGAP8
mCherry-UtrCH
mCherry-UtrCH
3XeGFP-RhoGAP8

**Figure 2.** RhoGAP1 labels early and recycling endosomes. **(A)** An embryo expressing 3XeGFP-RhoGAP1 and mCherry-Rab5, a marker of early endosomes. Arrowheads denote structures labeled by both constructs. **(B)** An embryo expressing 3XeGFP-RhoGAP1 and mCherry-Rab7, a marker of late endosomes. **(C)** An embryo expressing 3XeGFP-RhoGAP1, BFP-Rab5, and mCherry-Rab7. Several structures labeled by 3XeGFP-RhoGAP1 are not labeled by BFP-Rab5 (arrows). **(D)** An embryo expressing 3XeGFP-RhoGAP1, mCherry-Rab7, and BFP-Rab11, a marker of recycling endosomes. Many structures are labeled with both 3XeGFP-RhoGAP1 and BFP-Rab11 (double arrows). Scale bars: (A-B) 5 μm, (C-D) 2.5 μm,

# Figure 2

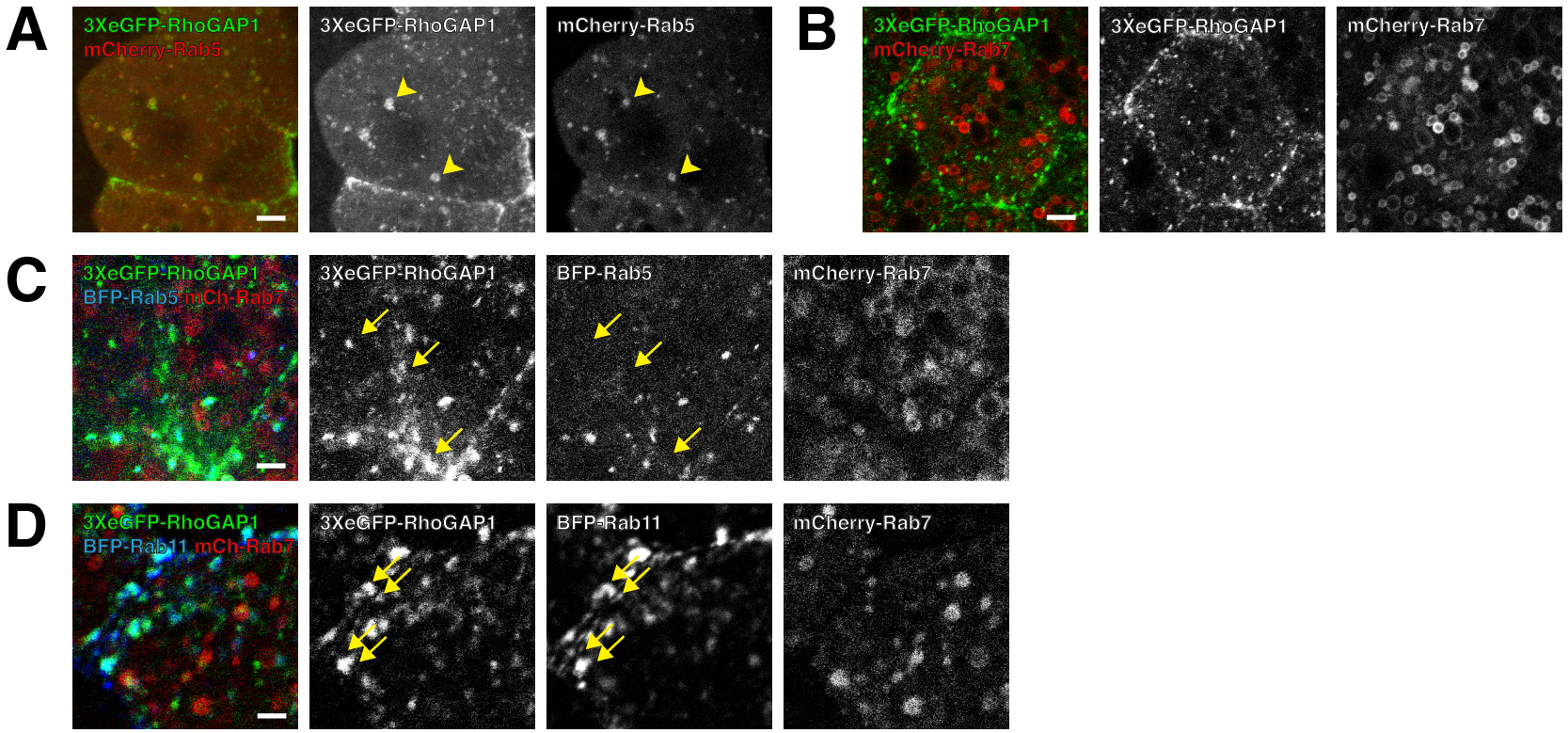
A
3XeGFP-RhoGAP1
mCherry-Rab5
3XeGFP-RhoGAP1
mCherry-Rab5
B
3XeGFP-RhoGAP1
mCherry-Rab7
3XeGFP-RhoGAP1
mCherry-Rab7
C
3XeGFP-RhoGAP1
BFP-Rab5 mCh-Rab7
3XeGFP-RhoGAP1
BFP-Rab5
mCherry-Rab7
D
3XeGFP-RhoGAP1
BFP-Rab11 mCh-Rab7
3XeGFP-RhoGAP1
BFP-Rab11
mCherry-Rab7

**Figure 3**. RhoGAP1 and RhoGAP8 localize to wound-induced multicellular purse strings. **(A)** A single cell within an embryo expressing 3XeGFP-RhoGAP1 was wounded (wound site indicated by "W"). 3XeGFP-RhoGAP1 localized to the leading edge of the ingressing wound (arrowhead). **(B)** An embryo expressing 3XeGFP-RhoGAP8 and mCherry-CAAX (a plasma membrane marker) was wounded. 3X-eGFP-RhoGAP8 localized to the leading edge of the ingressing wound (arrowheads). Wound site indicated by "W". See Movie 2. (**B'**) A kymograph from the line seen at *t* = 0:00 in (B), revealing enrichment of RhoGAP1 (arrowhead) at the leading edge of the wound. Times in min:sec with t = 0:00 corresponding to moment of wounding. Scale bars, 20 μm.

# Figure 3

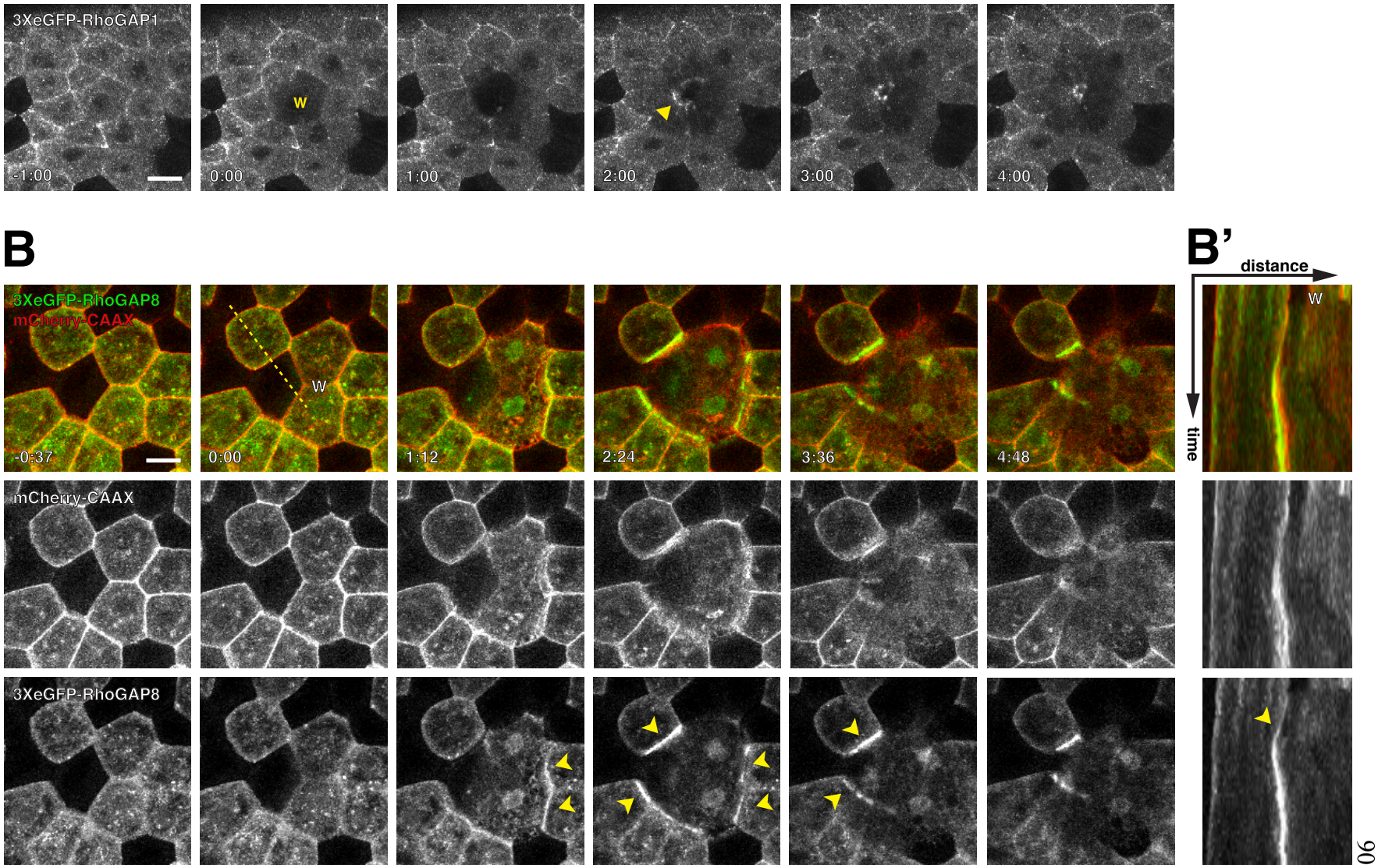
A
3XeGFP-RhoGAP1
W
-1:00
0:00
1:00
2:00
3:00
4:00
B
B'
3XeGFP-RhoGAP8
mCherry-CAAX
W
-0:37
0:00
1:12
2:24
3:36
4:48
distance
time
mCherry-CAAX
3XeGFP-RhoGAP8

**Figure 4.** Knockdown of RhoGAP1 results in increased F-actin and gastrulation defects. **(A)** Expression of RhoGAP1 in uninjected embryos or those injected with human Ago2 plus non-specific (NS) siRNA or siRNAs against RhoGAP1. **(B)** Low (left, 25X objective) and high (right, 63X objective) magnification views of fixed *Xenopus* embryos stained with Alexa Fluor 488-phalloidin 24 hrs after injection with human Ago2 plus non-specific (NS) siRNA or siRNAs against RhoGAP1. **(C)** Expression of RhoGAP1 in embryos injected with control morpholino or a morpholino against RhoGAP1. **(D)** Low magnification views of uninjected embryos or those injected with morpholinos (control or RhoGAP1) showing gastrulation defects in embryos with RhoGAP1 knockdown. Arrow denotes material that should have been contained by the closing blastopore, but was exuded and became trapped between the epithelium and vitelline envelope. Scale bars: (B) left, 50 μm; right, 20 μm (D) 1 mm.

# Figure 4

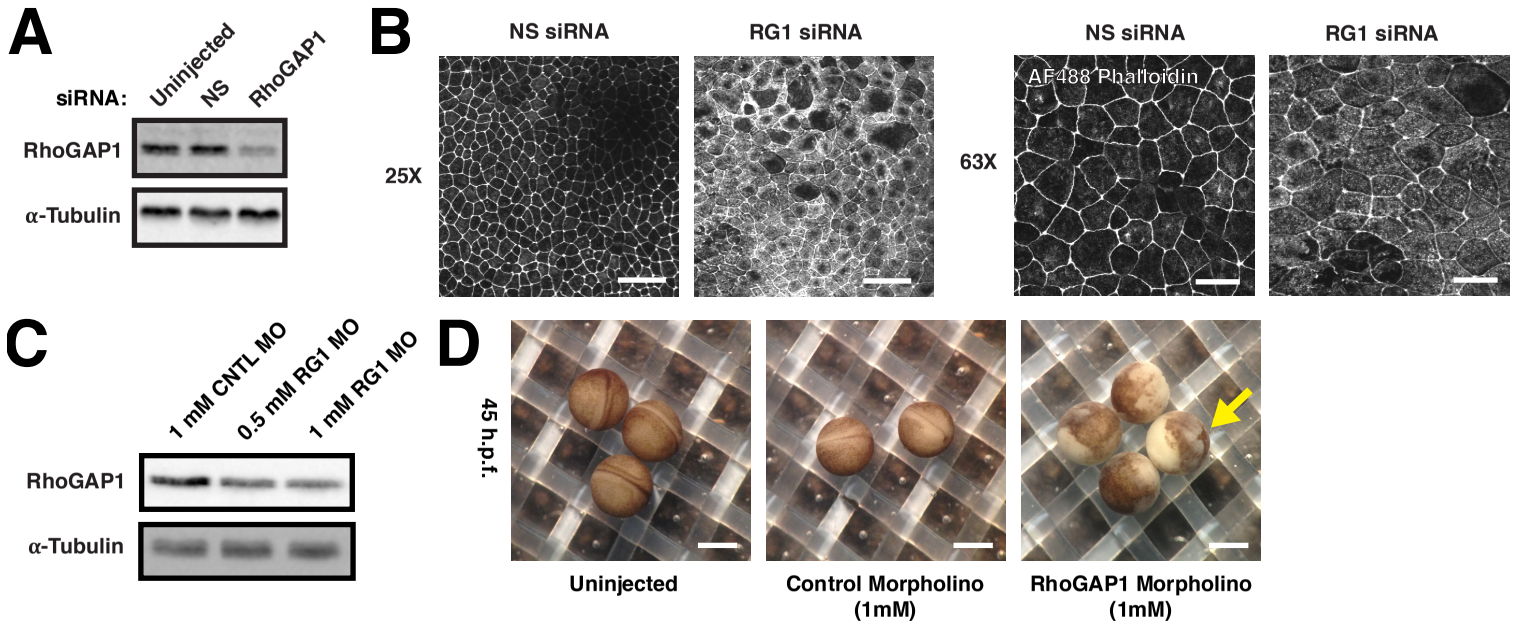
A
siRNA:
Uninjected
NS
RhoGAP1
RhoGAP1
α-Tubulin
B
NS siRNA
RG1 siRNA
NS siRNA
RG1 siRNA
25X
63X
AF488 Phalloidin
C
1 mM CNTL MO
0.5 mM RG1 MO
1 mM RG1 MO
RhoGAP1
α-Tubulin
D
45 h.p.f.
Uninjected
Control Morpholino (1mM)
RhoGAP1 Morpholino (1mM)

**Figure 5.** Wounding causes redistribution of RhoGAP1 in cells distal to wound site. **(A)** Multiple cells within an epithelium expressing 3XeGFP-RhoGAP1 and mCherry-UtrCH were wounded. Wounding resulted in increased cytoplasmic 3XeGFP-RhoGAP1 signal in cells distal to the wound (arrowheads). Wound site indicated by "W". **(B)** Enlargement of the boxed area in (A), showing loss of junctional 3XeGFP-RhoGAP1 localization (arrowheads) and a corresponding increase in junctional F-actin (double arrows). Wound is out of the frame, direction indicated by the arrow. See Movie 3. Times in min:sec with t = 0:00 corresponding to moment of wounding. Scale bars: (A) 20 μm, (B) 10 μm.

Figure 5

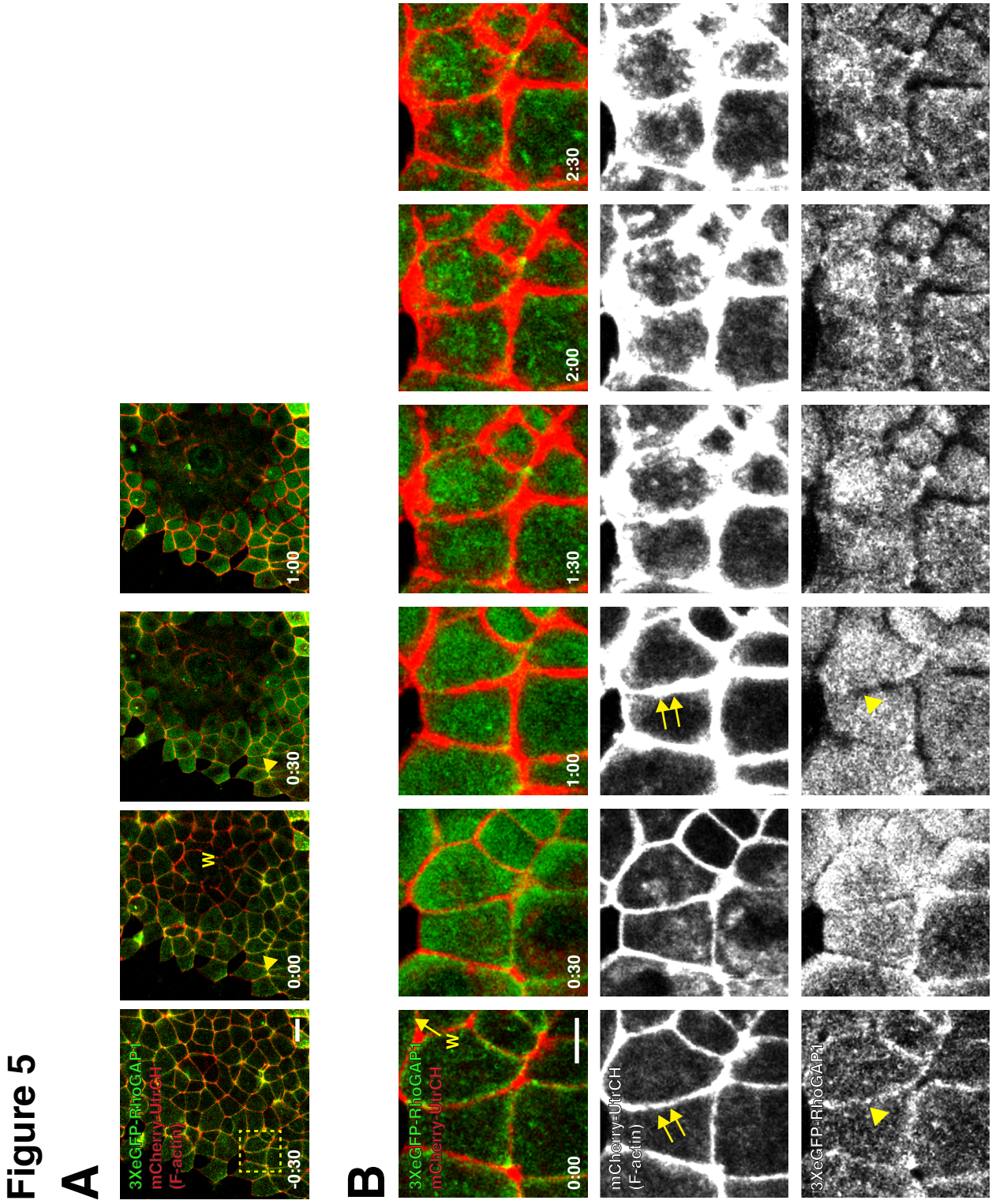
A
3XeGFP-RhoGAP1
mCherry-UtrCH
(F-actin)
-0:30
0:00
0:30
1:00
w
B
3XeGFP-RhoGAP1
mCherry-UtrCH
w
0:00
0:30
1:00
1:30
2:00
2:30
mCherry-UtrCH
(F-actin)
3XeGFP-RhoGAP1

**Figure 6.** Wound-induced signals are transduced far from the site of damage in embryonic epithelia. **(A)** A large wound was made in an embryo expressing eGFP-rGBD, a probe for active Rho. Wounding induces junctional eGFP-rGBD signal (arrowhead). **(A')** Enlargement of the boxed area from (A), highlighting the Rho activation at cell-cell junctions. Wound is out of the frame, direction indicated by the arrow. **(B)** An embryo expressing GCaMP5G (a probe for $Ca^{2+}$) was wounded, revealing the presence of a calcium wave that is translated across the surface of the embryo. See Movie 4. Times in min:sec with t = 0:00 corresponding to moment of wounding. Scale bars: (A) 20 μm, (A') 5 μm, (B) 100 μm.

# Figure 6

## A

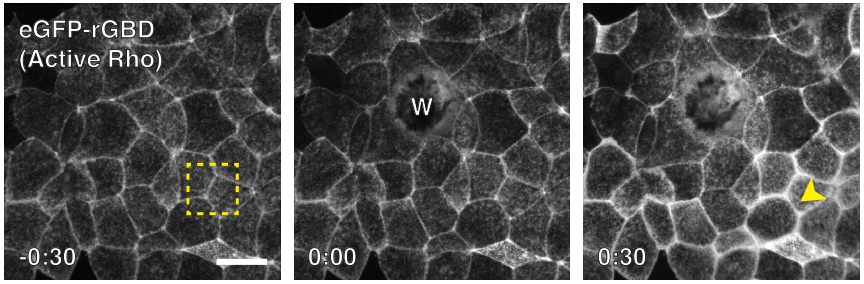
eGFP-rGBD
(Active Rho)
W
-0:30
0:00
0:30

## A’

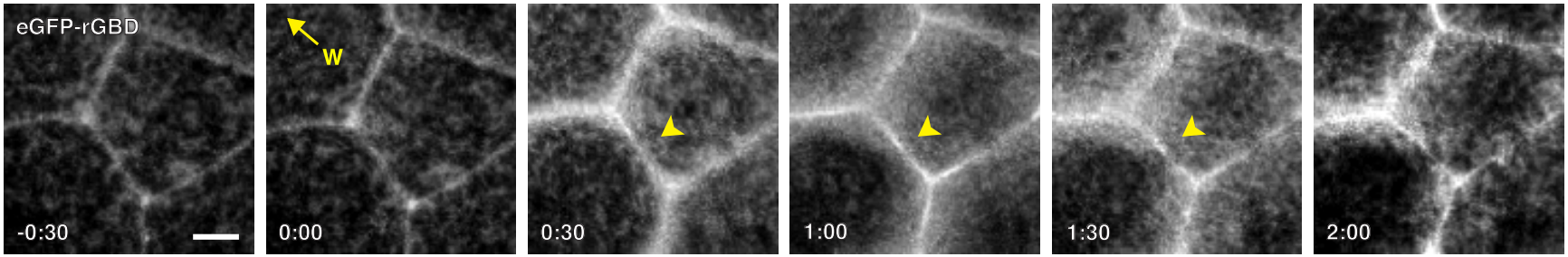
eGFP-rGBD
W
-0:30
0:00
0:30
1:00
1:30
2:00

## B

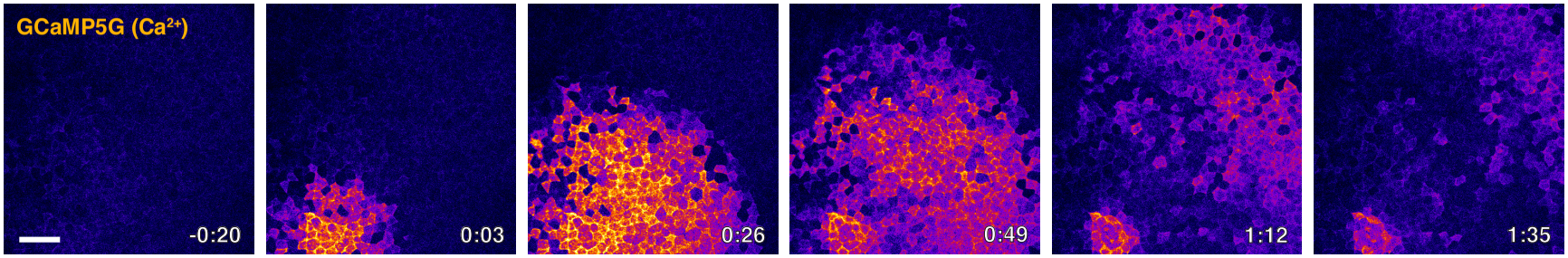
GCaMP5G (Ca2+)
-0:20
0:03
0:26
0:49
1:12
1:35

**Movie Legends**

**Movie 1.** A resting *Xenopus laevis* embryo expressing 3XeGFP-RhoGAP1, highlighting the dynamic nature of RhoGAP1-labelled vesicles (left), of which a conspicuous example was tracked (right, yellow line). From Figure 1D'.

**Movie 2.** A wounded embryo expressing mCherry-CAAX (red, probe for the plasma membrane; also, center grayscale sequence) and 3XeGFP-RhoGAP8 (green; also, right grayscale sequence)**.** From Figure 3B.

**Movie 3.** A wounded embryo expressing mCherry-UtrCH (red, probe for F-actin; also, center grayscale sequence) and 3XeGFP-RhoGAP1 (green; also, right grayscale sequence)**.** Wound is out of frame, towards the upper right-hand corner of the image sequence. From Figure 5B.

**Movie 4.** A wounded embryo expressing GCaMP5G (a probe for $Ca^{2+}$, pseudocolored with "Fire" LUT). From Figure 6B.

**Discussion**

This work describes the behavior and potential role of two Rho GTPase regulators, RhoGAP1 and RhoGAP8, in directing GTPase activity during the cell polarization events needed to reestablish epithelial integrity during multicellular wound repair. As was seen with single-cell wounds in oocytes (this work, Chapter 2), RhoGAP1 and RhoGAP8 are recruited to multicellular wounds (Figure 3). Additionally, I demonstrate that initially broad signals generated by damage (Figure 6) are later focused at the wound edge, a behavior also seen in single-cell wounds (this work, Chapter 4). Together, these results reveal striking parallels between single- and multicellular wound repair, a point of previous speculation (Clark et al., 2009; Sonneman and Bement, 2011).

The endosomal localization of RhoGAP1 and RhoGAP8 in *Xenopus laevis* embryonic epithelia mirrors what is seen oocytes (this work, Chapter 2). However, unlike in oocytes, many of the 3XeGFP-RhoGAP1- and 3XeGFP-RhoGAP8-positive endosomes are highly dynamic (Figure 1D'). While vesicles occasionally deviated from the cell periphery (e.g., Figure 1D'), it has not been determined whether they represent true movements into the cell center or movements along the apical cortex. Further, it remains unclear what, if any, purpose the junctional localization may serve in regulating Rho GTPase activity, although RhoGAP1 and RhoGAP8 may represent a sub-cortical pool of of GTPase regulators that can be delivered to areas of increased Rho GTPase activity when needed. For example, both Rho and Rac have been shown to be transiently elevated at cell-cell junctions of *X. laevis* embryonic epithelia, where they precede localized accumulation of actomyosin and likely serve a as measure to resist opposing tensile forces within the tissue (Reyes *et al.,* 2014; Breznau *et al.,* 2015). Further,

RhoGAP1 and RhoGAP8 localize to cell vertices (Figure 1), areas known to both be under high tension and recruit Rho GTPases (e.g., Oda *et al.,* 2014).

However, RhoGAP1 and RhoGAP8 do not appear to localize to the ingressing cytokinetic furrow (data not shown; Shiel *et al.,* 2015), a region with high Rho activity (Bement *et al.,* 2005). This discrepancy raises a more general question about localization of GTPase regulators; that is, why do two GAPs (MgcRacGAP and RhoGAP1) with the same *in vivo* substrate specificity (Rho) not get recruited to the same structure? As with *X. laevis* oocytes (this work, Chapter 2), it may not be the active GTPases per se that are directing localization of RhoGAP1 and RhoGAP8; rather, they may be directed to a specific location by an additional signaling event (e.g., lipid synthesis and/or accumulation, localization of a binding partner, or posttranslational modification). The diverse array of protein domains associated with GEF (DH/PH) and GAP domains (Moon and Zheng, 2003; Rossman *et al.,* 2005) provides cells with many means with which to control the spatiotemporal localization of Rho GTPase regulators; adding an additional layer of regulation beyond substrate recognition onto GEFs and GAPs may prevent spurious initiation of signaling feedback loops.

Laser ablation of single cells within epithelia induced accumulation of RhoGAP1 (Figure 3A) and RhoGAP8 (Figure 3, B and B') at the leading edge of the ingressing purse string. The delayed accumulation of RhoGAP1 and RhoGAP8 to multicellular wounds ($t \approx 2{:}00$; Figure 3, A and B) suggests they are recruited after activation of Rho ($t \approx 0{:}30$; Figure 6, A and A'; Clark *et al.,* 2009), consistent with observations from single-cell wounds in *X. laevis* oocytes (this work, Chapter 2). While never directly compared, the pattern with which Rho and Cdc42 are activated at multicellular wounds appears to match that seen in oocytes (Benink and Bement, 2005), i.e. a

zone of active Rho circumscribed by a zone of active Cdc42. It remains unclear whether RhoGAP1 and RhoGAP8 retain their positioning between the zones of active GTPases (this work, Chapter 2) in the context of multicellular repair.

Many of the signals released (i.e. growth factors, cytokines) to organize long-term collective cell migration to repair large wounds have been elucidated (reviewed in Gurtner *et al.,* 2008; Sonnemann and Bement, 2011), yet it remains unclear which factors are necessary and sufficient to initiate the response. Specifically, which factors are responsible for polarizing the cells at the leading edge of the wound? Wounding of an epithelium causes a nearly immediate rise in intracellular calcium in cells surrounding the site of damage that emanates outward in a wave-like manner (Figure 6B; see also Antunes *et al.*, 2012; Yoo *et al.*, 2012; Soto *et al*., 2013). Both release of ATP from wounded cells (Cavin-Nares *et al.,* 2012; Herrgen *et al.,* 2014; Takada *et al.,* 2014) and tension changes (Takada *et al.,* 2014; Xu and Chisholm, 2011) have been implicated in causing calcium increases within surrounding cells. However, few causal links exist between calcium signaling and Rho GTPase activation in wound repair (reviewed in Moe *et al.,* 2015), so the mechanism by which organisms convert a calcium wave to directed cell migration remains to be determined. Further, what dictates the cellular response to calcium increase? That is, while cells hundreds of microns away from the wound experience an elevation in calcium (Figure 6B), it is only a transient response. Only the cells adjacent (i.e. within a couple cell radii) to the wound edge display a prolonged calcium signal (Figure 6B; Antunes *et al.*, 2012), suggesting that additional, as of yet unidentified, players or processes are involved in shaping distinct cellular and molecular patterns at wounds from initially broad signals (Sonnemann and Bement, 2011).

The increases in F-actin and gastrulation failure seen in RhoGAP1 knockdown embryos are likely linked. Gastrulation consists of highly-complex, parallel events that involve both coordinated migration and changes in cell shape (reviewed in Solinca-Krezel, 2005). One of these coordinated events, epiboly, involves expansion of the incipient ectoderm over the surface of the developing embryo; the cell layer that facilitates epiboly is formed by radial intercalation of several cell layers into one (Keller, 1980). RhoGAP1 was found to be required for organizing Rho activity in a cellular behavior similar to intercalation, epithelial-to-mesenchymal transition (Clay and Halloran, 2013). Thus, the RhoGAP1 knockdown phenotype may represent to a disorganization of the contractile response; that is, single cells are unable to polarize to perform complex shape changes and movements, whereas increased contractility may inhibit migration of tissues.

With respect to cell polarization events initiated to close small wounds, it may be helpful to draw comparisons to the mechanisms utilized by cells within an epithelial sheet to extrude their neighbors in response to density-dependent and apoptotic cues (Eisenhoffer *et al.,* 2012; Rosenblatt *et al.,* 2001). Both wound repair and cell extrusion employ an actomyosin purse string to ingress inward (Clark *et al.,* 2009, Rosenblatt *et al.,* 2001; Marchiando *et al.,* 2011) and require contributions from functional cell-cell junctions (Marchiando *et al.,* 2011; Safferling *et al.,* 2013; Lubkov and Bar-Sagi, 2014; Michael *et al.*, 2016). Cell extrusion is initiated by production of sphingosine-1-phosphate (S1P) by the apoptotic cell that is recognized by receptors in surrounding cells (Gu *et al.,* 2011). Binding of S1P to its receptors induces translocation of p115RhoGEF to the plasma membrane (Meyer *et al.*, 2008; Slattum *et al.,* 2009) and subsequent polarization of the actomyosin cytoskeleton (Slattum *et al.,* 2009; Gu *et al.,*

2011). It remains unclear whether wounded cells are able to produce S1P prior to death, but given reports that S1P accelerates cutaneous wound repair (Kawanabe *et al.,* 2007; Serriere-Lanneau *et al.,* 2007) it, or a similar factor, are promising candidates to explain the polarization of cells at the wound edge.

Perhaps the most striking observation of this work is the redistribution of RhoGAP1 and RhoGAP8 away from cell-cell junctions in cells distal to large, multicellular wounds (Figure 5). While there are many reports of recruitment of Rho regulators to the plasma membrane in response to stimulus (e.g., Meyer *et al.,* 2008; Vaughan *et al.,* 2011; Ponik *et al.,* 2013; this work, Chapter 2), there are no, to the best of my knowledge, examples of stimulus-induced translocation away from a membranous compartment. Along with the observed increases in both junctional Rho activity (Figure 6, A and A') and F-actin polymerization (Figure 5), I propose the following model to explain this phenomenon: wound-induced increases in intracellular calcium (acting directly or indirectly; Figure 6B) cause translocation of RhoGAP1 and RhoGAP8 away from cell-cell junctions (Figure 5). No longer under the influence of localized GAPs, Rho activity (Figure 6, A and A') and subsequent signaling to downstream effectors are increased. The activated Rho effectors promote actomyosin assembly and contraction (Figure 5) to resist tensional changes in the epithelium due to wounding and the subsequent migration of the epithelium. Several key concepts within this model need elucidation; namely, the factor(s) responsible for, and consequences of, RhoGAP1 and RhoGAP8 redistribution. These, and obtaining increased temporal resolution to confirm the order of the proposed sequence events at junctions, represent promising avenues of investigation for future study.

## Methods

### *Plasmids*

*Xenopus laevis* RhoGAP1 and RhoGAP8 (accession numbers BC044312, BC072159) were obtained from Open Biosystems (IMAGE Clones 4681372, 4970462). RhoGAP1 was subcloned into 3XeGFP-pCS2 using BglII and EcoRI. RhoGAP8 was inserted into 3XeGFP-pCS2 with BspEI and XhoI. 6xHis- and GST- tagged versions of RhoGAP1 were generated for bacterial expression by excising full-length RhoGAP1 from 3XeGFP-RhoGAP1 using BglII and EcoRI and inserting it into the BamHI and EcoRI sites of pET28A and pGEX6P-1, respectively. The probes for active Rho (eGFP-rGBD), F-actin (mCherry-Utr), and the plasma membrane (mCherry-CAAX) were generated as previously described (Benink and Bement, 2005; Burkel *et al.,* 2007; Yu and Bement, 2007). pCMV-GCaMP5G was a gift from Douglas Kim & Loren Looger (Addgene plasmid # 31788). GCaMP5G was subcloned into pCS2+ with BamHI and EcoRI. The plasmid for human Ago2 (Liu *et al.,* 2004) was a gift from from Mike Sheets (University of Wisconsin-Madison). *Homo sapiens* Rab5 and Rab11 (accessions BC001267 and BC013348) and *Canis lupis* Rab7a (accession M35522) were obtained from Jon Audhya (University of Wisconsin-Madison) and subcloned into BFP-, eGFP-, and mCherry-pCS2 using BspEI and XhoI.

### *Embryo Acquisition*

Eggs and testes of *Xenopus laevis* were acquired via procedures approved by the University of Wisconsin-Madison Institutional Animal Care and Use Committee. Eggs from primed (human chorionic gonadotropin; MP Biomedicals) females were collected into a small

petri dish containing 1X Marc's Modified Ringer (MMR; 100 mM NaCl, 2 mM KCl, 2 mM $CaCl_2$, 1 mM $MgCl_2$, 5 mM HEPES, pH 7.4). Media was removed to 10% of its original volume to which a small portion of testis was added and manually teased apart with fine forceps. Nanopure water was added to dilute the remaining media to 0.1X MMR. Embryos were dejellied by brief cysteine treatment (2% w/v in 0.1X MMR, pH 7.8) followed by extensive washing with 1X and 0.1X MMR. Embryos were stored in 0.1X MMR at 16-18°C until injection.

***mRNA Preparation and Embryo Microinjection***

Messenger RNAs were transcribed *in vitro* using the mMessage mMachine SP6 Transcription Kit (Life Technologies) followed by purification using the RNeasy Mini Kit (Qiagen) per manufacturer's instructions. Ago2 mRNA was polyadenylated using the Poly(A) Polymerase Tailing Kit (Epicentre). Transcript size was verified on 1% agarose/formaldehyde denaturing gels versus Millennium Marker (Life Technologies) molecular weight standard. Embryos were injected at the two-cell stage with 5 nL of mRNA into each blastomere while immersed in 0.1X MMR supplemented with 5% Ficoll.

mRNAs for 3XeGFP-tagged RhoGAP1 and RhoGAP8 were injected at a needle concentration of 10 μg/mL. mCherry-UtrCH, mCherry-CAAX, eGFP-rGBD, and the fluorescently-tagged Rabs were injected at 20 μg/mL. GCaMP5G was injected at 63 μg/mL. Ago2-poly(A) mRNA was injected at 200 μg/mL. siRNA duplexes (5'-CAUCAAGGCCCUUUACAUUdTdT-3', 5'-CAUCCAACGAUGUUCAUCAdTdT-3', 5'-GAGGUUCAGCAGAAGUAUAdTdT-3', 5'-CUCUGAGCACUGAGGGAAUdTdT-3'; only sense strand shown; Sigma) were pooled and injected at 50 μM. Both the standard control (5'-

CCTCTTACCTCAGTTACAATTTATA-3') and RhoGAP1 morpholino (5'-GGTCGGACGC**CAT**CCTGATCTCT-3', start codon in bold) were used at 1 mM. Injected embryos were stored in 0.1X MMR at 16-18°C and mRNAs allowed to express for 24 hours prior to imaging or lysis.

***Fixation/Immunofluorescence***

Embryos were fixed overnight at room temperature in microtubule fixative solution (80 mM K-PIPES, 5 mM EGTA, 1 mM $MgCl_2$, 3.7% PFA, 0.25% glutaraldehyde, 0.2% Triton X-100, pH 7.4 ). Fixed embryos were dehydrated in a PBS:MeOH series and incubated overnight in 100% MeOH at -20°C. Cells were rehydrated with a MeOH:PBS series, quenched with 100 mM $NaBH_4$ in PBS for 4 hours, rinsed again with PBS, bisected and blocked overnight in TBSN + BSA (1X TBS, 0.1% NP-40, 5 mg/mL BSA) at 4°C. Anti-RhoGAP1 rabbit polyclonal antibodies were added (1:100 dilution) to samples and incubated overnight at 4°C. Cells were washed with TBSN + BSA overnight at 4°C, followed by an overnight incubation with secondary antibody (1:5000 Alexa Fluor 568 anti-rabbit secondary, Thermo Fisher Scientific). Unbound secondary was removed with an additional overnight round of washing with TBSN + BSA. Prior to imaging, embryos were dehydrated in a TBSN:MeOH series before clearing with Murry's Clear solution (2:1 benzyl alcohol, benzyl benzoate).

To visualize F-actin, embryos were fixed in "Superfix" buffer (100 mM KCl, 3 mM MgCl, 10 mM HEPES, 150 mM sucrose, 3.7% PFA, 10% DMSO, 2 mM EGTA, 0.1% glutaraldehyde, 0.02% Triton-X-100, pH 7.4) overnight at room temperature. Cells were washed 3 times in PBS, quenched with 100 mM $NaBH_4$ in PBS for 4 hours, rinsed again with PBS,

bisected, and blocked overnight in TBSN+ BSA (1X TBS, 0.1% NP-40, 5 mg/mL BSA) at 4°C. Alexa Fluor 488-Phalloidin (Thermo Fisher Scientific) was added to samples (1:100 dilution) and incubated overnight at 4°C. Unbound Alexa Fluor 488-Phalloidin was removed with an additional overnight round of washing with TBSN + BSA.

***Purification of Recombinant Proteins from Bacteria***

pGEX and pET28A constructs containing RhoGAP1 were transformed into BL21-CodonPlus (DE3)-RIPL competent cells (Agilent). Overnight cultures were added to fresh LB (1:100) and grown until $OD_{600} \approx 0.5$ at 37°C. Expression was induced with 0.1 mM IPTG for 4 hours at 37°C. Cells were collected by centrifugation (10 min at 5000 x g) and stored at -80°C until protein purification. Bacterial cell pellets expressing GST- were resuspended in solubilization buffer (1X PBS pH 7.5, 0.1% v/v Triton X-100, 1 mg/mL lysozyme, 10 µg/mL DNaseI, 0.5 µg/mL Leupeptin, 0.5 µg/mL Aprotinin, 0.5 µg/mL Pepstatin A, 40 µg/mL PMSF, 100 µg/mL Benzamidine, 0.5 µg/mL E64) and incubated at 4°C for 1 hour with gentle end-over-end mixing. Lysates were clarified by centrifugation at 21,100 x g for 15 min. The supernatant was incubated in batch format with glutathione-sepharose (GE Healthcare) for 1 hour at 4°C prior to adding to a column. The column was washed with 3 x 10 column volumes of wash buffer (1X PBS pH 7.5, 40 µg/mL PMSF, 100 µg/mL benzamidine) and recombinant protein was collected by addition of elution buffer (50 mM Tris pH 8.0, 10 mM glutathione, 80 µg/mL PMSF, 200 µg/mL benzamidine). Elution fractions were separated by SDS-PAGE (10% gel) followed by Coomassie Brilliant Blue staining. Desired fractions were pooled and concentrated using 10K MWCO Amicon Ultra-15 filters (Millipore). The buffer was exchanged in-filter to

remove glutathione to final conditions compatible with downstream applications (1X PBS, pH 7.5). The purity and concentration of the recombinant proteins were determined by SDS-PAGE and BCA Assay (Pierce), respectively. Aliquots were snap-frozen in liquid nitrogen prior to storage at -80°C. Purification of 6xHis-RhoGAP1 was performed as described above, with two notable exceptions: Ni-NTA agarose (Qiagen) and modified phosphate buffer (50 mM $NaH_2PO_4$, 300 mM NaCl, pH 8.0) supplemented with imidazole (10 mM for lysis, 20 mM for wash, 200 mM for elution) were used.

***Antibody Production and Purification***

Antisera was obtained from rabbits (Covance) injected with GST-RhoGAP1. Antibodies were purified using affinity chromatography against 6xHis-RhoGAP1. The affinity column was prepared by dialyzing 6xHis-RhoGAP1 in coupling buffer (0.1M $NaHCO_3$, 0.5 M NaCl, pH 8.3) prior to addition to CNBr-Sepharose 4B (Sigma Aldrich). The affinity resin washed with excess coupling buffer, blocked with 0.1 M Tris pH 8.0, and washed with alternating high salt washes (0.1 M NaOAc, 0.5 M NaCl, pH 4.0; 0.1 M Tris, 0.5 M NaCl, pH 8.8). Rabbit antiserum was diluted 1:1 with 20 mM Tris pH 7.5, passed through a 0.2 μm filter, and passed over the affinity column 5 times. Bound antibody was washed with 20 columns each of 20 mM Tris pH 7.5 and 20 mM Tris pH 7.5, 0.5 M NaCl prior to elution with 100 mM glycine pH 2.5. Elution fractions were collected into 1 M Tris pH 8.8 to neutralize antibody solutions. Antibody concentration within each fraction was determined by BCA assay (Pierce). Desired fractions were pooled, concentrated using 30K MWCO Amicon Ultra-15 filters (Millipore) and stored at 4°C, supplemented with 0.02% sodium azide, until use.

***Cell Lysis and Western Blotting***

Embryos were lysed by manual disruption in 10 mM imidazole, 50 mM KCl, 2.5 mM $MgCl_2$, 1 mM EGTA, 10 mM EDTA pH 7.8, 1 mM DTT, 0.5% (v/v) Triton X-100 with protease inhibitors (10 μM E-64, 4 mM pefabloc, 60 μg/ml chymostatin, 5 μg/ml leupeptin, 1 μg/ml pepstatin, 3.75 μg/ml aprotinin, 50 μM calpeptin, 50 μM ALLN). Lysates were centrifuged at 14,000 x g for 5 minutes followed by removal of the cytoplasmic fraction. Upon an additional centrifugation, clarified lysate was mixed with 6X Laemmli Buffer and stored at -80°C. Lysates were separated by SDS-PAGE (10% gels) and transferred onto nitrocellulose. Blots were blocked with 5% (w/v) milk in PBS for 1 hour at room temperature, incubated with primary antibody (1:500 rabbit α-RhoGAP1 and 1:500 mouse α-tubulin in 5% milk) overnight at 4°C, washed twice with excess 5% milk in PBS, and incubated with near-IR secondary antibodies (1:10000 Alexa Fluor 680-conjugated α-rabbit IgG, 1:10000 Alexa Fluor 790-conjugated α-mouse IgG ; Thermo Fisher Scientific) for 1 hour at room temperature. Membranes were washed 4 times with PBST (1X PBS pH 7.5, 0.1% [v/v] Tween-20) prior to analysis with an Odyssey Fc Imaging System (LI-COR Biosystems).

***Image Acquisition and Data Analysis***

Confocal microscopy was performed using a Nikon Eclipse Ti inverted microscope with 60X oil objective (1.4 NA) and Prairie View confocal system (Bruker) or an Axiovert 100M (Zeiss) inverted microscope with Lasersharp Confocal 1024 module (Bio-Rad) with a 63X oil objective (1.4 NA). Cells were wounded with illumination from a 488 nm uncaging laser

(Bruker) or 440 nm dye laser setup pumped by a MicroPoint 337 nm nitrogen laser (Andor). Imaging data were processed using Fiji (Schindelin *et al.*, 2012) and Volocity (Perkin-Elmer). Low magnification views of embryos were obtained using the camera of an iPhone 4S (Apple) though the eyepiece of a Stemi 1000 dissecting microscope (Zeiss). Kymography was performed by drawing a 10 pixel-wide line through the area of interest from a *z*-projected movie.

**Chapter 4**

Membrane Dynamics During Cellular Wound Repair

This chapter was published as:

Davenport NR, Sonnemann KJ, Eliceiri KW, Bement WM. Membrane Dynamics During Cellular Wound Repair. *Mol Biol Cell* 10.1091/mbc.E16-04-0223

**Abstract**

Cells rapidly reseal after damage, but how they do so is unknown. It has been hypothesized that resealing occurs due to formation of a patch formed from rapid fusion of intracellular compartments at the wound site. However, patching has never been directly visualized. Here we have studied membrane dynamics in wounded Xenopus laevis oocytes at high spatiotemporal resolution. Consistent with the patch hypothesis, we find that damage triggers rampant fusion of intracellular compartments, generating a barrier that limits influx of extracellular dextrans. Patch formation is accompanied by compound exocytosis, local accumulation and aggregation of vesicles, and rupture of compartments facing the external environment. Subcellular patterning is evident as annexin A1, dysferlin, diacylglycerol, active Rho, and active Cdc42 are recruited to compartments confined to different regions around the wound. We also find that a ring of elevated intracellular calcium overlaps the region where membrane dynamics are most evident and persists for several minutes. The results provide the first direct visualization of membrane patching during membrane repair, reveal novel features of the repair process, and show that a remarkable degree of spatial patterning accompanies damage-induced membrane dynamics.

**Introduction**

The capacity for self-repair is an essential trait of both individual cells and multicellular organisms. Not only do cells frequently incur plasma membrane disruptions large enough to warrant repair to prevent loss of cytoplasm or induction of proteolytic pathways by influx of extracellular calcium (McNeil and Ito, 1989), the inability of cells to mount a sufficient repair response is linked to a variety of disease states including diabetes (Howard et al., 2011), muscular dystrophies (Bansal et al., 2003), and vitamin deficiencies (Labazi et al., 2015).

While our understanding of cell repair is still fragmentary, work from several different systems indicates that in most if not all eukaryotic cells it hinges on at least two complementary, calcium-dependent pathways: a "resealing" response that limits exchange between the cytoplasm and the extracellular environment (Steinhardt et al., 1994; Terasaki et al., 1997; Cooper and McNeil, 2015), and a cytoskeletal response wherein the small GTPases, Rho, Rac and Cdc42 coordinate the assembly and closure of a F-actin and myosin-2 contractile array at the wound site (Mandato and Bement, 2001; Benink and Bement, 2005; Abreu-Blanco et al., 2011; 2014).

While there is consensus that the resealing event is critically important, exactly how it occurs is the subject of controversy. Perhaps the most parsimonious idea is the "patch" hypothesis in which calcium-dependent fusion of intracellular compartments with each other and with the plasma membrane generates a continuous membrane patch at the site of cell damage (Terasaki et al., 1997; McNeil et al., 2000). The patch hypothesis is supported by several lines of evidence including the demonstration that sea water injected into a sea urchin egg is rapidly

walled off from the surrounding cytoplasm (Terasaki et al., 1997) and by the demonstration that cell repair requires internal membrane compartments (McNeil et al., 2003).

However, fusion of internal compartments with each other has never been directly observed at sites of cell damage; this and other considerations have led some to question whether patching actually occurs (Andrews et al., 2015). Further, several other resealing mechanisms have been proposed (reviewed in Moe et al., 2015), including exocytosis (Steinhardt et al., 1994; Bi et al., 1995; Miyake and McNeil, 1995; Reddy et al., 2001), endocytosis (Indone et al., 2008), membrane excision (Jimenez et al., 2014), and plugging of membrane holes via compartment aggregates (Eddelman et al., 1997).

One of the major reasons our understanding of membrane resealing is limited in spite of its obvious importance is that the majority of analyses monitoring the dynamics of membranes after wounding have been performed at relatively low spatiotemporal resolution. To address this deficit, we employed a series of general and specific probes for lipids, proteins and intracellular signals with high-speed, high-resolution confocal imaging to characterize the membrane dynamics elicited by plasma membrane damage of Xenopus oocytes which have a robust and readily observable wound response (Bement et al., 1999). Using this approach, we provide the first direct visualization of patching. We also find that wounding elicits compound exocytosis and a novel behavior that we term “explodosis” in which membranous compartments rupture outward at the wound site. Further, we find that patching is accompanied by accretion of membranous compartments in association with two proteins previously implicated in cell repair —annexin and dysferlin—as well as the small GTPases Rho and Cdc42 in distinct subcellular patterns around wounds. Finally, we find that intracellular calcium remains locally elevated

around wounds for several minutes in a region overlapping the contractile array utilized to reestablish the integrity of the cytoskeleton.

**Results**

Live imaging of cell repair comes with several inherent challenges. First, repair is very rapid, commencing within a second or so of damage; second, the wound itself is a moving target as actomyosin-powered contraction brings the edges of the wound together beginning at ~30-60s post wounding; third, what is observed depends on the focal plane and the angle of imaging; fourth, what is seen also depends on the probe employed. To help overcome these challenges, we imaged using several different approaches—standard laser scanning confocal microscopy of single focal planes or, occasionally, z-stacks; fast swept field confocal microscopy (SFC) of z-stacks; two different imaging angles for single focal planes—en face (i.e. looking directly down on the wound) and oblique (i.e. wounding an area where the oocyte surface curves away from the coverslip so that regions both below and at the level of the plasma membrane can be viewed in the same plane). We combined these imaging approaches with several different probes, both generic and specific, for membranes, ions, and proteins. All of the membrane dynamics described below were observed with a minimum of two different probes; some (e.g. exocytosis, patching) were seen with three or more.

***Wounding triggers exocytosis and formation of large membrane compartments at wound sites***

Wounding of sea urchin eggs triggers local exocytosis of cortical secretory granules (cortical granules) (Bi et al., 1995; Miyake and McNeil, 1995). It seemed unlikely that

cortical granule exocytosis would also be triggered by wounding in frog oocytes, in that exocytosis in oocytes (in contrast to eggs, a later meiotic stage) is refractory to elevation of intracellular calcium (reviewed in Bement, 1992). Nonetheless, we tested this possibility by wounding oocytes in the presence of external dextran, which labels exocytosing cortical granules by incorporating into their lumen after they release their contents (Sokac et al., 2003). In spite of our expectations, wounding not only resulted in a rapid incorporation of dextran that was largely confined to the immediate wound site (Figure 1A, arrowheads; see also below), it also triggered progressive exocytosis of cortical granules up to ~15 μm distal to the wound site (Figure 1A, Movie 1).

As an alternative to dextran, we assessed exocytosis using FM 1-43, a cell-impermeant, lipophilic dye that is often used to study membrane repair; its fluorescence emission increases upon incorporation into hydrophobic environments. Fast imaging series (1-2 s time points) at the plane of the plasma membrane revealed exocytotic events as transient openings in the FM 1-43-stained PM (Figure 1B, Movie 2). In oblique views of oocyte wounds FM 1-43 revealed an additional feature of the wound response: accumulation of large, dynamic membranous compartments in the center of the wound (Figure 1C, Movie 3).

***Fusion of intracellular compartments at wound sites to generate a patch***

The rapid confinement of dextran to the immediate wound site and the formation of large, FM 1-43-staining compartments at wounds hinted at the possibility that dextran spreading might be limited by fusion of internal compartments—i.e. patch formation. However, FM 1-43, while readily staining the plasma membrane, cell surface projections, and other external structures at

wound sites, did not effectively label internal compartments of the oocyte prior to wounding, even when microinjected (not shown). We therefore wounded oocytes in the presence of dextran after staining with R18, a nonspecific membrane dye. R18 labeled both the plasma membrane (not shown) and, based on their size, distribution and abundance (Campanella and Andreucetti, 1977; see also below) the cortical granules (Figure 2, Movie 4). Immediately after wounding, the wound area contained dextran but was largely devoid of cortical granules (Figure 2, Movie 4). Dextran did not appear to diffuse away from the initial wound site but instead either remained constrained by tightly opposed cortical granules or spread incrementally in a manner suggestive of local membrane fusion or disruption (Figure 2, top; Movie 4; see also below). Indeed, higher magnification views showed that R18-labeled compartments could first fuse with each other, forming a larger compartment, and then subsequently incorporate dextran after apparently rupturing on the side bordering the dextran (Figure 2, bottom; enlargement 1), or undergo rupture and dextran incorporation without a prior fusion event (Figure 2, bottom; enlargement 2).

While these results showed that endogenous, membrane bound compartments—the cortical granules—participate in the repair process, further analysis of repair dynamics was hampered by the fact that the R18 was rapidly lost from cortical granules facing the wound edge. We therefore employed a fusion protein comprising eGFP fused to the C2 domain of protein kinase C beta (eGFP-C2), which binds to phosphatidylserine in the presence of elevated calcium and which has previously been shown to provide high contrast labeling of cortical granules following calcium elevation (Yu and Bement, 2007). The combination of R18, eGFP-C2 and dextran allowed us to track the fate of cortical granules at wound sites: upon wounding, multiple

R18-labelled compartments rapidly fuse, forming a compartment within which the dextran is contained (Figure 3, Movie 5). The C2 probe is rapidly recruited to the membrane of this compartment even as the R18 is lost and is retained there for ~10-60 s, providing a high contrast label of a continuous membrane layer that forms around the wound site. Further, the membrane labeled with C2 is contiguous with the plasma membrane, which still retains R18 labeling (Figure 3; t = 0:04-0:08). Because these results are exactly what is predicted by the patch hypothesis, we will hereinafter refer to the membranous structure that bounds the wound site as the "patch".

***Patching dynamics***

The high signal:noise provided by eGFP-C2 permitted us to analyze the patching process in more detail. Patches begin forming within several seconds of wounding and thereafter undergo essentially constant remodeling (Figure 4A, Movie 6). Specifically, on the immediate outside of the patch (i.e. in the extracellular space), strange, extremely dextran-rich structures grew slowly from the patch floor in a manner that frustrated all of our efforts at characterization. Further, the cytoplasmic region surrounding the patch accumulated membranous compartments, many of which become cross-linked with the patch and each other or the patch, as judged by accumulation of C2 probe at sites of contact and distortion of compartment shape (Figure 4, A' and B; Movies 6 and 7). The dextran remained confined to the exoplasmic side of the regions where compartments were tightly packed, even in the absence of a continuously labeled (with eGFP-C2) patch, suggesting that the packing was sufficient to form a barrier impermeable to dextran influx (e.g. Figure 4A').

The patch also served as a site of extensive membrane fusion. For example, the cytoplasmic compartments immediately abutting the patch often fused with it and then each other, as judged by dextran incorporation (Figure 4, A-B; Movies 6 and 7). Most of the compartments involved were likely cortical granules based on their size and intense labeling with eGFP-C2, however, much smaller, C2-poor compartments were also observed, reminding us that there may be many other compartments participating that are not labeled with the probes being employed (Figure 4, C and C').

The patch served as a site of compound exocytosis, with an initial fusion event being followed by one or more fusions with deeper (in the cytoplasm) compartments (Figure 5A, Movie 8). However, there did not appear to be a strict requirement for prior union with a plasma membrane containing compartment (i.e. either the plasma membrane itself or a compartment that had previously fused with the plasma membrane) in that eGFP-C2-labeled compartments were occasionally observed to fuse with each other first and then fuse with dextran-containing compartments (Figure 5B, Movie 9; see also Figure 2).

***Explodosis***

The foregoing results provided a paradox: wounding clearly elicits local fusion of intracellular compartments, which is expected to generate large, completely membrane-enclosed compartments at the wound site, and yet the patching membrane often appears to have no "roof"—i.e. it seems to be a single bilayer (e.g. Figure 4). The apparent rupture of the R18-labeled compartments observed in Figure 2 suggested a resolution to this paradox—compartments exposed to the extracellular medium might rupture outward. Consistent with this

mechanism, oblique, single optical plane movies of repair in eGFP-C2 labeled cells revealed that compartments facing the extracellular environment often popped open and then collapsed into a single membrane (Figure 6, A and A'; Movie 10). To better visualize this process in x, y, and z over time, we took advantage of the superior speed provided by swept field confocal microscopy (Bembenek et al., 2007; Castellano-Munoz et al., 2012; Ponomareva et al., 2016), which permits 12-20 z-plane stacks to be captured in 2 s (Figure 6, B and B', Movies 11-13). Figure 6 (B and B'; also Movies 12 and 13) shows a series where three small compartments first fuse with each other, forming a large, continuous compartment which subsequently ruptures on the side facing the outside of the cell. Because this behavior is fairly violent, and appears qualitatively different from other behaviors previously described, we refer to it as "explodosis".

***Human annexin A1 and dysferlin are rapidly recruited to membrane compartments around wounds***

Annexins have been implicated in cell repair in several systems (McNeil et al., 2006; Potez et al., 2011; Swaggart et al., 2014). To obtain insight into their potential roles in this process and to assess the potential of the oocyte system for heterologous analysis of human repair proteins, an eGFP-human annexin A1 fusion (eGFP-annexin) was generated and expressed in oocytes. Low magnification, en face movies showed rapid recruitment of eGFP-annexin to wounds where it localized to the PM in a tight ring bordering the wound and to membranous compartments both beneath the wound and on the interior of the wound region (Figure 7A, Movie 14). High magnification movies revealed that eGFP-annexin was recruited to small foci around wounds within 2-4 s (Figure 7B, Movie 15, and not shown). Recruitment of eGFP-

annexin to vesicles often preceded incorporation of dextran (Figure 7B, Movie 15), indicating that there is no requirement for PM-compartment fusion for annexin recruitment. Further, we observed few, if any, cases of fusion of compartments around the wound edge that were not eGFP-annexin-labeled, suggesting the possibility that annexin may participate in the fusion process (see Discussion). Movies made from oblique views often revealed discontinuous localization of eGFP-annexin on the "floor" of the wound site, consistent with it being a component of the patch (Figure 7, C and C'; Movie 16). However, this localization was typically transient (Movie 16), suggesting that, once formed, the patch is continually remodeled.

To extend the analysis of heterologous protein targeting to wounds, we assessed the dynamics of human dysferlin, a protein implicated in repair of skeletal muscle (Bansal et al., 2003; Lennon et al., 2003). The size of eGFP-dysferlin (~265 kD; mRNA of ~7 kb) precluded the use of in vitro-transcribed mRNA. We therefore expressed eGFP-human dysferlin (eGFP-dysferlin) in insect cells and purified it to homogeneity (Figure 7D). Following injection into oocytes, eGFP-dysferlin was cytoplasmic. However, upon wounding, it was recruited to both the plasma membrane and to intracellular compartments at the wound (Figure 7, E and E'). Like eGFP-annexin, eGFP-dysferlin was localized to a tight ring on the plasma membrane around the wound; unlike eGFP-annexin, eGFP-dysferlin did not extensively label all of the large compartments within the wound (Figure 7, E and E').

***Membrane remodeling continues long after initial plasma membrane damage***

It was evident from the above results that the wound response continued well after the first minute of wounding. However, it was also evident that several of the probes—R18, eGFP-

C2, eGFP-annexin—were often lost from a given membranous structure over time. We therefore analyzed wound dynamics using the C1 domain of protein kinase C beta fused to eGFP (eGFP-C1). This probe binds specifically to diacylglycerol, a signaling lipid previously shown to be generated at wound sites, to persist at wounds for several minutes, and to be required for proper wound repair (Vaughan et al., 2014). eGFP-C1 accumulated around wounds in a tight ring at the plasma membrane and also accumulated on membranous compartments around the wound site (Figure 8A; Movie 17; and not shown). Double labeling with mRFP-C1 and eGFP-C2 revealed that the PM DAG is initially concentrated within a broader ring defined by the eGFP-C2 probe (Figure 8B; Movie 18). Strikingly, while the eGFP-C2 signal wanes over the course of several minutes, eGFP-C1 remains concentrated on the PM and on membranous compartments underneath the wounds for at least 15 min (Figure 8C; Movie 19; and not shown). The DAG-labeled compartments are highly dynamic, and their behavior suggests that the wound response continues long after the initial healing is largely finished (Figure 8C, Movie 19).

***C2 recruitment parallels increases in intracellular free calcium***

In principle, targeting of the C2 domain to the wound site, as well as its eventual loss, could reflect changes in intracellular free calcium, changes in phosphatidylserine distribution, or both. However, previous results showed that while phosphatidylserine becomes more enriched around wound sites over time, this process is not evident until ~90 s post-wounding (Vaughan et al., 2014), well after the observed recruitment of eGFP-C2. It therefore seemed likely that the spatiotemporal recruitment pattern of eGFP-C2 was driven by calcium, with the preexisting (i.e. prewounding) membrane phosphatidylserine serving as a passive platform for C2 binding. To

test this possibility, we imaged C2 fused with BFP (BFP-C2) together with GCaMP5G, a circularly-permuted eGFP construct that has increased fluorescence in the presence of calcium ions (Akerboom et al., 2012). Wounding triggered a rapid (within 1 s) increase in fluorescent signal of GCaMP5G in a broad bloom around wounds (Figure 9; Movie 20; and not shown). However, within ~30 s, the bloom decreased rapidly, with the GCaMP5G eventually forming an ~8 μm disc of increased signal around the wound (Figure 9, Movie 20). The disc decreased in size steadily as healing progressed, and the GCaMP5G signal eventually disappeared within ~5 min (Figure 9, Movie 20, and not shown). Double labeling showed that BFP-C2 followed a similar pattern with the following differences: it took ~ 5-10 s for the BFP-C2 bloom to be evident (Figure 9, Movie 20); the area occupied by BFP-C2 was generally less broad than that occupied by GCaMP5G fluorescence (Figure 9); while the GCaMP5G signal was diffuse, as expected for a soluble calcium reporter, the BFP-C2 was sharply confined to the plasma membrane and on intracellular membrane compartments (Figure 9, Movie 20, see also Figures 3-6). Based on these results, the overall similarity of the timing and pattern of C2 recruitment and GCaMP5G signal, and the known ability of C2 to bind to phosphatidylserine in the presence of elevated calcium (Kohout et al., 2002), it is likely that changes in calcium are the primary driver of C2 recruitment and, conversely, C2 recruitment represents a reasonable surrogate for elevation of intracellular free calcium.

***Patterning of membrane dynamics***

Many of the foregoing results hinted at the possibility that the precise pattern formation events previously described at the level of the plasma membrane, wherein the small GTPases

Rho and Cdc42 form concentric zones of activity around each other (Benink and Bement, 2005) might be mirrored in some of the membrane dynamics elicited by wounding. That is, the distinct patterns of C1 and C2 accumulation, the tight focusing of annexin and dysferlin at the wound edge, and differential distribution of dextran-containing compartments (e.g., Figure 1A) hinted that the apparently promiscuous and chaotic membrane fusion events might be subject to more order than is apparent at first glance. In particular, because Rho and Cdc42 have been linked to membrane dynamics in other systems (reviewed in Ridley, 2006), we hypothesized that their activity might not be confined to the plasma membrane but might also be localized to the dynamic membrane compartments that form during healing. We first addressed this point by comparing the distribution of elevated intracellular free calcium, Cdc42 activity and Rho activity using triple labeling with GCaMP5G, BFP-wGBD and mCherry-2xrGBD (wGBD and rGBD are probes that specifically bind to active Cdc42 and active Rho, respectively; Benink and Bement, 2005). This approach revealed that the formation of the focused disc of intracellular free calcium preceded Rho and Cdc42 activation and that the highest concentration of elevated calcium within the disc precisely overlapped the Rho and the Cdc42 zone once the latter had formed around wounds (Figure 10, A and A'; Movie 21; results not shown). Eventually, the Cdc42 activity declined coincident with the fall of intracellular free calcium, while Rho activity persisted for much longer. These results, taken in conjunction with those above, indicate that intracellular free calcium, active Rho, and active Cdc42 are all concentrated in the same general region where patching and wound-induced compartment fusion occur and that the dynamics of active Cdc42 parallel those revealed by GCaMP5G and C2, while those of Rho parallel the dynamics of C1.

We then employed swept field confocal imaging to permit us to follow the dynamics of active Rho and active Cdc42 both at the PM level and much deeper (~3-10 um) with rapid acquisition (2-3 s intervals) during the course of wounding and repair. Imaging at the level of the plasma membrane clearly revealed that exocytotic events occur within both of the GTPase zones as they form and that such events continued as the zones close inward (Figure 10B, top; Movie 22). Such grazing views also occasionally revealed membranous compartments that appeared to be squeezed from the wound edge into the center of the wound (Figure 10B, top; Movie 22, bottom).

Remarkably, imaging the region beneath the plasma membrane revealed that the concentric pattern of active Rho and active Cdc42 evident at the PM was maintained beneath the PM around the wound, with each active GTPase confined to a different subset of membrane compartments: active Rho concentrated on compartments immediately abutting the wound, while active Cdc42 concentrated on compartments more distal to the wound (Figure 10B, bottom; Movie 23). The two sets of compartments displayed qualitatively different behavior: those compartments that harbored active Rho were relatively inert, while those associated with active Cdc42 were highly dynamic and displayed rapid shape changes, changes in the intensity of Cdc42 signal, and changes in position (Figure 10B, bottom; Movie 23).

**Figure 1.** Exocytosis occurs upon wounding. (A) A *Xenopus laevis* oocyte wounded in the presence of extracellular fluorescent dextran (Texas Red dextran). Intrusion of dextran into cell is initially limited to region proximal to the wound (arrowheads) but then compartments distal to the wound undergo exocytosis and imbibe dextran (first event indicated by arrow). See Movie 1. (B) An oblique view of oocyte wounded in media containing FM 1-43 (*N*-(3-triethylammoniumpropyl)-4-(4-(dibutylamino)styryl)pyridinium dibromide). Wound center is out of frame, towards the bottom of the image. Numbered arrowheads indicate sites of exocytosis, highlighted in enlarged insets. See Movie 2. (C) An oblique view of an oocyte wounded in the presence of FM 1-43. Arrowheads highlight membranous compartments labeled by FM 1-43 during repair. See Movie 3. **Times in min:sec with *t* = 0:00 corresponding to moment of wounding. Scale bars: (A) 10 µm, (B)(C) 5 µm, (B, insets) 1 µm.**

**Figure 1**

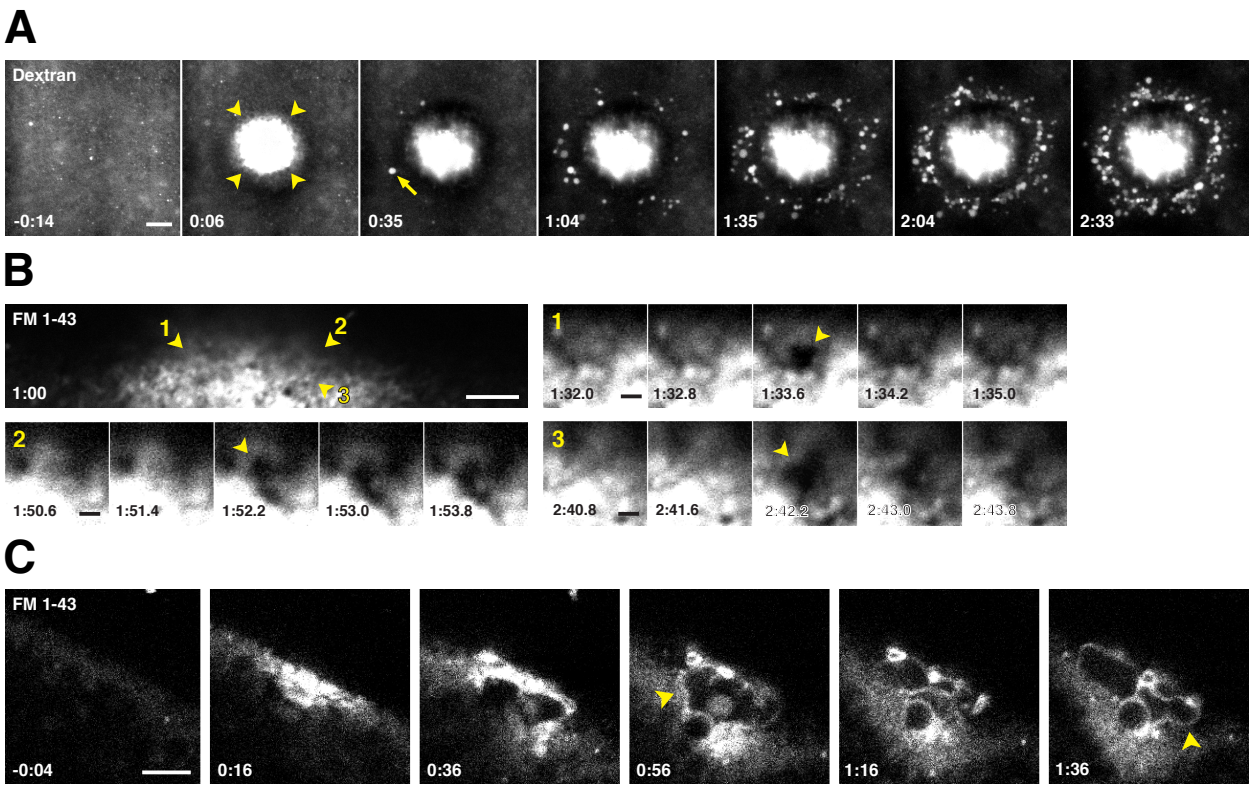
A
Dextran
-0:14
0:06
0:35
1:04
1:35
2:04
2:33
B
FM 1-43
1
2
3
1:00
1
1:32.0
1:32.8
1:33.6
1:34.2
1:35.0
2
1:50.6
1:51.4
1:52.2
1:53.0
1:53.8
3
2:40.8
2:41.6
2:42.2
2:43.0
2:43.8
C
FM 1-43
-0:04
0:16
0:36
0:56
1:16
1:36

**Figure 2. Extracellular dextran has limited access to the cytoplasm of wounded cells**. En face view of oocyte pre-stained with R18 (octadecyl rhodamine B chloride) and wounded in the presence of extracellular fluorescent dextran (Oregon Green 488 dextran). Areas highlighted by boxes at *t* = 0:04 enlarged to highlight wound dynamics. Enlargement of region 1 (bottom, left) shows fusion of two compartments (arrowheads) prior to rupture and imbibing of dextran at 0:14-0:16. Arrow shows fragment of compartment after rupture. Enlargement of region 2 (bottom, right) highlights a compartment at the wound edge (arrowheads) that is exposed to dextran upon rupture at 0:10. A fragment of the vesicle is visible after rupture (arrow). See Movie 4. **Times in min:sec with *t* = 0:00 corresponding to moment of wounding. Scale bars; 5 µm (top), 2.5 µm (bottom).**

# Figure 2

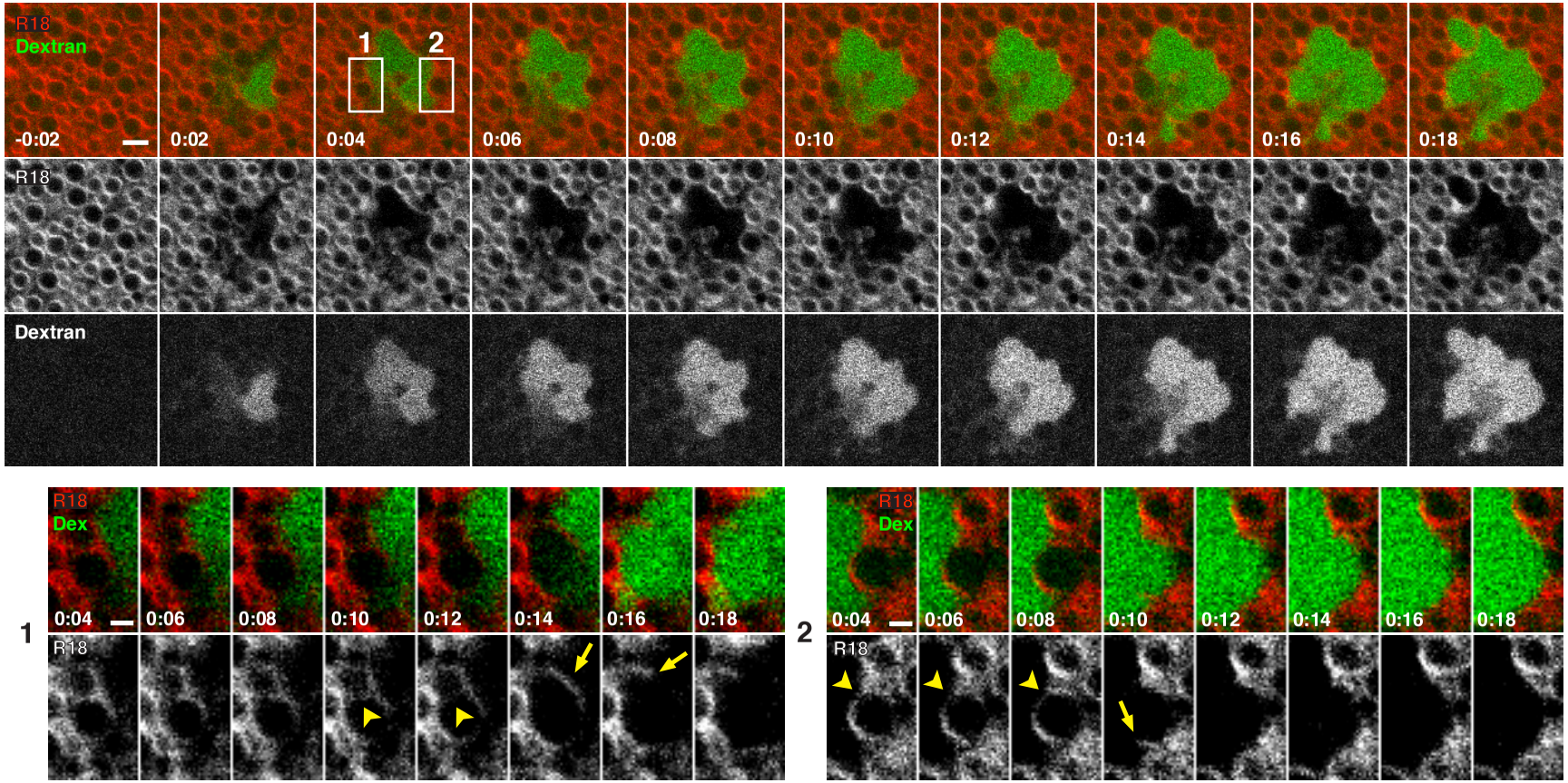
R18
Dextran
-0:02
0:02
1
2
0:04
0:06
0:08
0:10
0:12
0:14
0:16
0:18
R18
Dextran
1
R18
Dex
0:04
0:06
0:08
0:10
0:12
0:14
0:16
0:18
R18
2
R18
Dex
0:04
0:06
0:08
0:10
0:12
0:14
0:16
0:18
R18

**Figure 3**. **Vesicle-vesicle fusion at sites of plasma membrane disruption**. Oocyte expressing eGFP-PKCβ-C2 (a probe for phosphatidyserine and calcium) was pre-incubated with R18 and wounded in presence of fluorescent extracellular dextran (Alexa Fluor 647 dextran). Arrowhead at *t* = 0:00 denotes a R18-labelled vesicle that is about to undergo fusion. eGFP-C2 probe begins to label R18-stained compartments (arrow at *t* = 0:02) shortly after wounding. eGFP-C2-labeled compartment is contiguous with the plasma membrane (double arrows) and forms a barrier (asterisks) limiting dextran influx. See Movie 5. **Time in min:sec with *t* = 0:00 corresponding to moment of wounding. Scale bar, 5 μm.**

Figure 3

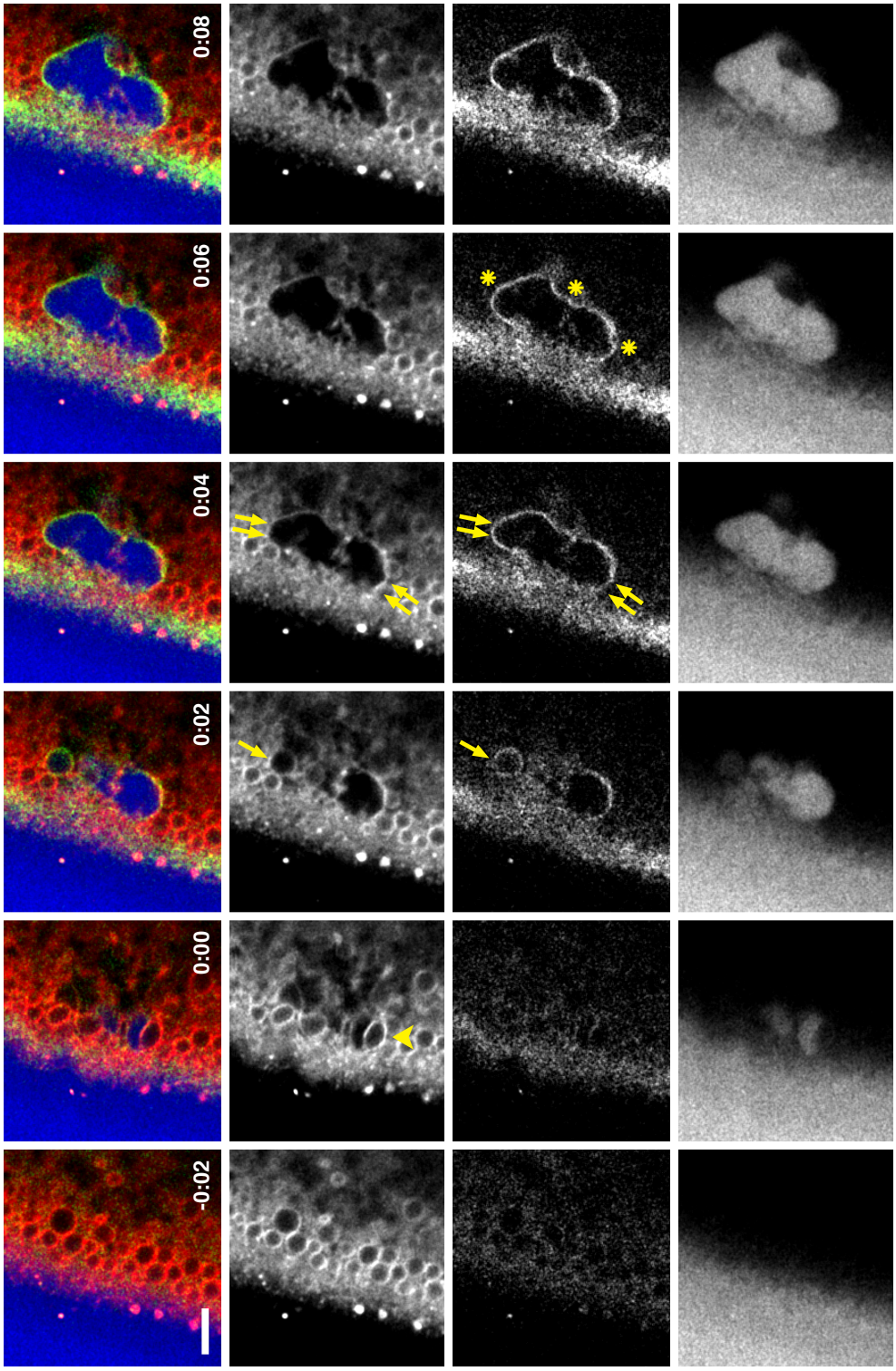
-0:02
0:00
0:02
0:04
0:06
0:08
R18
eGFP-PKCβ-C2
Dextran
R18
eGFP-PKCβ-C2
Dextran

**Figure 4**. **The C2 domain of PKCβ labels intracellular vesicles and wound patch.** (A) Oblique, low magnification view of oocyte expressing eGFP-PKCβ-C2 wounded in the presence of extracellular fluorescent dextran (Texas Red dextran). eGFP-PKCβ-C2 is rapidly recruited to wound and labels vesicles clustered around edge of wound. Brightly-stained structure (asterisk) of unknown identity appears in wound pit. See Movie 6. (A') Enlargement of (A) starting at *t* = 0:30, showing tightly packed, C2-labelled vesicles at wound edge (arrows) closely opposed to nascent patch (green line bordering wound). Large vesicle fuses with patch and imbibes dextran (0:32) and then fuses with another vesicle (0:36). (B) Cell expressing eGFP-PKCβ-C2 wounded presence of extracellular fluorescent dextran (Texas Red dextran). Single arrowheads denote membranous compartments incorporated into patch, double arrowheads denotes region of patch that progressively accumulates C2. (C) Oocyte expressing eGFP-PKCβ-C2 and stained with R18 prior to wounding. The vesicular structures labeled by the C2 probe upon wounding are also labeled by R18 (arrowhead). (C') Enlargement of (C) showing C2 probe labels most, but not all, compartments labeled by R18 (R18-labelled vesicles free of C2 signal are denoted by the arrowheads). **Times in min:sec with *t* = 0:00 corresponding to moment of wounding. Scale bars: (A)(A')(B)(C) 5 µm, (C') 2.5 µm.**

# Figure 4

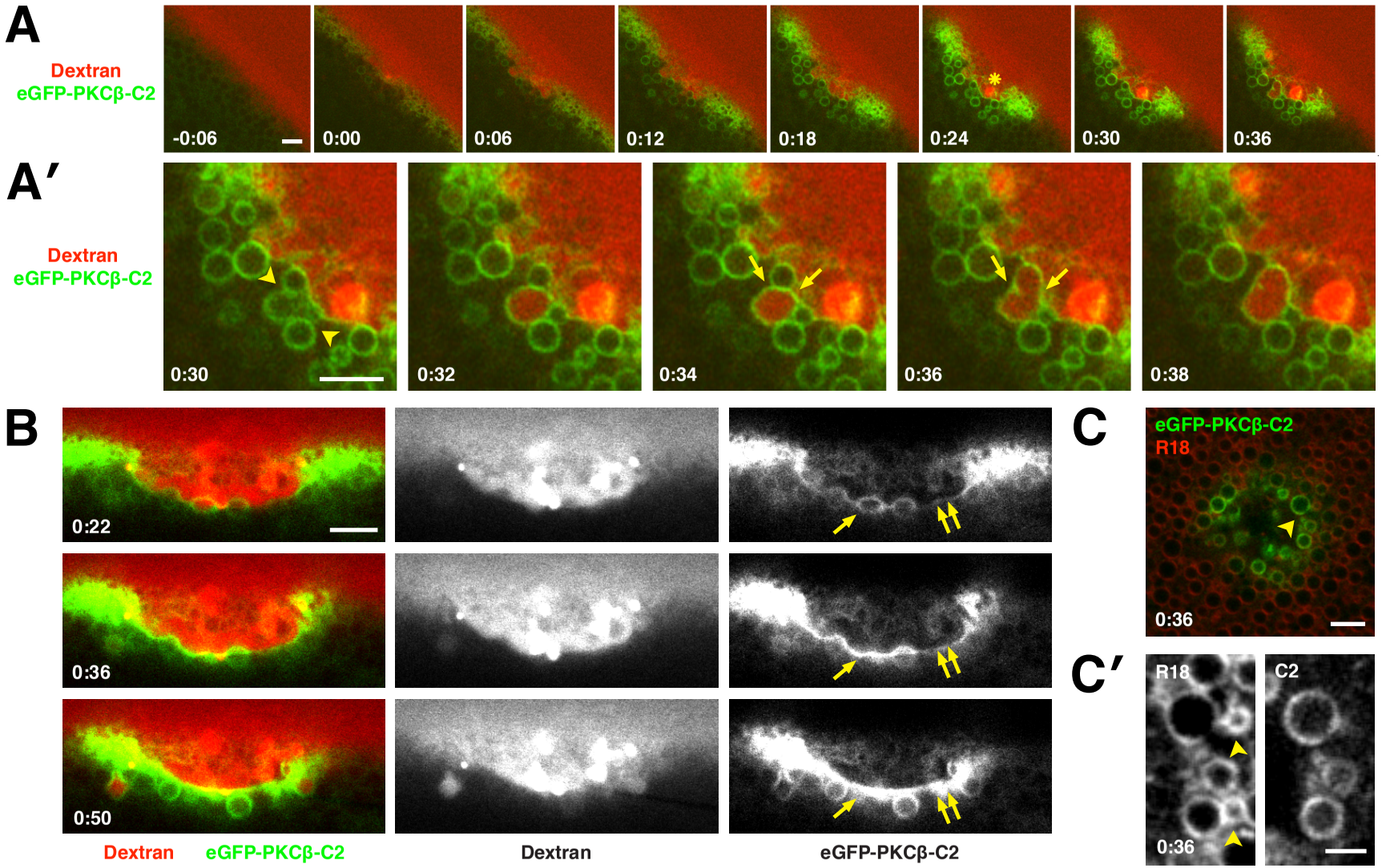
A
Dextran
eGFP-PKCβ-C2
-0:06
0:00
0:06
0:12
0:18
0:24
0:30
0:36
A′
Dextran
eGFP-PKCβ-C2
0:30
0:32
0:34
0:36
0:38
B
0:22
0:36
0:50
Dextran
eGFP-PKCβ-C2
Dextran
eGFP-PKCβ-C2
C
eGFP-PKCβ-C2
R18
0:36
C′
R18
C2
0:36

**Figure 5. Vesicle-vesicle fusion continues through wound repair**. (A) Oblique view of oocyte wounded in presence of extracellular fluorescent dextran (Texas Red dextran) reveals compound exocytosis occurs at wound edge (ie the site of patch formation). Compound exocytotic events indicated by arrowheads. See Movie 7. (B) Oblique, high magnification view of the edge of a wound in an oocyte expressing eGFP-PKCβ-C2 wounded in the presence of extracellular fluorescent dextran (Alexa Fluor 647 dextran, pseudocolored red). Small, tightly packed vesicles near wound edge (arrow) acquire C2, fuse with each other (0:48-0:54), then fuse with another large compartment (double arrows), thereby acquiring dextran (arrowheads). See Movie 8. **Time in min:sec with *t* = 0:00 corresponding to the moment of wounding. Scale bars: (A) 5 µm, (B) 2 µm.**

# Figure 5

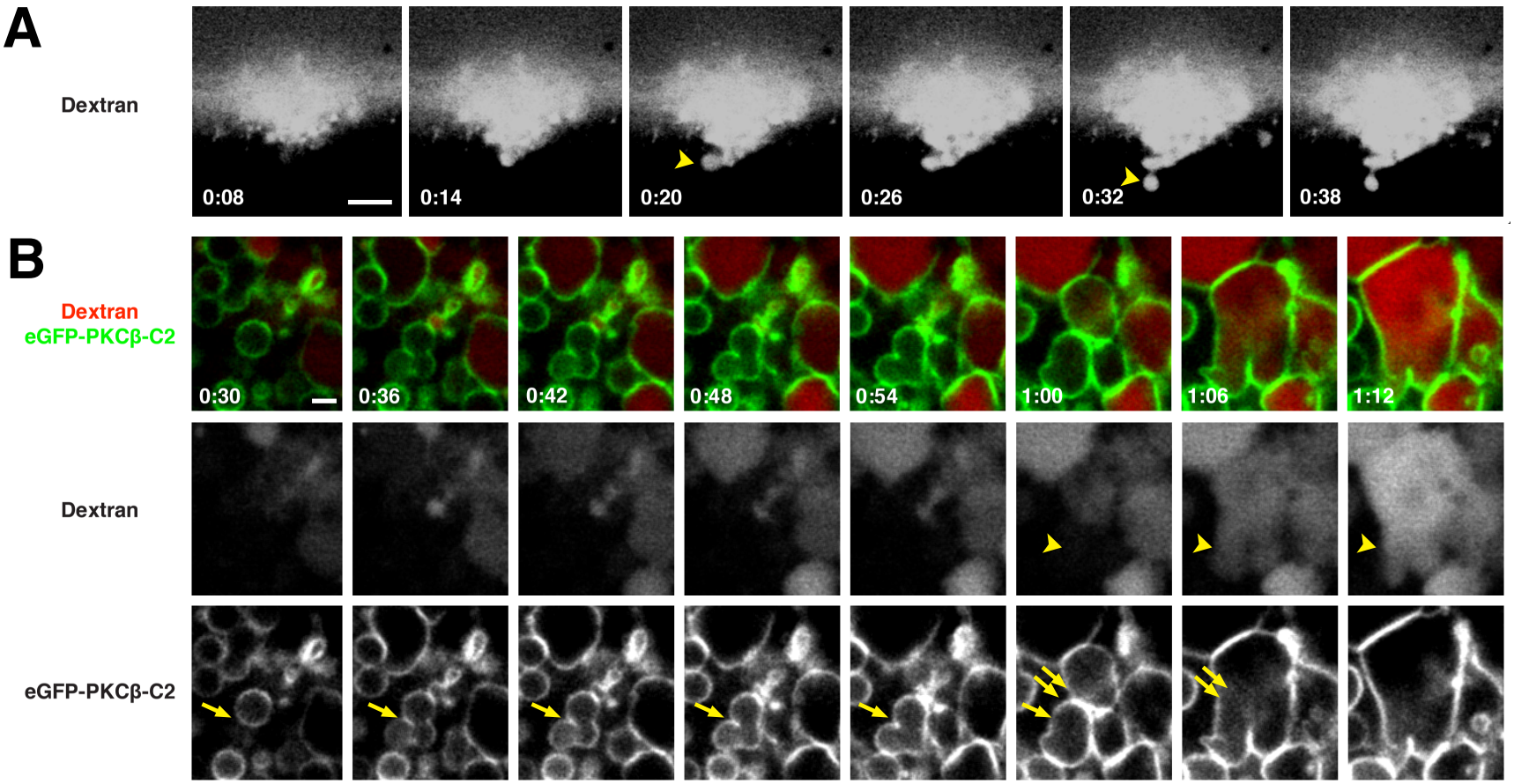
A
Dextran
0:08
0:14
0:20
0:26
0:32
0:38
B
Dextran
eGFP-PKCβ-C2
0:30
0:36
0:42
0:48
0:54
1:00
1:06
1:12
Dextran
eGFP-PKCβ-C2

**Figure 6. High speed imaging of vesicle-vesicle fusion and rupture.** (A) Still from single-focal plane movie showing oblique view of wounded oocyte expressing eGFP-PKCβ-C2. (A') Enlargement and movie series from same wound depicted in (A) showing growth, rupture and collapse of vesicles (see arrowhead) at the wound edge. See Movie 9 which shows several cycles of growth, rupture and collapse of vesicles. (B) Still from a high-resolution 4D movie showing wounded oocyte expressing eGFP-PKCβ-C2 forming a large compartment (see arrowheads) at the wound edge that was no longer visible several frames later (not shown). (B') Enlargement of (B), along the *xy*-plane (left) and *xz*-plane (right) reveals fusion of smaller compartments prior to rupture of apical portion of membrane and subsequent collapse of entire compartment. See Movies 11 and 12. **Time in min:sec with *t* = 0:00 corresponding to the moment of wounding. Scale bars, 5 µm.**

# Figure 6

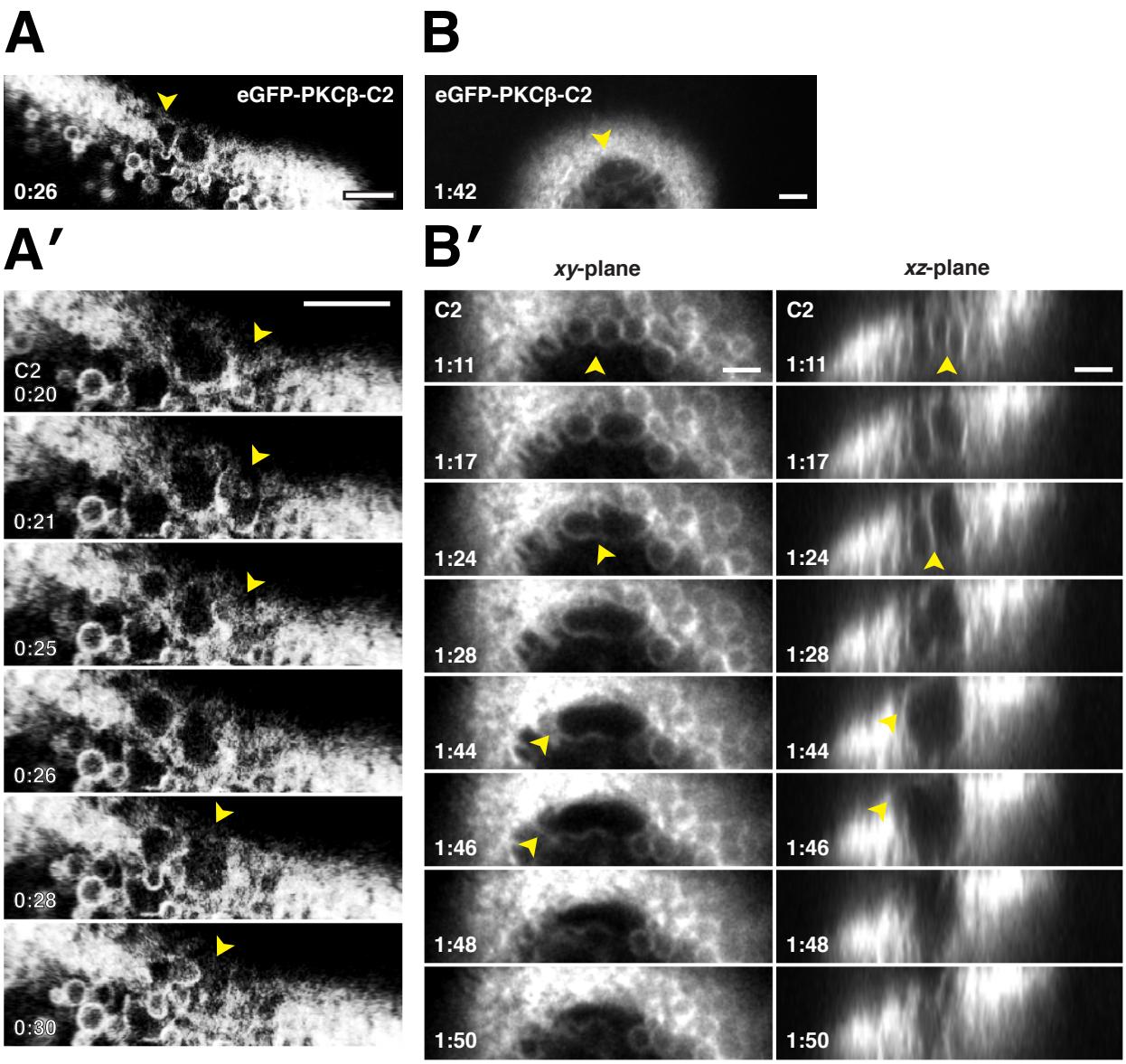
A
eGFP-PKCβ-C2
0:26
B
eGFP-PKCβ-C2
1:42
A′
C2
0:20
0:21
0:25
0:26
0:28
0:30
B′
xy-plane
xz-plane
C2
1:11
1:17
1:24
1:28
1:44
1:46
1:48
1:50

**Figure 7. Human annexin A1 and dysferlin are recruited to membranous structures at wounds**. (A) Low magnification, en face view of wounded oocyte expressing eGFP-annexin A1. Annexin is recruited to cortical foci (0:18), vesicles at wound edge (0:38) and a tight ring around plasma membrane (1:18). See movie Movie 14. (B) En face view of oocyte expressing eGFP-annexin A1 wounded in presence of fluorescent extracellular dextran (Alexa Fluor 647 dextran). Annexin is recruited to foci (arrowheads) and to vesicles prior to dextran incorporation (arrows). At increasing times post wounding annexin also labels compartments in the wound interior (1:38). See Movie 15. (C) Oblique view of a cell expressing eGFP-annexin A1 wounded in the presence of extracellular fluorescent dextran (not shown) showing a eGFP-annexin A1 accumulating at nascent patch (arrowheads). See movie 16. (C') Still from (C) demonstrating eGFP-annexin A1-labelled compartments (green) fuse to form a barrier that excludes extracellular fluorescent dextran (red, Alexa Fluor 647 dextran) from the cytoplasm. (D) Coomassie-stained SDS-PAGE gel showing recombinant FLAG-eGFP-hDysferlin_isoform 1 purified from *Sf9* cells. (E) Oocyte wounded after microinjection with recombinant FLAG-eGFP-hDysferlin. (E') Enlargement of region indicated by an arrowhead in (B) showing recruitment of dysferlin to tight ring at plasma membrane bordering the wound and to vesicles at wound edge. **Time in min:sec with *t* = 0:00 corresponding to the moment of wounding. Scale bars, 5 µm.**

# Figure 7

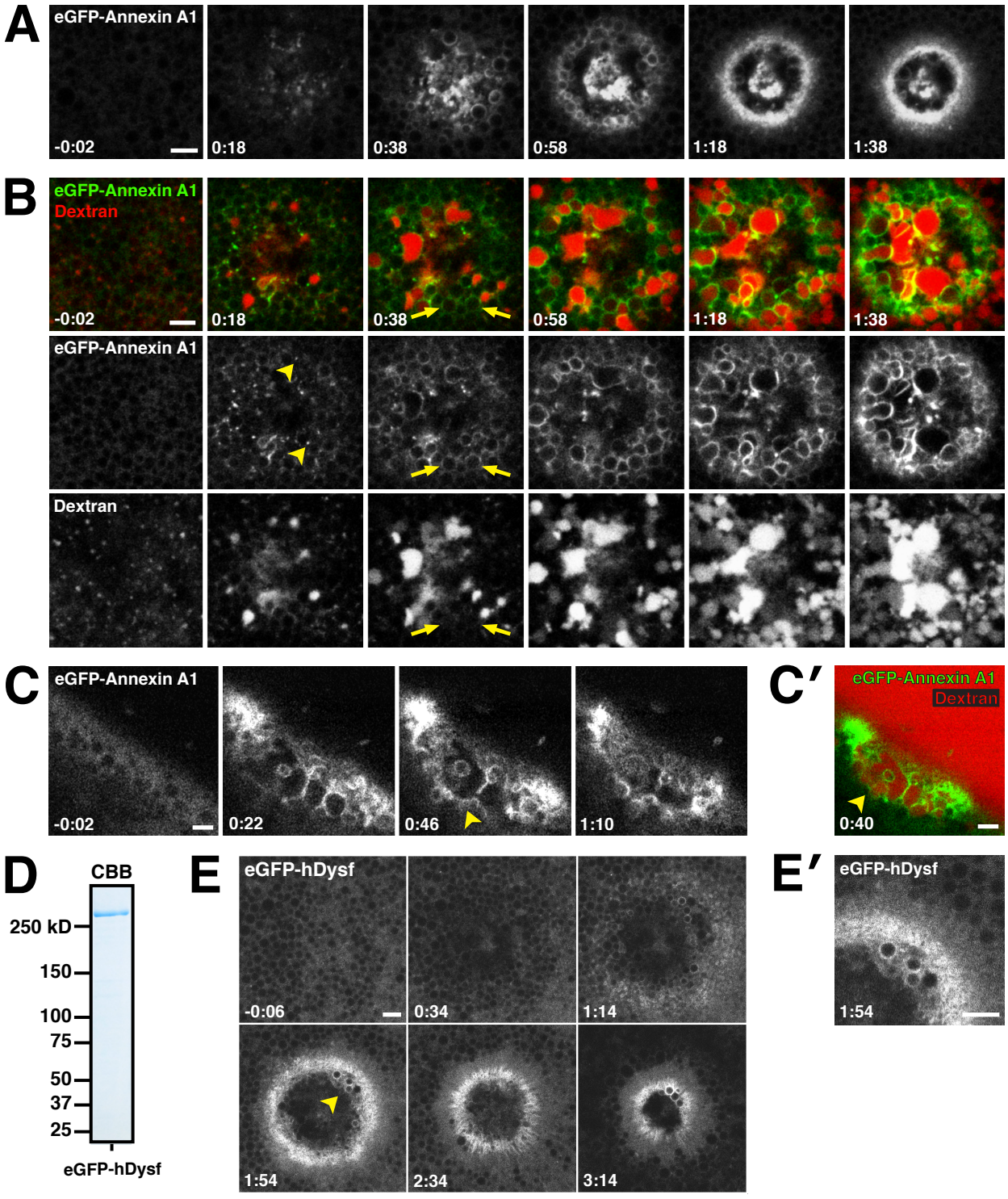
A
eGFP-Annexin A1
-0:02
0:18
0:38
0:58
1:18
1:38
B
eGFP-Annexin A1
Dextran
eGFP-Annexin A1
Dextran
C
eGFP-Annexin A1
-0:02
0:22
0:46
1:10
C′
eGFP-Annexin A1
Dextran
0:40
D
CBB
250 kD
150
100
75
50
37
25
eGFP-hDysf
E
eGFP-hDysf
-0:06
0:34
1:14
1:54
2:34
3:14
E′
eGFP-hDysf
1:54

**Figure 8. Wound-induced lipid domains persist throughout membrane repair**. (A) En face view of wounded eGFP-PKCβ-C1 expressing oocyte. C1 labels both small (arrowhead at *t* = 2:00) and large (arrow at *t* = 4:40) membrane structures upon wounding. See Movie 17. (B) Cells expressing mRFP-PKCβ-C1 and eGFP-PKCβ-C2 reveal lipid patterning around wounds. C1 accumulates at the leading edge of wounds, whereas C2 is more broadly distributed. See Movie 18. (C) A *z*-view of membrane dynamics after wounding, as seen with mRFP-PKCβ-C1 and eGFP-PKCβ-C2. Remodeling of wound area and patch continues long after the initial membrane disruption and loss of C2 with C1 evident on presumptive patch as well as vesicles surrounding patch (arrow). See Movie 19. **Time in min:sec with *t* = 0:00 corresponding to the moment of wounding. Scale bar, 5 µm.**

# Figure 8

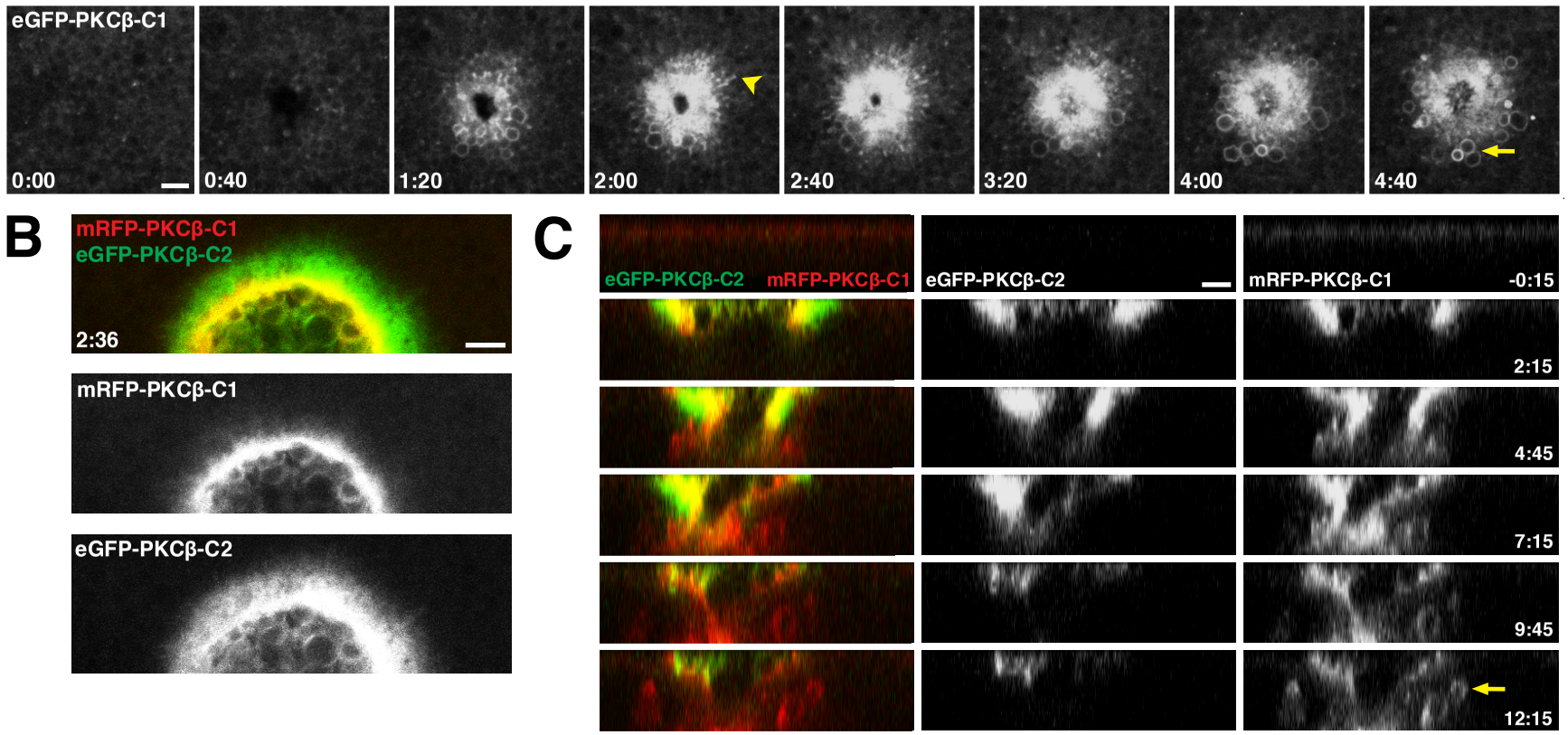
A
eGFP-PKCβ-C1
0:00
0:40
1:20
2:00
2:40
3:20
4:00
4:40
B
mRFP-PKCβ-C1
eGFP-PKCβ-C2
2:36
mRFP-PKCβ-C1
eGFP-PKCβ-C2
C
eGFP-PKCβ-C2
mRFP-PKCβ-C1
eGFP-PKCβ-C2
mRFP-PKCβ-C1
-0:15
2:15
4:45
7:15
9:45
12:15

**Figure 9. C2 accumulation follows elevation of intracellular calcium**. Oblique view of wounded oocyte expressing GCaMP5G and BFP-PKCβ-C2. Increased calcium (detected by GCaMP5G) initially extends far from the site of membrane damage before being confined to a ring around the wound edge at later time points. The pattern of C2 recruitment follows that of calcium elevation, although the GCaMP5G signal is broader and more diffuse while C2 is concentrated on the plasma membrane and on vesicles (arrowheads). See Movie 20. **Time in min:sec with *t* = 0:00 corresponding to the moment of wounding. Scale bar, 10 µm.**

Figure 9

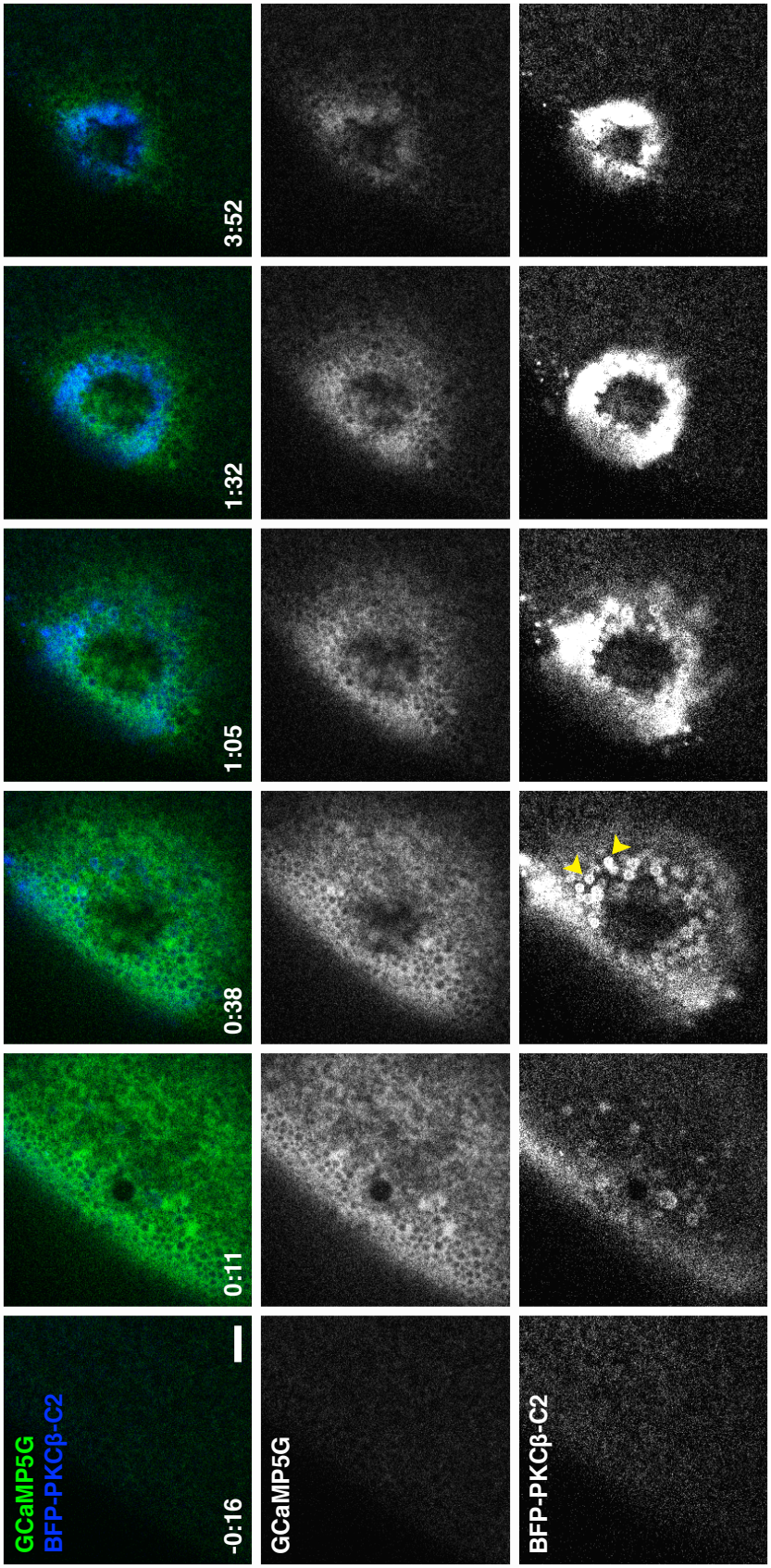
GCaMP5G
BFP-PKCβ-C2
-0:16
0:11
0:38
1:05
1:32
3:52
GCaMP5G
BFP-PKCβ-C2

**Figure 10. Patterning of elevated calcium, Rho and Cdc42**. (A) Low magnification, en face view of wounded oocyte expressing BFP-wGBD, mCherry-2XrGBD, and GCaMP5G; the ring of calcium elevation overlaps the Rho and Cdc42 activity zones. (A') A line scan from (A) showing positions of active Rho and Cdc42 with respect to calcium. The increased calcium spans both zones, with peak intensity of the GCaMP5G signal closer to the peak of Cdc42 activity than that of Rho. (B) En face views of wounded oocyte expressing mRFP-wGBD and eGFP-rGBD from two different focal planes. $z$ = 0 μm (top row, Movie 22) corresponds to a surface view whereas $z$ = -3 μm (bottom row, Movie 23) represents a subcortical view. Active Rho (arrowheads) and Cdc42 (arrows) are present on compartments other than the plasma membrane at wounds. **Time in minutes:seconds, with $t$ = 0:00 corresponding to the moment of wounding. Scale bars, 10 μm.**

# Figure 10

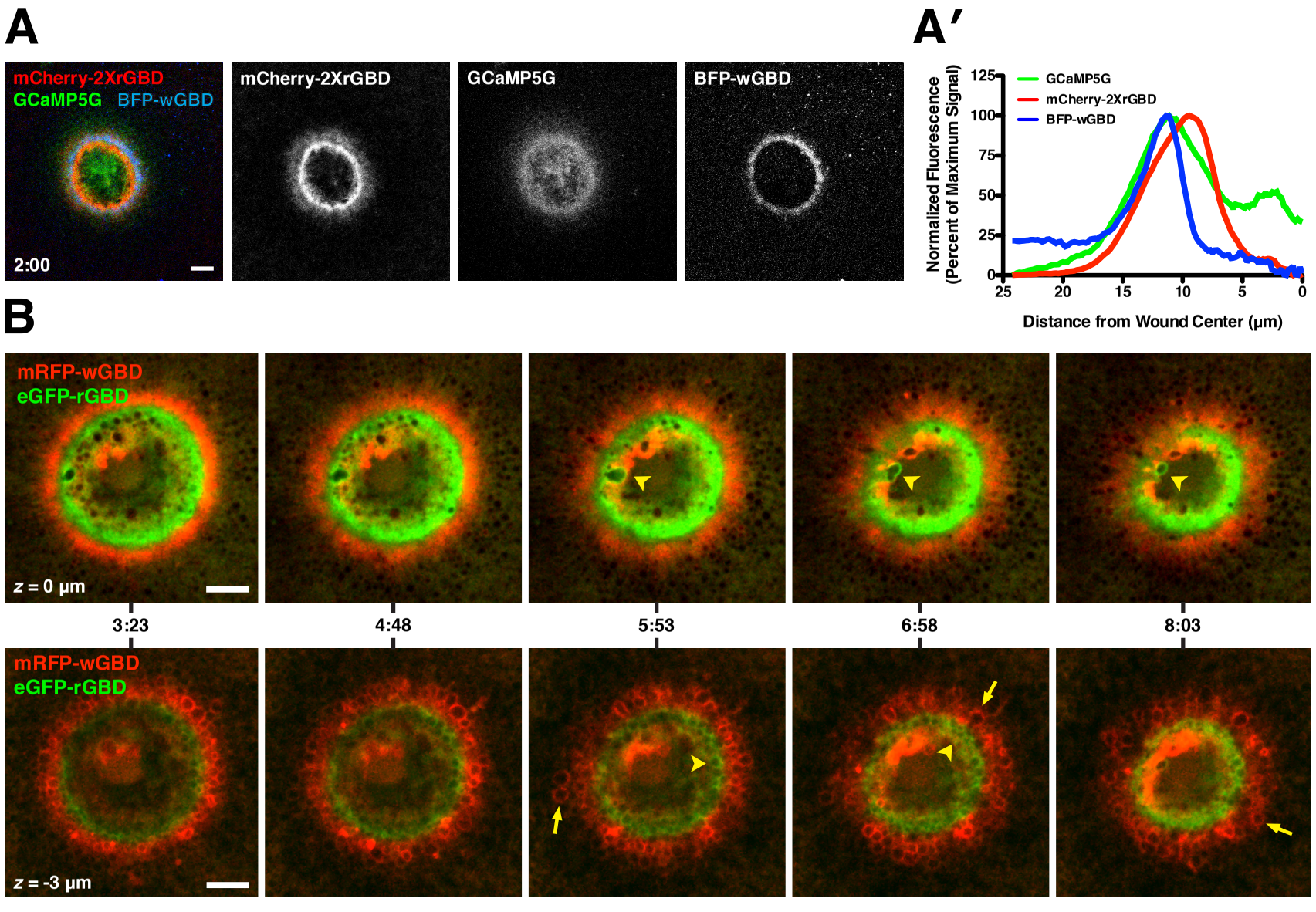
A
mCherry-2XrGBD
GCaMP5G BFP-wGBD
2:00
mCherry-2XrGBD
GCaMP5G
BFP-wGBD
A′
Normalized Fluorescence (Percent of Maximum Signal)
125
100
75
50
25
0
GCaMP5G
mCherry-2XrGBD
BFP-wGBD
25
20
15
10
5
0
Distance from Wound Center (µm)
B
mRFP-wGBD
eGFP-rGBD
z = 0 µm
3:23
4:48
5:53
6:58
8:03
mRFP-wGBD
eGFP-rGBD
z = -3 µm

**Figure 11. Schematic diagram of membrane dynamics at single-cell wounds.** (A-F) Representative time course of wound-induced membrane dynamics. (A) Resting plasma membrane with proximal intracellular membranous compartments. Double-headed arrows represent incipient membrane fusion events. Upon wounding (B), calcium enters the cell, causing fusion of intracellular vesicles with each other and the plasma membrane to form a patching membrane (C). Intracellular compartments continue to fuse with both the patch and the plasma membrane distal to the site of damage (D-F). The extracellular face of the patch ruptures outward (E; denoted by the arrowheads) in a process known as “explodosis”; this allows for resolution of a double-membrane structure and formation of a continuous barrier between the cytoplasm and the extracellular environment (F). Membrane fusion and remodeling events occur long after the initial resealing events.

# Figure 11

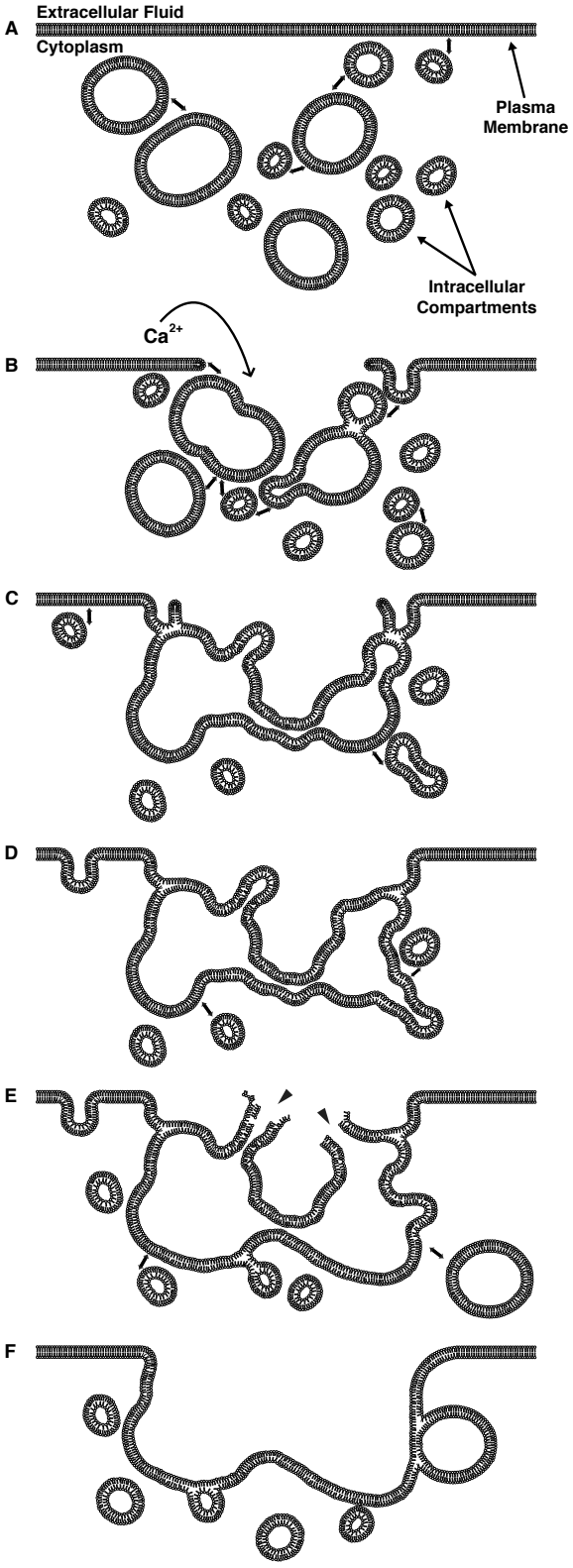
A
Extracellular Fluid
Cytoplasm
Plasma Membrane
Intracellular Compartments
B
$Ca^{2+}$
C
D
E
F

**Movie Legends**

**Movie 1.** A *Xenopus laevis* oocyte wounded in the presence of extracellular Texas Red dextran. From Figure 1A.

**Movie 2**. An oblique view of an oocyte wounded in the presence of extracellular FM 1-43. From Figure 1B.

**Movie 3.** An oblique view of an oocyte wounded in the presence of extracellular FM 1-43. From Figure 1C.

**Movie 4.** An oocyte pre-stained with R18 (red) was wounded in the presence of extracellular Alexa Fluor 488 dextran (green). From Figure 2.

**Movie 5.** An oblique view of a R18-stained (red) oocyte expressing eGFP-PKCβ-C2 (green; probe for phosphatidylserine) that was wounded in the presence of extracellular Alexa Fluor 647 dextran (blue). From Figure 3.

**Movie 6.** An oblique view of an oocyte expressing eGFP-PKCβ-C2 that was wounded in the presence of extracellular Texas Red dextran. From Figure 4, A and A'.

**Movie 7.** An oblique view of an oocyte wounded in the presence of extracellular Texas Red dextran. Focal plane was altered during second half of movie. From Figure 4B.

**Movie 8.** An oblique view of an oocyte wounded in the presence of extracellular Texas Red dextran. Focal plane was altered during second half of movie. From Figure 5A.

**Movie 9.** An oblique view of an oocyte expressing eGFP-PKCβ-C2 that was wounded in the presence of extracellular Alexa Fluor 647 dextran (pseudocolored red). Focal plane begins at cell surface before moving to cell interior. From Figure 5B.

**Movie 10.** An oblique view of a wounded oocyte expressing eGFP-PKCβ-C2. From Figure 6, A and A'.

**Movie 11.** A high resolution *z*-projection of a wounded oocyte expressing eGFP-PKCβ-C2. From Figure 6B.

**Movie 12.** Magnification of Movie 10 along the *xy*-plane. From Figure 7B', left.

**Movie 13.** Magnification of Movie 10 along the *xz*-plane. From Figure 7B', right.

**Movie 14.** A wounded oocyte expressing eGFP-tagged human annexin A1. From Figure 7A.

**Movie 15.** An en face view of an oocyte expressing eGFP-tagged human annexin A1 wounded in the presence of extracellular Texas Red dextran . From Figure 7B.

**Movie 16.** An oblique view of an oocyte expressing eGFP-tagged human annexin A1 wounded in the presence of extracellular Texas Red dextran . From Figure 7, C and C'.

**Movie 17.** mRFP-PKCβ-C1 was used to track diacylglycerol accumulation at wounds. From Figure 8A.

**Movie 18.** mRFP-PKCβ-C1 (red) and eGFP-PKCβ-C2 (green) were used to track diacylglycerol and phosphatidylserine, respectively, at wounds. From Figure 8B.

**Movie 19.** *z*-view of a wounded oocyte expressing mRFP-PKCβ-C1 (red) and eGFP-PKCβ-C2 (green). From the same cell depicted in Figure 8C.

**Movie 20.** GCaMP5G (green) and BFP-PKCβ-C2 (blue) were injected into oocytes to track intracellular calcium after wounding. From Figure 9.

**Movie 21.** A wounded oocyte expressing GCaMP5G (green, probe for $Ca^{2+}$), mCherry-2XrGBD (red, probe for active Rho), and BFP-wGBD (blue, probe for active Cdc42). From Figure 10A.

**Movie 22.** Surface view ($z$ = 0 μm) of a wounded oocyte expressing eGFP-rGBD (green, probe for active Rho) and mRFP-wGBD (red, probe for active Cdc42). The bottom frame is a magnification of eGFP-rGBD signal, shown in grayscale. From Figure 10B, top row.

**Movie 23.** Subcortical view ($z$ = -3 μm) of wounded oocyte expressing eGFP-rGBD (green, probe for active Rho) and mRFP-wGBD (red, probe for active Cdc42). The bottom frame is a magnification of mRFP-wGBD signal, shown in grayscale. Same event as in Movie 21. From Figure 10B, bottom row.

**Discussion**

In this study we sought to explain a centuries-old observation: when the surface (plasma membrane) of a cell is disrupted, a "film" or barrier layer is quickly erected at the site of damage to prevent loss of cytoplasm (see Heilbrunn, 1928, for review of the early literature). Electron microscopy studies suggest that this barrier is at least partly comprised of membranes (e.g. Gingell, 1970; Bluemink, 1972; Krause et al., 1994; Miyake and McNeil, 1995), and in keeping with this notion, a variety of membrane-binding proteins and membrane compartments have been implicated in cell repair (see Moe et al., 2015). However, the cellular mechanisms that lead to barrier formation have remained elusive, giving rise to a variety of models including resealing via exocytosis, endocytosis, scission, aggregation and patching. Our results provide the first direct demonstration of patching: we have visualized fusion of internal compartments with each other at the sites of wounds, we have shown that this results in formation of larger compartments that limit diffusion of fluorescent dextran, and we have shown that these larger compartments are contiguous with the plasma membrane (Figure 11).

Are the observations described here specific to oocytes? That is, are they applicable to other systems or are they merely a consequence of utilizing a large cell with a readily accessible cache of cortical granules, compartments that undergo calcium-dependent membrane fusion at fertilization? The former possibility seems most congruent with the available data. First, as noted above, cortical granules in Xenopus oocytes cannot be stimulated to undergo exocytosis even by exposure to calcium ionophore, a manipulation that triggers rapid exocytosis in Xenopus eggs (e.g. Charbonneau and Grey, 1984). Further, even in eggs, calcium elevation via fertilization or calcium ionophore treatment triggers neither compound exocytosis nor granule-

granule fusion—the fusion event is strictly heterotypic with the granules fusing with the plasma membrane. Thus, the behavior seen following wounding is qualitatively different than what occurs in response to other stimuli, as expected if damage triggers a promiscuous fusion response of internal compartments. Second, cortical granules are not required for repair in later stages of Xenopus development in that Xenopus blastomeres, which lack cortical granules, readily close PM disruptions (Clark et al., 2009). Third, cell types that are commonly regarded as healing slowly, namely invertebrate neurons, display the same wound response hallmarks seen in fast-healing cells: calcium dependence (Yawo and Kuno, 1985), contraction at the wound edge (Krause et al., 1994), and accumulation of vesicles at the site of damage (Eddleman et al., 1997). Fourth, other aspects of the healing response, such as Rho GTPase dependent assembly of actin filaments and myosin-2 at the wound site are conserved across diverse phyla and cell types, both slow and fast healing (Sonnemann and Bement, 2011; Abreu-Blanco et al., 2014). In addition, the pattern of dysferlin recruitment observed in this study is consistent with findings from muscle cells (e.g. Lek et al., 2013; McDade et al., 2014). Thus, we suspect that at least some features of the response observed here will occur in other systems, albeit based on different pools of intracellular compartments.

We also provide evidence that calcium remains locally elevated for several minutes after wounding, confirming earlier reports that even cells that are able to quickly halt the influx of high-molecular weight dextrans nevertheless exhibit increased plasma membrane permeability to ions for minutes (Fein and Terasaki, 2005; Luxardi et al., 2014). In transected axons, calcium concentrations at the cut edge remain elevated into the low millimolar range for approximately a minute (Ziv and Spira, 1995) and elevated above physiological concentrations for over an hour

(Eddleman et al., 2000). Further, even in cultured mammalian cells it has been reported that the wound remains open for several minutes (Jimenez et al., 2014).

These observations are surprising in that it has been assumed that if plasma membrane holes are not immediately and completely resealed, calcium inrush will rapidly kill the cell. However, our results show that after an initial "bloom" of calcium elevation triggered by wounding, the calcium signal rapidly shrinks back until it is tightly confined to a ring overlying the site where the Rho GTPases are active and the majority of the dramatic membrane dynamics are taking place. We suspect this focusing reflects the remarkable capability of cells to sequester and buffer cytosolic calcium (Ziv and Spira, 1993; Allbritton et al., 1992). If so, it follows that extensive vesicle cross-linking by membrane-associated proteins such as annexins (Blackwood and Ernst, 1990), dysferlin (Bansal et al., 2003), MG53 (Cai et al., 2009), or the enigmatic 'tethering factor' (McNeil and McNeil, 2005) in parts of the wound may be sufficient to slow calcium influx to within the range of cellular buffering capacity. Consistent with this notion, we found that tightly packed vesicles appeared to serve as barriers to dextran diffusion in the cytoplasm. Further, we found that human annexin A1 is rapidly recruited to wound sites and extensively labels not only the plasma membrane, but also sites of vesicle-vesicle contact.

In this light, prolonged local elevation of calcium would be viewed as an important feature of the healing process rather than a sign and cause of incipient cell death. That is, protracted calcium elevation at the wound would be analogous to keeping steady pressure on a laceration, i.e. the calcium serves to drive vesicle fusion or/or aggregation to limit loss of material from the cell until the contractile array can be assembled and ingress to heal the defect. This idea is particularly appealing in that calcium elevation is known to be the trigger for Rho

GTPase activation (Benink and Bement, 2005; Abreu-Blanco et al., 2014) and, as shown here, the calcium ring overlaps both the Rho and Cdc42 zone. Moreover, the calcium-dependent kinase PKCβ is required for proper organization of the Rho GTPase activity zones at wounds (Vaughan et al., 2014). Since calcium is also known to drive the production of DAG (Kunkel et al., 2007), a key determinant of PKCβ localization, it appears that post-wound calcium serves as an initial signaling gradient from which subcellular patterns may be formed to assemble the factors needed to drive wound closure.

Our results also provide potential resolutions to two conceptual challenges imposed by the patch hypothesis: how the double membrane compartment predicted by patching is converted into a single membrane and how a membrane patch derived from fusion of one or more intracellular compartments manages to serve as a functioning plasma membrane when (presumably) the proteins and lipids comprising the membranes of the intracellular compartments differ significantly from those of the plasma membrane. With respect to conversion of a double-membrane to a single membrane, the observation of explodosis provides a simple solution: rather than fusing with the plasma membrane (as in exocytosis), some of the patching-generated compartments rupture on their exoplasmic faces leaving a single membrane. With respect to how a patching membrane provides a fully functional replacement for the plasma membrane, we suggest that it doesn't. Instead, we propose that the patching membrane is replaced via the extensive remodeling that begins almost as soon as it is formed and which, based on the results of DAG imaging, continues for 15 min or more after the initial damage. Such a mechanism could work alone or in conjunction with other mechanisms such as scission

mediated by ESCRT proteins (Jimenez et al., 2014) or actomyosin-powered contraction (Sonnemann and Bement, 2011).

Finally, we would add a technical observation to the effect that in spite of our efforts to be thorough in terms of probes employed and imaging regimes, we are almost certainly missing many important events. We base this statement on the fact that essentially every probe we tried revealed something different about the healing process. Even the presumably inert dextran labeled not only compartments that fused with the plasma membrane, but intensely stained mysterious structures that formed in the wound pit. We therefore assume that other sets of probes would reveal additional features of the healing process. Further, because we focused on membrane dynamics within the cell, the remarkable membranous elaborations seen using EM and other approaches (e.g. Bluemink, 1972; Jimenez et al., 2014; Moe et al., 2015; Figure 2) were largely ignored.

## Methods

### *Plasmids*

The probes containing the C1 or C2 domains of *Xenopus laevis* PKCβ were generated as previously described (Yu and Bement, 2007). BFP-PKCβ-C2 was constructed by excising eGFP from eGFP-PKCβ-C2 using BamHI and BspEI and replacing it with BFP. pCMV-GCaMP5G was a gift from Douglas Kim & Loren Looger (Addgene plasmid # 31788). GCaMP5G was subcloned into pCS2+ with BamHI and EcoRI. Human Annexin A1 (accession number BC001275) was obtained from Open Biosystems (Clone 345615) and subcloned into eGFP-pCS2+ using BspE1 and XbaI. The probes for active GTPases, mRFP-wGBD and eGFP-

rGBD, were generated as previously described (Sokac *et al.,* 2003; Benink and Bement, 2005). BFP-wGBD was constructed by excising mRFP from mRFP-wGBD using BamHI and BspEI and replacing it with BFP. mCherry-2xrGBD was constructed by adding an additional rGBD between the BspEI and XhoI sites of mCherry-rGBD. Human dysferlin isoform 1 (accession number NM_003494.3) was obtained from the Jain Foundation and subcloned into eGFP-pCS2+. A FLAG sequence was added by PCR to the N-terminus of eGFP, and the resultant FLAG-eGFP-hDysf construct was subcloned into pFastBac1 using NotI.

***Oocyte Acquisition and Preparation***

Ovarian tissue was procured from *Xenopus laevis* females via surgical procedures approved by the University of Wisconsin-Madison Institutional Animal Care and Use Committee. Tissue was stored in 1X Modified Barth's Solution (88 mM NaCl, 1 mM KCl, 2.4 mM $NaHCO_3$, 0.82 mM $MgSO_4$, 0.33 mM $NaNO_3$, 0.41 mM $CaCl_2$, 10 mM HEPES, pH 7.4; supplemented with 100 µg/mL gentamycin sulfate, 6 µg/mL tetracycline, 25 µg/mL ampicillin) at 16-18°C. Follicle cells were removed from oocytes by enzymatic digestion ([8 mg/mL Type I collagenase; Life Technologies] in 1X Barth's for 1 hour at 16-18°C on 60 rpm rotating plate) followed by manual dissociation with fine forceps. Defolliculated oocytes were stored in 1X Barth's (changed daily) until use.

***mRNA Preparation and Oocyte Microinjection***

Messenger RNAs were transcribed *in vitro* using the mMessage mMachine SP6 Transcription Kit (Life Technologies) followed by purification using RNeasy Mini Kit (Qiagen)

per manufacturer's instructions. Transcript size was verified on 1% agarose/formaldehyde denaturing gels versus Millennium Marker (Life Technologies) molecular weight standard. Oocytes were injected while in 1X Barth's with a 40 nL injection volume. Cells were allowed to recover at least 30 minutes between injections. Probes for active GTPases (wGBDs and rGBDs) were each injected a final needle concentration of 125-167 μg/mL. eGFP-AnnexinA1 was injected at 50-100 μg/mL. GCaMP5G was injected at 125 μg/mL. eGFP-, and BFP-PKCβ C2 were injected at 50 μg/mL. eGFP- and mRFP-PKCβ C1 was injected at 250-500 μg/mL. FLAG-eGFP-hDysf was injected at 1.5 μM, corresponding to a needle concentration of 400 μg/mL. Injected oocytes were stored in 1X Barth's at 16-18°C and mRNAs allowed to express for 24 hours prior to imaging. Oocytes injected with FLAG-eGFP-hDysferlin were allowed to recover for at 24 hours prior to imaging.

***Cell Labelling***

Cellular membranes were labeled by 30-60 minute pre-incubation with octadecyl rhodamine B chloride (R18) or N-(3-triethylammoniumpropyl)-4-(4-(dibutylamino)styryl)pyridinium dibromide (FM1-43) at 1 μM or 5-20 μM in 1X Barth's, respectively. Fluorescent dextrans were added to 1X Barth's , at 10-100 μM final concentration, 10-60 minutes prior to wounding; dextran sizes were 3,000 Da (Texas Red dextran) or 10,000 Da (Oregon Green 488 and Alexa Fluor 647 dextrans).

***Purification of Recombinant Proteins From Insect Cells***

Dysferlin constructs in pFastBac1 were transformed into DH10Bac competent *E. coli* (Thermo Fisher Scientific) and positive clones selected by blue/white screening. Recombinant bacmids were isolated and subsequently transfected into *Sf9* cells using Cellfectin II reagent (Thermo Fisher Scientific). Highly expressing clones were selected and virus amplified for two additional generations. *Sf9* cells ($2.2 \times 10^7$ per plate) were infected with high titer baculovirus and allowed to incubate for 72 hours at 27°C. Infected cells were collected by centrifugation (5 minutes at 500 x g) and stored at -80°C until protein purification.

Baculovirus-infected *Sf9* cell pellets were resuspended in 5 volumes of solubilization buffer (1X PBS pH 7.5, 1% v/v Triton X-100, 0.5 µg/mL Leupeptin, 0.5 µg/mL Aprotinin, 0.5 µg/mL Pepstatin A, 40 µg/mL PMSF, 100 µg/mL Benzamidine, 0.5 µg/mL E64) and incubated at 4°C for 1 hour with gentle end-over-end mixing. Lysates were clarified by centrifugation at 21,100 x g for 15 min. The supernatant was incubated in batch format with anti-FLAG-M2 agarose beads (Sigma) for 1 hour at 4°C prior to adding to a column. The column was washed with 3 x 10 column volumes of wash buffer (1X PBS pH 7.5, 40 µg/mL PMSF, 100 µg/mL benzamidine) and recombinant protein was eluted with 1M arginine, pH 4.4 into an equal volume of collection buffer (50 mM HEPES pH 8.5, 200 mM KCl, 80 µg/mL PMSF, 200 µg/mL benzamidine). Elution fractions were separated by SDS-PAGE (4-12% gradient gel) followed by Coomassie Brilliant Blue staining. Desired fractions were pooled and concentrated using 100K MWCO Amicon Ultra-15 filters (Millipore). The buffer was exchanged in-filter to remove residual arginine to final conditions compatible with downstream applications (25 mM HEPES pH 7.5, 100 mM KCl, 10% glycerol). The purity and concentration of the recombinant proteins

were determined by SDS-PAGE and BCA Assay (Pierce), respectively. Aliquots were snap-frozen in liquid nitrogen prior to storage at -80°C.

***Image Acquisition, Wounding, and Data Analysis***

Laser Scanning and Swept Field confocal microscopy was performed using Nikon Eclipse Ti inverted microscopes and Nikon 60X CFI Plan APO oil objectives (1.4 NA) with either Prairie Point Scanner or Opterra Multipoint confocal systems (Bruker). Cells were wounded with illumination from a 488 nm uncaging laser (Bruker) or 440 nm dye laser setup pumped by a MicroPoint 337 nm nitrogen laser (Andor). The wounding laser is nominally diffraction limited, manually activated for ~1 sec with a ~5-10 Hz repetition rate, and the source laser (per manufacturer specifications) has a maximal output of 400 μJ/pulse. Imaging data were processed using Fiji (Schindelin *et al*., 2012) and Volocity (Perkin-Elmer). The line scan in Figure 10A' was made in Fiji by performing a radial reslice around the wound center and making an average intensity projection of the resultant stack. The fluorescence intensity along the line extending from the wound center was plotted in Prism 5 (GraphPad). Each channel was normalized such that the maximum and minimum fluorescence intensity values for that channel became 100% and 0%, respectively. All of the results reported here were representative of 20 to >100 wounds. Moreover, the membrane behaviors reported here including exocytosis, patching and explodosis were repeatedly observed with 3-5 different probes (e.g. exocytosis was revealed by dextrans, FM 1-43, wGBD and rGBD; patching was strongly revealed by C2, C1, and GFP-annexin, and weakly revealed by R18 and explodosis was revealed by C2, C1, GFP-annexin and wGBD). Thus, while we cannot exclude the possibility that some probes (e.g. dextran) altered

the wound response in some way, we can say with consequence that none of these behaviors were a consequence of having a particular probe (e.g. dextran) present during wounding.

# Chapter 5

Conclusions

Cells frequently undergo shape changes that require polarization of subcellular components (Bement and von Dassow, 2014; Ngok *et al.,* 2014). Precise mechanistic explanations for how many of the molecular patterns accompanying polarization events can be generated, sculpted, and spatially maintained within a shared cytoplasm remain surprisingly elusive. The results presented in this dissertation reflect my efforts to characterize the mechanism behind a critical, evolutionarily-conserved example of subcellular pattern formation: wound repair.

In Chapter 2, I described my continuation of a candidate screen to identify Rho GTPase regulators responsible for activation and segregation of distinct subcellular Rho GTPase activity zones in *Xenopus laevis* oocytes. I identified two such regulators, RhoGAP1 and RhoGAP8, that appear to be responsible for defining the width of the Rho activity zone. In Chapter 3, I extended my characterization of RhoGAP1 and RhoGAP8 to examine their role in embryonic wound repair. I discovered that both RhoGAP1 and RhoGAP8 localize to the leading edge of multicellular wounds. Further, loss of RhoGAP1 in embryos leads to an increase in F-actin and gastrulation defects, suggesting a role for RhoGAP1 in regulating morphogenesis. Lastly, Chapter 4 details how intracellular compartments can be combined at wounds to create a temporary barrier between the cytoplasm and extracellular environment, therein providing what appears to be the first direct visual confirmation of the "patch hypothesis" (Terasaki *et al*., 1997; McNeil *et al*., 2000). Further, high-speed microscopy revealed distinct subcellular localization of membranous compartments, membrane lipids, and intracellular calcium. Here, I address some open questions raised by my results, suggest future lines of inquiry, and discuss the broader impact of my work on studies of wound repair and GTPase regulation.

***Localization of RhoGAP1 and RhoGAP8***

What is the basis for the distinct wound-induced localization of RhoGAP1 and RhoGAP8 (i.e. between the zones of active Rho and Cdc42)? In addition to localizing to single- (Chapter 2, Figure 2) and multicellular wounds (Chapter 3, Figure 3), RhoGAP1 and RhoGAP8 localize to the cytokinetic ring during polar body emission (unpublished results), a process that requires concentric zones of active Rho and Cdc42 (Ma *et al.*, 2006). It remains to be seen whether this localization pattern is reflected in other systems or processes, but the reports of RhoGAP1 localization at the leading edge of migrating cells (Shen *et al.,* 2008) and the existence of distinct GTPase activity zones in that very location (Machacek *et al.,* 2009; Martin *et al.,* 2016) lends credence to this possibility. Wounds in *X. laevis* oocytes produce GTPase activity zones that are larger, more homogenous, and more persistent than those found in other contexts (Benink and Bement, 2005; Machacek *et al.,* 2009), thereby providing an excellent system to study the mechanisms that control this distinct localization pattern.

Endosomal localization of Rho GTPase regulators appears to be common (McCrea *et al*., 2008; Mori *et al*., 2014; Steenblock *et al.*, 2014). Of note, delivery of Rab11-positive vesicles is required for properly localized Rac activity during protrusion in *Drosophila* S2 cells (Ramel *et al.,* 2013); however, a specific Rac regulator was not identified. Nevertheless, the results align with a model (Chapter 3) where endosomes serve as a "reservoir" that allows for delivery of a regulator to its target only when it is needed. The signals that mediate the intracellular distribution of RhoGAP1 and RhoGAP8 remain elusive; the three possible localization states (endosomal, cytoplasmic, and plasma membrane) is suggestive of multiple layers of regulation.

***Control of the Zone of Active Rho by RhoGAP1 and RhoGAP8***

What are the functional consequences of RhoGAP1 and RhoGAP8 modulating Rho zone width during wound repair? Our current model suggests that by limiting the outward spread of the Rho zone, RhoGAP1 and RhoGAP8 likely keep Abr from spreading outward, thereby preserving the Cdc42 zone (Vaughan *et al.,* 2011). Active Cdc42 has a role in promoting assembly of wound-associated actin (Benink and Bement, 2005), which due to positive feedback from a putative as-of-yet unidentified GEF (Vaughan *et al.,* 2011; Burkel *et al.,* 2012; Simon *et al.,* 2013), helps organize the GTPase activity treadmill (Burkel *et al.,* 2012).

Another possible consequence of modulating Rho zone width is the rate of wound closure. Preliminary results suggest that wounds in *X. laevis* oocytes with narrow Rho zones due to low-level overexpression of RhoGAP1 (e.g., Chapter 2, Figure 8) close faster than those made in control cells (unpublished results). There is some evidence for this phenomenon in another Rho-dependent process, cytokinesis. MgcRacGAP, a GAP for Rho, is responsible for confining RhoA activity to the cytokinetic furrow (Miller and Bement, 2009) and overexpression of MgcRacGAP not only narrows the zone of active Rho (Miller and Bement, 2009), but also increases the speed of cytokinetic apparatus ingression (William Bement, personal communication). A zone narrowing phenotype, and any potential increase in speed, is likely highly sensitive to GAP concentration; that is, above a critical threshold, the Rho inactivation rate would outstrip that of any potential activation by RhoGEF (Ect2 for cytokinesis [Tatsumoto *et al.,* 1999], Abr for wound repair [Vaughan *et al.*, 2011]) and cause collapse of the Rho zone, as I observed with high-level RhoGAP1 overexpression (e.g., Chapter 2, Figure 4).

How could RhoGAP1, a Rho inactivator, increase the rate of a Rho-dependent process? One possible explanation for this observation is that as a consequence of less Rho activity, there may be less myosin-2 activity at the wound edge; this could lead to a more constructive contraction (i.e. motors not working against each other), thereby leading to more rapid closure. Consistent with this possibility, overexpression of constitutively-active Rho, which increases myosin contractility, inhibits closure of the wound array (Benink and Bement, 2005).

One prediction from RhoGAP1-induced Rho zone narrowing would be increased turnover of Rho at the trailing edge of the Rho zone. I propose (both paradoxically and perhaps heretically) that localized Rho inactivation, rather than activation per se, is the driver of wound closure. That is, the position of RhoGAP1 at the trailing edge of the Rho zone acts as a "fence" to increase the pool of inactive Rho, allowing RhoGDI to extract Rho from the plasma membrane and redistribute it back to the Rho zone. This continual focusing would allow for efficient, and therefore rapid, application of force at the wound edge, as described above. This hypothesis is supported by three suspicious coincidences worth considering: the onset of wound array ingression occurs at approximately the same time as Rho zone spatial turnover bias begins (Burkel *et al.,* 2012; my unpublished results), spatial bias in Rho turnover does not occur until approximately the time that RhoGAP1 localizes to wounds (Burkel *et al.,* 2012; Chapter 2, Figure 2F), and multicellular wound arrays do not ingress until after RhoGAP1 and RhoGAP8 localize to the wound edge (Chapter 3, Figure 3).

A striking feature of the wound array itself may present the means to test the above hypothesis: non-circular (elliptic) wounds ingress faster along their long axis (Mandato and Bement, 2001). By examining Rho zone width and turnover rates (Burkel *et al.,* 2012) with

respect to ingression velocity at various regions around non-circular wounds, it should be possible to examine the link between GTPase turnover and wound closure rates. These experiments and further analysis of wound closure rates in cells overexpressing RhoGAP1 are subjects of future study and have broad implications for other Rho GTPase-dependent processes.

***Robustness***

Perhaps one of the most remarkable, yet overlooked, features of wound repair is robustness. Wound robustness refers not to the impressive scale with which a response can be mounted to recover from removal of significant portions of plasma membrane (Bement and Capco, 1991; Terasaki *et al.,* 1997), but rather the resiliency of the process to perturbations that would disrupt or halt other processes capable of altering cell morphology (e.g., cytokinesis). For example, blebbistatin, a potent inhibitor of myosin-2 (Straight *et al.,* 2003) can halt cytokinesis but is only capable of slowing wound repair (Burkel *et al.,* 2012).

What is the basis of wound robustness? Some of it may be a result of necessity - wound repair is an emergency response and needs to be accomplished quickly with the cellular components on hand. This is much different than cell division that can halt for long periods of time as observed, for example, when cells have not satisfied the spindle assembly checkpoint. Of course, the outcomes have different requirements - cell division requires fidelity, whereas wound repair likely requires speed. Additional robustness may derive from functional redundancy; that is, multiple regulators may be localized at the wound to perform a particular function - RhoGAP1 and RhoGAP8 seem to fall into that category.

The conservation of the single-cell wound response, both mechanistically and with respect to the molecular participants across many taxa (reviewed in Sonnemann and Bement, 2011) suggests that repair is an ancient process. Furthermore, the first single-cell organisms would have been subject to similar stresses as modern life; thus, some of the aforementioned robustness in the wound response may have ancient origins. For example, the amoeba *Dictyostelium* has been reported to not require myosin for wound repair (Yumura *et al.,* 2014), or even cytokinesis (Neujahr *et al.*, 1997). Similar results were observed in animal cells, with respect to both cytokinesis (Ma *et al.,* 2012) and wound repair (Burkel *et al.,* 2012). Rather, it appears that actin crosslinking, and not myosin motor activity per se, is necessary for ingression of the cytoskeletal array (Weber *et al.,* 1999; Ma *et al.,* 2012); myosin activity likely serves to focus the contractile arrays and make their ingression more efficient (Burkel *et al.,* 2012). It is currently unknown if other actin crosslinkers associate with the wound array.

What are the minimal cellular components needed to mount a wound response? Given the aforementioned functional redundancy within the wound response and use of wound components in other cellular functions, it may be difficult to determine in an *in vivo* model. Yet, armed with approximate concentrations of the relevant proteins in *X. laevis* eggs (Wühr *et al.,* 2014) and the ability to produce recombinant proteins in an eukaryotic system (Chapters 2 and 4), it may be possible to reconstitute key components of the wound response (e.g., Rho GTPase signal treadmills) on supported lipid bilayers (Castellana and Cremer, 2007). An *in vitro* model of wound repair would be a powerful tool to dissect the complex and dynamic processes occurring at the wound array, and thus might inform cytoskeletal rearrangements in other contexts (e.g., cell motility and cytokinesis).

A technical hurdle that will need to be overcome to improve on previous *in vitro* studies of GTPase regulator function is the production and use of prenylated GTPases. Most GEF or GAP assays, including the one used in my studies (Chapter 2), utilize recombinant GTPases purified from bacteria, which lack the necessary enzymes to post-translationally modify the GTPases. As such, the GTPases are unable to associate with membranes, which may alter the substrate specificity of GEFs or GAPs (e.g. Molnár *et al.,* 2001). Thus, to produce a physiologically relevant reconstitution, the most faithfully reproduced components will be necessary. Towards this end, significant progress has been made in producing *X. laevis* Rho GTPases (Kevin Sonnemann, personal communication).

A glaring deficiency of wound repair studies is the assessment of efficacy of the damage response. That is, what comprises a "good" wound response? Is it the speed with which a wound is closed, the strength of a wound to withstand subsequent forces on the cell, or the ability to cope with multiple wounds? After all, the sarcomeric degeneration that defines muscular dystrophies does not result from a single membrane deficiency or wounding event; rather, it represents the cumulative effects of repeated events that lead to loss of dystrophic tissues. Most single-cell wound repair studies have only tracked the ingression of the wound for several minutes (e.g., Benink and Bement, 2005; Vaughan *et al.,* 2011; 2014), and two that tracked repair for longer (overnight; Clark *et al.,* 2012; Vaughan *et al.,* 2014) were only assessing cellular viability. As a result, many potential wound regulators may have been overlooked merely because they failed to mount an immediate response (i.e. within ~5 minutes). It would be intriguing to reexamine, at high resolution, the wound many hours after damage to determine the

process by which the contractile array is disassembled and the cortex restored to its pre-wounded state.

***Calcium at Wounds***

Based on the results presented in Chapter 4 (Figures 8-10) and other studies (Ziv and Spira, 1993;1995; Eddleman *et al.,* 1997; 1998; Luxardi *et al.*, 2014), there is significant evidence that intracellular calcium remains elevated throughout the repair process, even in cells that are thought to heal quickly. Does the sustained intracellular calcium reflect defects within the plasma membrane (PM), or does it suggest passage of calcium through ion channels? With respect to the former, the rapidity with which fluorescent dextrans are excluded from the cytoplasm at sites of damage (Chapter 4, Figures 1-4) suggests a barrier is quickly erected at the sites of wounds. While this does not preclude calcium permeability of the patching membrane, in that dextrans are much larger than calcium ions, the sustained calcium at the wound appears to be primarily focused on the contractile array, outside of the nascent patch (Chapter 4, Figure 10). This suggests that the majority of wound-associated calcium in *X. laevis* is passing through ion channels.

In addition to the extracellular media, there are two major intracellular sources of calcium: the endoplasmic reticulum (ER) and mitochondria. Resident proteins from both the ER and mitochondria have been identified in wound proteome screens (Mellgren, 2010; Sharma *et al.,* 2012). However, given that both compartments are in close proximity to the PM (Gingell 1970; Giordano *et al.,* 2013), this association may be incidental rather than from active participation in the wound repair process. Further, it is currently unclear whether the initial

calcium "bloom" seen at wounds (Chapter 4, Figure 9) reflects influx of extracellular calcium, release from intracellular stores, or a combination of the two.

The ring of intracellular calcium at wounds displays a striking behavior: it moves inward with the contractile array (Chapter 4, Figures 9 and 10). Since calcium is diffusible (albeit in a very limited way; see Allbritton *et al.,* 1992) within the cytoplasm, this suggests that either the wound array is transiently activating calcium channels as it ingresses (e.g. Yatani *et al.,* 2005) or that the source of calcium is physically linked to the closing wound. In keeping with the latter possibility, the close proximity of the ER, the primary intracellular calcium store, to the wound array and its associated ring of calcium is striking. Two proteins of note are known to link the PM to the ER: the extended synaptotagmins (E-syts) and stromal interaction molecule 1 (STIM1). E-syts are ER integral membrane proteins that possess cytosolic C2 domains; the C2 domains of E-syts can bind plasma membrane $PI(4,5)P_2$ in a calcium-dependent manner (Giordano *et al.,* 2013). STIM1, another ER integral protein, acts as $Ca^{2+}$ sensor for the ER lumen; when lumenal $Ca^{2+}$ drops, STIM dimerizes and binds to the PM $Ca^{2+}$ channel Orai1, thereby activating influx of extracellular calcium to replenish ER $Ca^{2+}$ stores (Liou *et al.,* 2007).

Thus, I propose the following model to explain calcium dynamics during wound repair: wound events above a certain threshold (the product of size, time required for patching, and extracellular calcium concentration) are able to trigger calcium-induced calcium release from the ER (reviewed in Endo, 2009), resulting in the broad calcium "bloom" commonly seen at wounds (Chapter 4, Figures 9-10). The release of calcium from the ER locally depletes lumenal stores, triggering store-operated calcium entry through the PM (see Parekh and Putney, 2005) by STIM1-mediated activation of the $Ca^{2+}$ channel Orai1 (Liou *et al.,* 2007). The PM-ER linkage is

further strengthened by calcium-induced binding of E-syts to $PI(4,5)P_2$, a membrane lipid known to be enriched in wounds (Vaughan *et al.,* 2014). The calcium passing across the PM is transiently exposed to the cytoplasm before getting pumped into the ER (Montero *et al.,* 1993), allowing for interaction with wound-associated calcium binding proteins. The physical ER-PM linkage ensures that the calcium ring is in the correct location to most efficiently drive ingression of the contractile array. Dissolution of the ER-PM complex at the end of wound repair may result from lipid remodeling that occurs upon wound closure (Chapter 4, Figure 8).

While the above model is speculative, its plausibility is supported by several lines of evidence. Mainly, the coincidence that $Mg^{2+}$ is inhibitory to cell repair (Steinhardt *et al.,* 1994), and has also been shown to be an inhibitor of both ER and PM $Ca^{2+}$ channels (Meissner *et al.,* 1986; Delpianoa and Altura, 1996). However, it must be noted that this may also represent an inhibition of SNARE-mediated fusion events (Park *et al.,* 2015), which have shown to be required for successful wound repair (Steinhardt *et al.,* 1994; Bi *et al.,* 1995; Shen *et al.,* 2005). Further, preliminary results indicate that *X. laevis* E-Syt2A is concentrated at wounds (unpublished results). Both the relative ease with which cellular calcium dynamics can be manipulated (either pharmacologically or by altering composition of the extracellular media; Parekh and Putney, 2005; Endo, 2009) and dearth of knowledge with respect to wound-induced calcium elevation warrants further investigation in *X. laevis.*

As discussed in Chapter 1, the wound response is physically scalable, i.e. able to respond to wounds both large and small. This scalability also appears to have a molecular basis; for example, some small wounds do not elicit a conspicuous response (e.g. GTPase activation or contraction). These events may represent a rapid sealing of the defect (Chapter 4) that limits

calcium entry to subthreshold levels (Steinhardt *et al.,* 1994). Many wounds that are slightly larger, and thereby able to activate the Rho GTPases, nevertheless close faster than what is required to observe RhoGAP1 and RhoGAP8 recruitment (unpublished results). Thus, it appears the subcellular patterns generated at wounds are similar to many seen in morphogen signaling during embryonic development; that is, the response to stimulus is dependent on duration of signal (Yan and Lin, 2009). While many signals are generated at wounds (Benink and Bement, 2005; Vaughan *et al.,* 2011; 2014), calcium influx appears to be the primary driver of wound repair. Thus, the longer calcium signal is maintained, the more downstream signals will be generated.

Another similarity between multicellular- and single-cell pattern formation is the generation of signaling gradients. The results from Chapter 4 (Figure 9) suggest a steep calcium gradient exists at the wound array; the C2 probe (Yu and Bement, 2007; calcium affinity of 5 μM, Kohout *et al.,* 2002) is recruited to a more-refined ring than GCaMP5G (Akerboom *et al.,* 2012; calcium affinity of 460 nM). Use of other genetically-encoded calcium sensors along a range of calcium-binding affinities (e.g., Wu *et al.,* 2013; Suzuki *et al.,* 2014) could further refine our understanding of wound-associated calcium and explain the localization and behavior of other proteins known to participate in wound repair (Moe *et al.,* 2015).

### *Impact of these Results on Further Wound Repair Studies*

The results presented in Chapter 4 may influence the design of future studies that add cell-impermeant compounds to extracellular media to assess their effects on wound repair. Given the rapidity with which a barrier is erected between the cytoplasm and the extracellular

space, it may not be possible to see an effect from a drug, as it may not have enough time to encounter their presumptive targets. Thus, it may be necessary to use cell-permeant alternatives or inject the drug into the cell before wounding (e.g., Burkel *et al.,* 2012) to see an effect. Further, it may be difficult to draw comparisons to pharmacological treatments in other cell types (e.g., Cai *et al.,* 2009a), as the resealing rate may be slower, thus allowing greater access of extracellular materials to the cytoplasm.

The effects of overnight overexpression (both wild-type and putative dominant negative forms) of constructs expressed from injected mRNA should be considered prior to drawing conclusions from phenotypes. This was perhaps most evident in overexpression of the C-terminal fragment of RhoGAP1 (Chapter 2, Figure 4). As noted in Chapter 2, the GAP domain of RhoGAP1 is quite potent *in vivo,* requiring ~1% of the injected mRNA than that of the full-length construct to elicit a similar phenotype (i.e. loss of the Rho zone and disorganization of the Cdc42 zone). It was incredibly difficult to wound oocytes overexpressing the C-terminus, likely as a result of global loss of tension by inhibition of actomyosin contraction. Thus, it may often be difficult to determine whether the observed phenotypes result from localized activity of the injected construct or are rather due to global defects in the cytoskeleton due to overnight overexpression. It may then be helpful to inject recombinant protein (like those purified in Chapters 2 and 4) immediately prior to imaging to reduce the chances of off-target effects. This approach has the added benefit confirming *in vitro* activity of recombinant proteins and would allow for greater control the amount of exogenous protein the cell encounters as it will not be dependent on time, as is injection of mRNAs.

***"Big data"***

If a picture is worth a thousand words, then what of an image sequence consisting of 12 *z*-sections collected over 500 time points? When the added complexity of three separate image channels is considered, the resulting number quickly becomes astronomical. Thus is the dilemma we face with the high acquisition rates capable with swept field microscopy (Chapter 4; Bembenek *et al*., 2007; Castellano-Munoz *et al*., 2012; Ponomareva *et al.,* 2016). While compressing the data (e.g., maximum intensity projections in *z*) may help in some cases, some distinct behaviors that occur at different focal planes (e.g. Chapter 4, Figure 10B) may be lost during the process. Therefore, while our wound repair studies are by no means "high-throughput," we are quickly approaching a point where our ability to collect data has surpassed our ability to process and analyze. As a result, new methods to increase the rate of image processing are needed.

Current efforts from our lab to automate image analysis have the potential to not only expedite the workflow, but to also allow us to draw relationships between wound parameters (e.g., zone width or rate of closure) throughout the entire wound repair process. In short, the method requires the user to roughly encircle where a target is localized and, from that initial input step, the computer can determine the localization of said target for all time points in a movie (Matt Larson and Alison Moe, personal communication). This is in contrast to previous studies of wound repair, which compared one or two time points per manipulation by manually-derived measurements (Chapter 2, Benink and Bement, 2005; Burkel *et al.,* 2007; 2012; Vaughan *et al.,* 2011; 2014). Further, the improved image processing techniques can also be adapted to

extract features from specific focal planes. These techniques should allow us to discern subtleties in wound behavior that have previously eluded us.

Modeling has become a powerful tool for understanding Rho GTPase zone dynamics in transient contractile arrays (Bement *et al.,* 2006; 2015; Simon *et al.,* 2013; Holmes *et al.,* 2015). Not only is modeling able to confirm or explain *in vivo* results, but it can reveal conditions or novel features that must be present to explain observed behavior at the wound array (e.g., Simon *et al.,* 2013). Yet, a model is only as powerful as the parameters used to generate it; in this regard, recent progress in determining intracellular protein concentrations (unpublished results; see also Wühr *et al.,* 2014), biochemical properties (Chapter 2, Figure 1; Burkel *et al.*, 2012), and localization of targets at the wound array (see above) has generated data that will advance our efforts to make a more physiologically relevant, and therefore useful, *in silico* wound array model.

***Parting Thoughts***

"Curiouser and curiouser!" - Alice, in *Alice's Adventures in Wonderland* by Lewis Carroll

The wound repair response is far more complex that we could have ever imagined. Every new probe used to examine a particular process at wounds inevitably raises more questions than it answers. Further, new imaging technologies are allowing us to clearly visualize novel or poorly-characterized processes, such as explodosis and patching (Chapter 4). Using *X. laevis* as a model for wound healing continues to prove its value, not only for its insight into the repair process, but also for dissecting key components of other transient contractile arrays. The results I presented in this dissertation exemplify that point; Chapter 4 describes, with perhaps best clarity

to date, the myriad of events and cellular components utilized to repair plasma membrane defects, whereas Chapters 2 and 3 characterize two Rho GTPase regulators at wounds that likely regulate cytoskeletal rearrangements in other vital cellular processes. These results, and other recent discoveries from our lab, have the potential to make widely-applicable contributions to our field. As such, I look forward to future wound repair studies with great enthusiasm.

## References

Abreu-Blanco MT, Verboon JM, Parkhurst SM (2011). Cell wound repair in Drosophila occurs through three distinct phases of membrane and cytoskeletal remodeling. *J Cell Biol* **193**:455-64.

Abreu-Blanco MT, Verboon JM, Liu R, Watts JJ, Parkhurst SM (2012). Drosophila embryos close epithelial wounds using a combination of cellular protrusions and an actomyosin purse string. *J Cell Sci* **125**(24):5984-97.

Abreu-Blanco, MT, Verboon JM, Parkhurst SM (2014). Coordination of Rho family GTPase activities to orchestrate cytoskeleton responses during cell wound repair. *Curr Biol* **24**(2):144–155.

Adamson P, Paterson HF, Hall A (1992). Intracellular localization of the P21 rho proteins. *J Cell Biol* **119**(3):617–627.

Aghazadeh B, Lowry WE, Huang XY, Rosen MK (2000). Structural basis for relief of autoinhibition of the Dbl homology domain of proto-oncogene Vav by tyrosine phosphorylation. *Cell* **102**:625–633.

Ahn YH, Gibbons DL, Chakravarti D, Creighton CJ, Rizvi ZH, Adams HP, Pertsemlidis A, Gregory PA, Wright JA, Goodall GJ, Flores ER, Kurie JM (2012). ZEB1 drives prometastatic actin cytoskeletal remodeling by downregulating miR-34a expression. *J Clin Invest.* **122**(9): 3170-83.

Akerboom J, Chen TW, Wardill TJ, Tian L, Marvin JS, Mutlu S, Calderón NC, Esposti F, Borghuis BG, Sun XR, *et al.* (2012). Optimization of a GCaMP calcium indicator for neural activity imaging. *J Neurosci* **32**(40):13819-40.

Alfaro-Aco R, Petry S (2015). Building the Microtubule Cytoskeleton Piece by Piece. *J Biol Chem* **290**(28):17154-62.

Allbritton NL, Meyer T, Stryer L (1992). Range of messenger action of calcium ion and inositol 1,4,5-trisphosphate. *Science* **258**(5089):1812–5.

Amann KJ, Pollard TD (2001). The Arp2/3 complex nucleates actin filament branches from the sides of pre-existing filaments. *Nat Cell Biol* **3**(3):306-10.

Andersen OS, Koeppe RE 2nd (2007). Bilayer thickness and membrane protein function: an energetic perspective. *Annu Rev Biophys Biomol Struct* **36**:107–130.

Andrade D, Rosenblatt J (2011). Apoptotic regulation of epithelial cellular extrusion. *Apoptosis* **16**:491–501.

Andrews NW, Almeida PE, Corrotte M (2014). Damage control: cellular mechanisms of plasma membrane repair. *Trends Cell Biol* **24**(12):734-42.

Andrews NW, Perez F (2015). The plasma membrane repair shop: Fixing the damage. *Semin Cell Dev Biol* **45**:1.

Antunes M, Pereira T, Cordeiro JV, Almeida L, Jacinto A (2013). Coordinated waves of actomyosin flow and apical cell constriction immediately after wounding. *J Cell Biol* **202**(2): 365-79.

Aravind L, Neuwald AF, Ponting CP (1999). Sec14p-like domains in NF1 and Dbl-like proteins indicate lipid regulation of Ras and Rho signaling. *Curr Biol.* **9**(6):R195-7.

Arun SN, Xie D, Howard AC, Zhong Q, Zhong X, McNeil PL, Bollag WB (2013). Cell wounding activates phospholipase D in primary mouse keratinocytes. *J Lipid Res* **54**(3):581–591.

Baek SH, Kwon YC, Lee H, Choe KM (2010). Rho-family small GTPases are required for cell polarization and directional sensing in Drosophila wound healing. *Biochem Biophys Res Commun* **394**(3):488-92.

Bansal D, Miyake K, Vogel SS, Groh S, Chen CC, Williamson R, McNeil PL, Campbell KP (2003). Defective membrane repair in dysferlin-deficient muscular dystrophy. *Nature* **423**:168-72.

Barak LS, Yocum RR (1981). 7-Nitrobenz-2-oxa-1,3-diazole (NBD)--phallacidin: synthesis of a fluorescent actin probe. *Anal Biochem* **110**(1):31-8.

Barfod ET, Zheng Y, Kuang WJ, Hart MJ, Evans T, Cerione RA, Ashkenazi A (1993). Cloning and expression of a human CDC42 GTPase-activating protein reveals a functional SH3-binding domain. *J Biol Chem* **268**(35):26059-62.

Bembenek JN, Richie CT, Squirrell JM, Campbell JM, Eliceiri KW, Poteryaev D, Spang A, Golden A, White JG (2007). Cortical granule exocytosis in C. elegans is regulated by cell cycle components including separase. *Development* **134**:3837-48.

Bement WM (1992). Signal transduction by calcium and protein kinase C during egg activation. *J Exp Zool* **263**:382-97.

Bement WM, Capco DG (1991). Analysis of inducible contractile rings suggests a role for protein kinase C in embryonic cytokinesis and wound healing. *Cell Motil Cytoskeleton* **20**(2): 145–57.

Bement WM, von Dassow G (2014). Single cell pattern formation and transient cytoskeletal arrays. *Curr Opin Cell Biol* **26**:51-59.

Bement WM, Forscher P, Mooseker MS (1993). A novel cytoskeletal structure involved in purse string wound closure and cell polarity maintenance. *J Cell Biol* **121**(3):565–578.

Bement WM, Mandato CA, Kirsch, MN (1999). Wound-induced assembly and closure of an actomyosin purse string in Xenopus oocytes. *Curr Biol* **9**(11):579-87.

Bement WM, Benink HA, von Dassow G (2005). A microtubule-dependent zone of active RhoA during cleavage plane specification. *J Cell Biol* **170**(1):91–101.

Bement WM, Miller AL, von Dassow G (2006). Rho GTPase activity zones and transient contractile arrays. *Bioessays* **28**(10):983-93.

Bement WM, Leda M, Moe AM, Kita AM, Larson ME, Golding AE, Pfeuti C, Su KC, Miller AL, Goryachev AB, von Dassow G (2015). Activator-inhibitor coupling between Rho signalling and actin assembly makes the cell cortex an excitable medium. *Nat Cell Biol* **17**(11):1471-83.

Benink HA, Bement WM (2005). Concentric zones of active RhoA and Cdc42 around single cell wounds. *J Cell Biol* **168**(3):429-39.

Berridge MJ (1984). Inositol trisphosphate and diacylglycerol as second messengers. *Biochem J* **220**(2):45–360.

Bi GQ, Alderton JM, Steinhardt RA (1995). Calcium-regulated exocytosis is required for cell membrane resealing. *J Cell Biol* **131**(2):1747–58.

Bishop AL, Hall A (2000). Rho GTPases and their effector proteins. *Biochem J* **348**(2): 241–255.

Blackwood RA, Ernst JD (1990). Characterization of Ca2(+)-dependent phospholipid binding, vesicle aggregation and membrane fusion by annexins. *Biochem J* **266**:195-200.

Bluemink JG (1972). Cortical wound healing in the amphibian egg: an electron microscopical study. *J Ultrastruct Res* **41**(1):95-114.

Borena BM, Martens A, Broeckx SY, Meyer E, Chiers K, Duchateau L, Spaas JH (2015). Regenerative Skin Wound Healing in Mammals: State-of-the-Art on Growth Factor and Stem Cell Based Treatments. *Cell Physiol Biochem* **36**(1):1-23.

Boulter E, Garcia-Mata R, Guilluy C, Dubash A, Rossi G, Brennwald PJ, Burridge K (2010). Regulation of Rho GTPase crosstalk, degradation and activity by RhoGDI1. *Nat Cell Biol* **12**(5): 477-83.

Bretscher A, Edwards K, Fehon RG (2002). ERM proteins and Merlin: Integrators at the cell cortex. *Nat Rev Mol Cell Biol* **3:**586–599.

Breznau EB, Semack AC, Higashi T, Miller AL (2015). MgcRacGAP restricts active RhoA at the cytokinetic furrow and both RhoA and Rac1 at cell-cell junctions in epithelial cells. *Mol Biol Cell* **26**(13):2439-55.

Brock J, Midwinter K, Lewis J, Martin P (1996). Healing of incisional wounds in the embryonic chick wing bud: characterization of the actin purse-string and demonstration of a requirement for Rho activation. *J Cell Biol* **135**(4):1097-107.

Bulina ME, Chudakov DM, Britanova OV, Yanushevich YG, Staroverov DB, Chepurnykh TV, Merzlyak EM, Shkrob MA, Lukyanov S, Lukyanov KA (2006). A genetically encoded photosensitizer. *Nat Biotechnol* **24**(1):95-9.

Burkel BM, von Dassow G, Bement WM (2007).Versatile fluorescent probes for actin filaments based on the actin-binding domain of utrophin. *Cell Motil Cytoskeleton* **64**(11):822-32.

Burkel BM, Benink HA, Vaughan EM, von Dassow G, Bement WM (2012). A Rho GTPase signal treadmill backs a contractile array. *Dev Cell* **23**(2):384–396.

Cai C, Masumiya H, Weisleder N, Matsuda N, Nishi M, Hwang M, Ko JK, Lin P, Thornton A, Zhao X *et al.* (2009a). MG53 nucleates assembly of cell membrane repair machinery. *Nat Cell Biol* **11**(1):56–64.

Cai C, Weisleder N, Ko JK, Komazaki S, Sunada Y, Nishi M, Takeshima H, Ma J (2009b). Membrane Repair Defects in Muscular Dystrophy Are Linked to Altered Interaction between MG53, Caveolin-3, and Dysferlin. *J Biol Chem* **284**(23):15894–15902.

Campanella C, Andreuccetti P (1977). Ultrastructural observations on cortical endoplasmic reticulum and on residual cortical granules in the egg of Xenopus laevis. *Dev Biol* **56**:1–10.

Castellana ET, Cremer PS (2007). Imaging large arrays of supported lipid bilayers with a macroscope. *Biointerphases* **2**(2):57-63.

Castellano-Muñoz M, Peng AW, Salles FT, Ricci AJ (2012). Swept field laser confocal microscopy for enhanced spatial and temporal resolution in live-cell imaging. *Microsc Microanal* **18**:753-60.

Carter SB (1967). Effects of cytochalasins on mammalian cells. *Nature* **213**(5073):261-4.

Chambers R (1917). Microdissection studies. I. The visible structure of cell protoplasm and death changes. *Am J Physiol* **43**:1–12.

Chang DC, Reese TS (1990). Changes in membrane structure induced by electroporation as revealed by rapid-freezing electron microscopy. *Biophys J* **58**(1):1-12.

Charbonneau M, Grey RD (1984). The onset of activation responsiveness during maturation coincides with the formation of the cortical endoplasmic reticulum in oocytes of Xenopus laevis. *Dev Biol* **102**: 90-7.

Clark AG, Miller AL, Vaughan E, Yu H-YE, Penkert R, Bement WM (2009). Integration of single and multicellular wound responses. *Curr Biol* **19**(16):1389–1395.

Clay MR, Halloran MC (2013). Rho activation is apically restricted by Arhgap1 in neural crest cells and drives epithelial-to-mesenchymal transition. *Development* **140**(15):3198–3209.

Cocucci E, Racchetti G, Podini P, Rupnik M, Meldolesi J (2004). Enlargeosome, an exocytic vesicle resistant to nonionic detergents, undergoes endocytosis via a nonacidic route. *Mol Biol Cell.* **15**(12):5356-68.

Cooper ST, McNeil PL (2015). Membrane Repair: Mechanisms and Pathophysiology *Physiol Rev* **95**:1205–1240.

Corrotte M, Almeida PE, Tam C, Castro-Gomes T, Fernandes MC, Millis BA, Cortez M, Miller H, Song W, Maugel TK, Andrews NW (2013). Caveolae internalization repairs wounded cells and muscle fibers. *Elife* **2**:e00926.

Covian-Nares JF, Koushik SV, Puhl HL 3rd, Vogel SS (2010). Membrane wounding triggers ATP release and dysferlin-mediated intercellular calcium signaling. *J Cell Sci* **123**(11):1884-93.

Crick F (1970). Diffusion in embryogenesis. *Nature* **225**:420–22.

Davidson LA, Ezin AM, Keller R (2002). Embryonic wound healing by apical contraction and ingression in Xenopus laevis. *Cell Motil Cytoskeleton* **53**(3):163-76.

de Madrid BH, Greenberg L, Hatini V (2015). RhoGAP68F controls transport of adhesion proteins in Rab4 endosomes to modulate epithelial morphogenesis of Drosophila leg discs. *Dev Biol* **399**(2):283-95.

Delpiano MA, Altura BM (1996). Transmembrane currents in capillary endothelial cells are modulated by external Mg2+ ions. *Adv Exp Med Biol* **410**:115-8.

Di Paolo G, De Camilli P(2006). Phosphoinositides in cell regulation and membrane dynamics. *Nature* **443**:651-657.

Dovas A, Couchman JR (2005). RhoGDI: multiple functions in the regulation of Rho family GTPase activities. *Biochem J* **390**(1):1-9.

Dovas A, Choi Y, Yoneda A, Multhaupt HA, Kwon SH, Kang D, Oh ES, Couchman JR (2010). Serine 34 phosphorylation of rho guanine dissociation inhibitor (RhoGDIalpha) links signaling from conventional protein kinase C to Rho GTPase in cell adhesion. *J Biol Chem* **285**:23296–23308.

Driever W, Nüsslein-Volhard C (1988a). A gradient of bicoid protein in Drosophila embryos. *Cell* **54**:83–93.

Driever W, Nüsslein-Volhard C (1988b). The bicoid protein determines position in the Drosophila embryo in a concentration-dependent manner. *Cell* **54**:95–104.

Driever W, Nüsslein-Volhard C (1989). The bicoid protein is a positive regulator of hunchback transcription in the early Drosophila embryo. *Nature* **337**(6203):138-43.

Eddleman CS, Ballinger ML, Smyers ME, Godell CM, Fishman HM, Bittner GD (1997). Repair of plasmalemmal lesions by vesicles. *Proc Natl Acad Sci U S A* **94**:4745–50.

Eddleman CS, Ballinger ML, Smyers ME, Fishman HM, Bittner GD (1998). Endocytotic formation of vesicles and other membranous structures induced by Ca2+ and axolemmal injury. *J Neurosci* **18**(11):4029–41.

Eddleman CS, Bittner GD, Fishman HM (2000). Barrier permeability at cut axonal ends progressively decreases until an ionic seal is formed. *Biophys J* **79**(4):1883–90.

Eisenhoffer GT, Loftus PD, Yoshigi M, Otsuna H, Chien CB, Morcos PA, Rosenblatt J (2012). Crowding induces live cell extrusion to maintain homeostatic cell numbers in epithelia. *Nature* **484**(7395):546-9.

Endo M (2009). Calcium-induced calcium release in skeletal muscle. *Physiol Rev* **89**(4):1153-76.

Evans E, Heinrich V, Ludwig F, Rawicz W (2003). Dynamic Tension Spectroscopy and Strength of Biomembranes. *Biophys. J.* **85**(4):2342-2350.

Fadok VA, Voelker DR, Campbell PA, Cohen JJ, Bratton DL, Henson PM (1992). Exposure of phosphatidylserine on the surface of apoptotic lymphocytes triggers specific recognition and removal by macrophages. *J Immunol* **148**(7):2207-16.

Fein A, Terasaki M (2005). Rapid increase in plasma membrane chloride permeability during wound resealing in starfish oocytes. *J Gen Physiol* **126**(2):151-9.

Ferguson MW, O'Kane S (2004). Scar-free healing: from embryonic mechanisms to adult therapeutic intervention. *Philos Trans R Soc Lond B Biol Sci* **359**(1445):839-50.

Formaglio P, Tavares J, Ménard R, Amino R (2014). Loss of host cell plasma membrane integrity following cell traversal by Plasmodium sporozoites in the skin. *Parasitol Int* **63**(1): 237-44.

Garrett MD, Self AJ, van Oers C, Hall A (1989). Identification of distinct cytoplasmic targets for ras/R-ras and rho regulatory proteins. *J Biol Chem* **264**(1):10-3.

Geeraerts MD, Ronveaux-Dupal MF, Lemasters JJ, Herman B (1991). Cytosolic free Ca2+ and proteolysis in lethal oxidative injury in endothelial cells. *Am J Physiol* **261**:C889-96.

Gennerich A, Vale RD (2009). Walking the walk: how kinesin and dynein coordinate their steps. *Curr Opin Cell Biol* **21**(1):59-67.

Gerke V, Moss SE (2002). Annexins: from structure to function. *Physiol Rev* **82**:331–371.

Gingell D (1970). Contractile responses at the surface of an amphibian egg. *J Embryol Exp Morphol* **23**:583-609.

Giordano F, Saheki Y, Idevall-Hagren O, Colombo SF, Pirruccello M, Milosevic I, Gracheva EO, Bagriantsev SN, Borgese N, De Camilli P (2013). PI(4,5)P(2)-dependent and Ca(2+)-regulated ER-PM interactions mediated by the extended synaptotagmins. *Cell* **153**(7):1494-509.

Gozen I, Dommersnes P (2014). Pore dynamics in lipid membranes. *Eur Phys J Spec Top* **223**: 1813–1829.

Graham DL, Eccleston JF, Lowe PN (1999). The conserved arginine in rho-GTPase-activating protein is essential for efficient catalysis but not for complex formation with Rho-GDP and aluminum fluoride. *Biochemistry* **38**(3):985-91.

Graham TR (2004). Flippases and vesicle-mediated protein transport. *Trends Cell Biol* **14**(12): 670-7.

Grimsrud PA, Carson JJ, Hebert AS, Hubler SL, Niemi NM, Bailey DJ, Jochem A, Stapleton DS, Keller MP *et al.* (2012). A quantitative map of the liver mitochondrial phosphoproteome reveals posttranslational control of ketogenesis. *Cell Metab* **16**(5):672-83.

Gu Y, Forostyan T, Sabbadini R, Rosenblatt J (2011). Epithelial cell extrusion requires the sphingosine-1-phosphate receptor 2 pathway. *J Cell Biol* **193**(4):667-76.

Gurtner GC, Werner S, Barrandon Y, Longaker MT (2008). Wound repair and regeneration. *Nature* **453**:314-21.

Heasman J (2006). Maternal determinants of embryonic cell fate. *Semin Cell Dev Biol* **17**:93–98.

Heilbrunn LV (1928). The colloid chemistry of protoplasm, Berlin : Gebrüder Borntraeger.

Heilbrunn LV (1930). The action of various salts on the first stage of the surface precipitation reaction in arbacia egg protoplasm. *Protoplasma* **11**:558–573.

Heissler SM, Sellers JR (2016). Various themes of myosin regulation. *J Mol Biol* pii: S0022-2836(16)00041-3.

Heo J, Campbell SL (2006). Ras regulation by reactive oxygen and nitrogen species. *Biochemistry* **45**(7):2200-10.

Herrgen L, Voss OP, Akerman CJ (2014). Calcium-dependent neuroepithelial contractions expel damaged cells from the developing brain. *Dev Cell* **31**(5):599-613.

Hibino M, Itoh H, Kinosita K Jr (1993). Time courses of cell electroporation as revealed by submicrosecond imaging of transmembrane potential. *Biophys J* **64**(6):1789-800.

Holmes WR, Liao L, Bement WB, Edelstein-Keshet L (2015). Modeling the roles of protein kinase Cβ and η in single-cell wound repair. *Mol Biol Cell* **26**(22):4100–4108.

Holtfreter J (1943). Properties and functions of the surface coat in amphibian embryos. *J Exp Zool* **93**:251–323.

Howard AC, McNeil AK, Xiong F, Xiong W-C, McNeil PL (2011a). A Novel Cellular Defect in Diabetes: Membrane Repair Failure. *Diabetes* **60**(11):3034–3043.

Howard AC, McNeil AK, McNeil PL (2011b). Promotion of plasma membrane repair by vitamin E. *Nat Commun* **2**:597.

Hülskamp M, Pfeifle C, Tautz D (1990). A morphogenetic gradient of hunchback protein organizes the expression of the gap genes Krüppel and knirps in the early Drosophila embryo. *Nature*. **346**(6284):577-80.

Hutagalung AH, Novick PJ (2011). Role of Rab GTPases in membrane traffic and cell physiology. *Physiol Rev* **91**(1):119-49.

Hwang M, Ko J, Weisleder N, Takeshima H, Ma J (2011). Redox-dependent oligomerization through a leucine zipper motif is essential for MG53-mediated cell membrane repair. *Am J Physiol Cell Physiol* **301**:C106–C114.

Idone V, Tam C, Goss JW, Toomre D, Pypaert M, Andrews NW (2008). Repair of injured plasma membrane by rapid Ca2+-dependent endocytosis. *J Cell Biol* **180**(5):905–14.

Jacinto A, Wood W, Woolner S, Hiley C, Turner L, Wilson C, Martinez-Arias A, Martin P (2002). Dynamic analysis of actin cable function during Drosophila dorsal closure. *Curr Biol* **12**(14):1245-50.

Jaffe AB, Hall A. (2005) Rho GTPases: biochemistry and biology. *Annu Rev Cell Dev Biol* **21**:247-69.

Jaiswal JK, Lauritzen SP, Scheffer L, Sakaguchi M, Bunkenborg J, Simon SM, Kallunki T, Jäättelä M, Nylandsted J (2014). S100A11 is required for efficient plasma membrane repair and survival of invasive cancer cells. *Nat Commun* **5**:3795.

Jedd G, Chua NH (2000). A new self-assembled peroxisomal vesicle required for efficient resealing of the plasma membrane. *Nat Cell Biol* **2**(4):226-31.

Jimenez AJ, Maiuri P, Lafaurie-Janvore J, Divoux S, Piel M, Perez F (2014). ESCRT machinery is required for plasma membrane repair. *Science* **343**(6174):1247136.

Johnson VE, Stewart W, Smith DH (2013). Axonal Pathology in Traumatic Brain Injury. *Exp Neurol* **246**:35–43.

Johnstone CN, Castellví-Bel S, Chang LM, Bessa X, Nakagawa H, Harada H, Sung RK, Piqué JM, Castells A, Rustgi AK (2004). ARHGAP8 is a novel member of the RHOGAP family related to ARHGAP1/CDC42GAP/p50RHOGAP: mutation and expression analyses in colorectal and breast cancers. *Gene* **336**(1):59-71.

Jones CM, Smith JC (1998). Establishment of a BMP-4 morphogen gradient by long-range inhibition. *Dev Biol* **194**(1):12-7.

Katayama M, Kawata M, Yoshida Y, Horiuchi H, Yamamoto T, Matsuura Y, Takai Y (1991). The posttranslationally modified C-terminal structure of bovine aortic smooth muscle rhoA p21. *J Biol Chem* **266**(19):12639-45.

Kawanabe T, Kawakami T, Yatomi Y, Shimada S, Soma Y (2007). Sphingosine 1-phosphate accelerates wound healing in diabetic mice. *J Dermatol Sci* **48**(1):53-60.

Keller RE (1980). The cellular basis of epiboly: an SEM study of deep-cell rearrangement during gastrulation in Xenopus laevis. *J Embryol Exp Morphol* **60**:201-34.

Kimura K, Ito M, Amano M, Chihara K, Fukata Y, Nakafuku M, Yamamori B, Feng J, Nakano T, Okawa K, *et al.* (1996). Regulation of myosin phosphatase by Rho and Rho-associated kinase (Rho-kinase). *Science* **273**:245-248.

Kleineke J, Düls C, Söling HD (1979). Subcellular compartmentation of guanine nucleotides and functional relationships between the adenine and guanine nucleotide systems in isolated hepatocytes. *FEBS Lett* **107**(1):198-202.

Klima A, Foissner I (2011). Actin-dependent deposition of putative endosomes and endoplasmic reticulum during early stages of wound healing in characean internodal cells. *Plant Biol (Stuttg)* **13**(4):590-601.

Kono K, Saeki Y, Yoshida S, Tanaka K, Pellman D (2012). Proteasomal degradation resolves competition between cell polarization and cellular wound healing. *Cell* **150**:151–64.

Kohout SC, Corbalán-García S, Torrecillas A, Goméz-Fernandéz JC, Falke JJ (2002). C2 domains of protein kinase C isoforms alpha, beta, and gamma: activation parameters and calcium stoichiometries of the membrane-bound state. *Biochemistry* **41**(38):11411-24.

Krause TL, Fishman HM, Ballinger ML, Bittner GD (1994). Extent and mechanism of sealing in transected giant axons of squid and earthworms. *J Neurosci* **14**(11):6638–51.

Kuhlmann N, Wroblowski S, Knyphausen P, de Boor S, Brenig J, Zienert AY, Meyer-Teschendorf K, Praefcke GJ, Nolte H, Krüger M, *et al*. (2015). Structural and mechanistic insights into the regulation of the fundamental Rho-regulator RhoGDIα by lysine acetylation. *J Biol Chem* pii: jbc.M115.707091.

Kunkel MT, Toker A, Tsien RY, Newton AC (2007). Calcium-dependent regulation of protein kinase D revealed by a genetically encoded kinase activity reporter. *J Biol Chem* **282(**9):6733-42.

Kureishi Y, Kobayashi S, Amano M, Kimura K, Kanaide H, Nakano T, Kaibuchi K, Ito M (1997). Rho-associated kinase directly induces smooth muscle contraction through myosin light chain phosphorylation. *J Biol Chem* **272**:12257-12260.

La Claire JW Jr (1983). Inducement of wound motility in intact giant algal cells. *Exp Cell Res* **145**:63–69.

Labazi M, McNeil AK, Kurtz T, Lee TC, Pegg RB, Angeli JPF, Conrad M, McNeil PL (2015). The antioxidant requirement for plasma membrane repair in skeletal muscle. *Free Rad Bio Med* **84**:246-253.

Lancaster CA, Taylor-Harris PM, Self AJ, Brill S, van Erp HE, Hall A (1994). Characterization of rhoGAP. A GTPase-activating protein for rho-related small GTPases. *J Biol Chem* **269**(2): 1137-42.

Lehmann R, Nüsslein-Volhard C (1991). The maternal gene nanos has a central role in posterior pattern formation of the Drosophila embryo. *Development* **112**(3):679-91.

Lennon NJ, Kho A, Bacskai BJ, Perlmutter SL, Hyman BT, Brown RH Jr (2003). Dysferlin interacts with annexins A1 and A2 and mediates sarcolemmal wound-healing. *J Biol Chem* **278**(50):50466-73.

Leonard DA, Lin R, Cerione RA, Manor D (1998). Biochemical studies of the mechanism of action of the Cdc42-GTPase-activating protein. *J Biol Chem* **273**(26):16210-5.

Li J, Zhang S, Soto X, Woolner S, Amaya E (2013). ERK and phosphoinositide 3-kinase temporally coordinate different modes of actin-based motility during embryonic wound healing. *J Cell Sci* **126**(21):5005-17.

Ligeti E, Settleman J (2006). Regulation of RhoGAP specificity by phospholipids and prenylation. *Methods Enzymol* **406**:104-17.

Limaye PB, Apte UM, Shankar K, Bucci TJ, Warbritton A, Mehendale HM (2003). Calpain released from dying hepatocytes mediates progression of acute liver injury induced by model hepatotoxicants. *Toxicol Appl Pharmacol* **191**(3):211-26.

Lin P, Zhu H, Cai C, Wang X, Cao C, Xiao R, Pan Z, Weisleder N, Takeshima H, Ma J (2012). Nonmuscle myosin IIA facilitates vesicle trafficking for MG53-mediated cell membrane repair. *FASEB J.* **26**(5):1875–1883.

Lioi AB, Reyes Rodriguez AL, Funderburg NT, Feng Z, Weinberg A, Sieg SF (2012). Membrane damage and repair in primary monocytes exposed to human β-defensin-3. *J Leukoc Biol* **92**(5): 1083–1091.

Liou J, Fivaz M, Inoue T, Meyer T (2007). Live-cell imaging reveals sequential oligomerization and local plasma membrane targeting of stromal interaction molecule 1 after Ca2+ store depletion. *Proc Natl Acad Sci U S A* **104**(22):9301-6.

Los FCO, Randis TM, Aroian RV, Ratner AJ (2013). Role of Pore-Forming Toxins in Bacterial Infectious Diseases. *Microbiol Mol Biol Rev* **77**(2):173–207.

Low BC, Seow KT, Guy GR (2000). The BNIP-2 and Cdc42GAP homology domain of BNIP-2 mediates its homophilic association and heterophilic interaction with Cdc42GAP. *J Biol Chem* **275**(48):37742-51.

Lubkov V, Bar-Sagi D (2014). E-cadherin-mediated cell coupling is required for apoptotic cell extrusion. *Curr Biol* **24**(8):868-74.

Luisoni S, Suomalainen M, Boucke K, Tanner LB, Wenk MR, Guan XL, Grzybek M, Coskun Ü, Greber UF (2015). Co-option of Membrane Wounding Enables Virus Penetration into Cells. *Cell Host Microbe* **18**(1):75-85.

Lund E, Sheets MD, Imboden SB, Dahlberg JE (2011). Limiting Ago protein restricts RNAi and microRNA biogenesis during early development in Xenopus laevis. *Genes Dev* **25**(11):1121-31.

Luxardi G, Reid B, Maillard P, Zhao M (2014). Single cell wound generates electric current circuit and cell membrane potential variations that requires calcium influx. *Integr Biol (Camb)* **6**(7):662-72.

Ma C, Benink HA, Cheng D, Montplaisir V, Wang L, Xi Y, Zheng PP, Bement WM, Liu XJ (2006). Cdc42 Activation Couples Spindle Positioning to First Polar Body Formation in Oocyte Maturation. *Curr Biol* **16**(2):214–220.

Ma X, Kovács M, Conti MA, Wang A, Zhang Y, Sellers JR, Adelstein RS (2012). Nonmuscle myosin II exerts tension but does not translocate actin in vertebrate cytokinesis. *Proc Natl Acad Sci U S A* **109**(12):4509–4514.

Macara IG (2004). Par proteins: partners in polarization. *Curr Biol* **14**:R160–R162.

Machacek M, Hodgson L, Welch C, Elliott H, Pertz O, Nalbant P, Abell A, Johnson GL, Hahn KM, Danuser G (2009). Coordination of Rho GTPase activities during cell protrusion. *Nature* **461**(7260):99-103.

Mandato CA, Bement WM (2001). Contraction and polymerization cooperate to assemble and close actomyosin rings around Xenopus oocyte wounds. *J Cell Biol* **154**(4):785-97.

Mandato CA, Bement WM (2003). Actomyosin transports microtubules and microtubules control actomyosin recruitment during Xenopus oocyte wound healing. *Curr Biol* **13**(13): 1096-105.

Marchiando AM, Shen L, Graham WV, Edelblum KL, Duckworth CA, Guan Y, Montrose MH, Turner JR, Watson AJ (2011). The epithelial barrier is maintained by in vivo tight junction expansion during pathologic intestinal epithelial shedding. *Gastroenterology* **140**(4): 1208-1218.e1-2.

Martin K, Reimann A, Fritz RD, Ryu H, Jeon NL, Pertz O (2016). Spatio-temporal co-ordination of RhoA, Rac1 and Cdc42 activation during prototypical edge protrusion and retraction dynamics. *Sci Rep* **6**:21901.

Martin P, Lewis J (1992). Actin cables and epidermal movement in embryonic wound healing. *Nature* **360**(6400):179-83.

McCrea HJ, Paradise S, Tomasini L, Addis M, Melis MA, De Matteis MA, De Camilli P (2008). All known patient mutations in the ASH-RhoGAP domains of OCRL affect targeting and APPL1 binding. *Biochem Biophys Res Commun* **369**(2):493-9.

McDade JR, Archambeau A, Michele DE (2014). Rapid actin-cytoskeleton–dependent recruitment of plasma membrane–derived dysferlin at wounds is critical for muscle membrane repair. *FASEB J* **28**(8):3660–3670.

McDade JR, Michele DE (2014). Membrane damage-induced vesicle–vesicle fusion of dysferlin-containing vesicles in muscle cells requires microtubules and kinesin. *Hum Mol Genet* **23**(7), 1677–1686.

McNeil A, McNeil PL (2005). Yolk granule tethering: a role in cell resealing and identification of several protein components. *J Cell Sci* **118**(20):4701-8.

McNeil AK, Rescher U, Gerke V, McNeil PL (2006). Requirement for annexin A1 in plasma membrane repair. *J Biol Chem* **281**(46):35202–7.

McNeil PL, Ito S (1989). Gastrointestinal cell plasma membrane wounding and resealing in vivo. *Gastroenterology.* **96**:1238–48.

McNeil PL, Ito S (1990). Molecular traffic through plasma membrane disruptions of cells in vivo. *J Cell Sci* **96**:549-56.

McNeil PL, Khakee R (1992). Disruptions of muscle fiber plasma membranes. Role in exercise-induced damage. *Am J Pathol* **140**:1097–109.

McNeil PL, Muthukrishnan L, Warder E, D'Amore PA (1989). Growth factors are released by mechanically wounded endothelial cells. *J Cell Biol* **109**(2): 811–822.

McNeil PL, Miyake K, Vogel SS (2003). The endomembrane requirement for cell surface repair. *Proc Natl Acad Sci U S A* **100**(8):4592-4597.

McNeil PL, Vogel SS, Miyake K, Terasaki M (2000). Patching plasma membrane disruptions with cytoplasmic membrane. *J Cell Sci* **113**(11):1891-902.

Meissner G, Darling E, Eveleth J (1986). Kinetics of rapid Ca2+ release by sarcoplasmic reticulum. Effects of Ca2+, Mg2+, and adenine nucleotides. *Biochemistry* **25**(1):236-44.

Mellgren RL (2010). A Plasma Membrane Wound Proteome: REVERSIBLE EXTERNALIZATION OF INTRACELLULAR PROTEINS FOLLOWING REPARABLE MECHANICAL DAMAGE. *J Biol Chem* **285**(47):36597–36607.

Merriam RW, Christensen K (1983). A contractile ring-like mechanism in wound healing and soluble factors affecting structural stability in the cortex of Xenopus eggs and oocytes. *J Embryol Exp Morphol.* **75**:11-20.

Meyer BH, Freuler F, Guerini D, Siehler S (2008). Reversible translocation of p115-RhoGEF by G(12/13)-coupled receptors. *J Cell Biochem* **104**(5):1660-70.

Michael M, Meiring JC, Acharya BR, Matthews DR, Verma S, Han SP, Hill MM, Parton RG, Gomez GA, Yap AS (2016). Coronin 1B Reorganizes the Architecture of F-Actin Networks for Contractility at Steady-State and Apoptotic Adherens Junctions. *Dev Cell* **37**(1):58-71.

Miller AL, Bement WM (2009). Regulation of cytokinesis by Rho GTPase flux. *Nat Cell Biol* **11**(1):71-77.

Miller ME, Adhikary S, Kolokoltsov AA, Davey RA (2012). Ebolavirus Requires Acid Sphingomyelinase Activity and Plasma Membrane Sphingomyelin for Infection. *J Virol* **86**(14): 7473–7483.

Minoshima Y, Kawashima T, Hirose K, Tonozuka Y, Kawajiri A, Bao YC, Deng X, Tatsuka M, Narumiya S, May WS Jr, *et al.* (2003). Phosphorylation by aurora B converts MgcRacGAP to a RhoGAP during cytokinesis. *Dev Cell* **4**(4):549-60.

Mitchison T, Kirschner M (1984). Dynamic instability of microtubule growth. *Nature* **312**:237–242.

Miyake K, McNeil PL (1995). Vesicle accumulation and exocytosis at sites of plasma membrane disruption. *J Cell Biol* **131**(2):1737–45.

Miyake K, McNeil PL, Suzuki K, Tsunoda R, Sugai N (2001). An actin barrier to resealing. *J Cell Sci* **114**(19):3487–94.

Moe AM, Golding AE, Bement WM (2015). Cell healing: Calcium, repair and regeneration. *Semin Cell Dev Biol* **45**:18-23.

Montero M, Alonso-Torre SR, Alvarez J, Sanchez A, García-Sancho J (1993). The pathway for refilling intracellular Ca2+ stores passes through the cytosol in human leukaemia cells. *Pflugers Arch* **424**(5-6):465-9.

Moon SY, Zheng Y (2003). Rho GTPase-activating proteins in cell regulation. *Trends Cell Biol* **13**(1):13-22.

Mori M, Saito K, Ohta Y (2014). ARHGAP22 localizes at endosomes and regulates actin cytoskeleton. *PLoS One* **9**(6):e100271.

Moskwa P, Paclet MH, Dagher MC, Ligeti E (2014). Autoinhibition of p50 Rho GTPase-activating protein (GAP) is released by prenylated small GTPases. *J Biol Chem* **280**(8):6716-20.

Needham D, Nunn RS (1990). Elastic deformation and failure of lipid bilayer membranes containing cholesterol. *Biophys J* **58**(4):997–1009.

Neujahr R, Heizer C, Gerisch G (1997). Myosin II-independent processes in mitotic cells of Dictyostelium discoideum: redistribution of the nuclei, re-arrangement of the actin system and formation of the cleavage furrow. *J Cell Sci* **110**(2):123-37.

Newport J, Kirschner M (1982). A major developmental transition in early Xenopus embryos: I. characterization and timing of cellular changes at the midblastula stage. *Cell* **30**(3):675-86.

Ngok SP, Lin WH, Anastasiadis PZ (2014). Establishment of epithelial polarity--GEF who's minding the GAP? *J Cell Sci* **127**(15):3205-15.

Nomanbhoy TK, Cerione RA (1996). Characterization of the interaction between RhoGDI and Cdc42Hs using fluorescence spectroscopy. *J Biol Chem* **271**:10004–10009.

Oancea E, Meyer T (1998). Protein kinase C as a molecular machine for decoding calcium and diacylglycerol signals. *Cell* **95**:307-318.

Ochoa WF, Garcia-Garcia J, Fita I, Corbalan-Garcia S, Verdaguer N, Gomez-Fernandez JC (2001). Structure of the C2 domain from novel protein kinase C epsilon. A membrane binding model for Ca(2+)-independent C2 domains. *J Mol Biol* **311**:837-849.

Oda Y, Otani T, Ikenouchi J, Furuse M (2014). Tricellulin regulates junctional tension of epithelial cells at tricellular contacts through Cdc42. *J Cell Sci* **127**(19):4201-12.

Orchard RC, Kittisopikul M, Altschuler SJ, Wu LF, Süel GM, Alto NM (2012). Identification of F-actin as the dynamic hub in a microbial-induced GTPase polarity circuit. *Cell* **148**(4):803-15.

Orrenius S, Zhivotovsky B, Nicotera P (2003). Regulation of cell death: the calcium-apoptosis link. *Nat Rev Mol Cell Biol* **4**(7):552-65.

Parekh AB, Putney JW Jr (2005). Store-operated calcium channels. *Physiol Rev* **85**(2):757-810.

Park Y, Seo JB, Fraind A, Pérez-Lara A, Yavuz H, Han K, Jung SR, Kattan I, Walla PJ, Choi M *et al.* (2015). Synaptotagmin-1 binds to PIP(2)-containing membrane but not to SNAREs at physiological ionic strength. *Nat Struct Mol Biol* **22**(10):815-23.

Perrie WT, Smillie LB, Perry SV (1973). A phosphorylated light-chain component of myosin from skeletal muscle. *Biochem J* **135**(1):151-164.

Peshkin L, Wühr M, Pearl E, Haas W, Freeman RM Jr, Gerhart JC, Klein AM, Horb M, Gygi SP, Kirschner MW (2015). On the Relationship of Protein and mRNA Dynamics in Vertebrate Embryonic Development. *Dev Cell* **35**(3):383-94.

Petrof BJ, Shrager JB, Stedman HH, Kelly AM, Sweeney HL (1993). Dystrophin protects the sarcolemma from stresses developed during muscle contraction. *Proc Natl Acad Sci U S A* **90**(8):3710-4.

Pettus EH, Povlishock JT (1996). Characterization of a distinct set of intra-axonal ultrastructural changes associated with traumatically induced alteration in axolemmal permeability. *Brain Res* **722**:1–11.

Pollard TD (2007). Regulation of actin filament assembly by Arp2/3 complex and formins. *Annu Rev Biophys Biomol Struct*. **36**:451-77.

Pollard TD (2010). Mechanics of cytokinesis in eukaryotes. *Curr Opin Cell Biol* **22**(1):50–56.

Ponik SM, Trier SM, Wozniak MA, Eliceiri KW, Keely PJ (2013). RhoA is down-regulated at cell-cell contacts via p190RhoGAP-B in response to tensional homeostasis. *Mol Biol Cell* **24**(11):1688-99, S1-3.

Ponomareva OY, Eliceiri KW, Halloran MC (2016). Charcot-Marie-Tooth 2b associated Rab7 mutations cause axon growth and guidance defects during vertebrate sensory neuron development. *Neural Dev* **11**:2.

Pontius JU, Wagner L, Schuler GD (2003). UniGene: a unified view of the transcriptome. In: The NCBI Handbook. Bethesda (MD): National Center for Biotechnology Information.

Potez S, Luginbühl M, Monastyrskaya K, Hostettler A, Draeger A, Babiychuk EB (2011). Tailored protection against plasmalemmal injury by annexins with different Ca2+ sensitivities. *J Biol Chem* **286**(20):17982–91.

Ramel D, Wang X, Laflamme C, Montell DJ, Emery G (2013). Rab11 regulates cell-cell communication during collective cell movements. *Nat Cell Biol* **15**(3):317-24.

Ramsey SD, Newton K, Blough D, McCulloch DK, Sandhu N, Reiber GE, Wagner EH (1999). Incidence, outcomes, and cost of foot ulcers in patients with diabetes. *Diabetes Care* **22**(3): 382-7.

Rebagliati MR, Weeks DL, Harvey RP, Melton DA (1985). Identification and cloning of localized maternal RNAs from Xenopus eggs. *Cell* **42**(3):769-77.

Reddy A, Caler EV, Andrews NW (2001). Plasma membrane repair is mediated by Ca(2+)-regulated exocytosis of lysosomes. *Cell* **106**(2):157–69.

Reyes CC, Jin M, Breznau EB, Espino R, Delgado-Gonzalo R, Goryachev AB, Miller AL (2014). Anillin regulates cell-cell junction integrity by organizing junctional accumulation of Rho-GTP and actomyosin. *Curr Biol* **24**(11):1263-70.

Rezvanpour A, Santamaria-Kisiel L, Shaw GS (2011). The S100A10-Annexin A2 Complex Provides a Novel Asymmetric Platform for Membrane Repair. *J Biol Chem* **286**(46):40174–40183.

Ridley AJ, Self AJ, Kasmi F, Paterson HF, Hall A, Marshall CJ, Ellis C (1993). rho family GTPase activating proteins p190, bcr and rhoGAP show distinct specificities in vitro and in vivo. *EMBO J* **12**(13):5151-60.

Rodriguez OC, Schaefer AW, Mandato CA, Forscher P, Bement WM, Waterman-Storer CM (2003). Conserved microtubule-actin interactions in cell movement and morphogenesis. *Nat Cell Biol* **5**(7):599-609.

Rogers KW, Schier AF (2011). Morphogen gradients: from generation to interpretation. *Annu Rev Cell Dev Biol* **27**:377-407.

Rohatgi R, Ma L, Miki H, Lopez M, Kirchhausen T, Takenawa T, Kirschner MW (1999). The interaction between N-WASP and the Arp2/3 complex links Cdc42-dependent signals to actin assembly. *Cell* **97**:221–231.

Rohatgi R, Ho HH, Kirschner MW (2000). Mechanism of N-Wasp Activation by Cdc42 and Phosphatidylinositol 4,5-Bisphosphate. *J Cell Biol* **150**(6):1299–1310.

Rosenblatt J, Raff MC, Cramer LP (2001). An epithelial cell destined for apoptosis signals its neighbors to extrude it by an actin- and myosin-dependent mechanism. *Curr Biol* **11**(23): 1847-57.

Rossman KL, Der CJ, Sondek J (2005). GEF means go: turning on RHO GTPases with guanine nucleotide-exchange factors. *Nat Rev Mol Cell Biol* **6**(2):167-80.

Roubinet C, Cabernard C (2014). Control of asymmetric cell division. *Curr Opin Cell Biol* **31**:84-9.

Rous P, Jones FS (1916). A METHOD FOR OBTAINING SUSPENSIONS OF LIVING CELLS FROM THE FIXED TISSUES, AND FOR THE PLATING OUT OF INDIVIDUAL CELLS. *J Exp Med* **23**(4):549–555.

Safferling K, Sütterlin T, Westphal K, Ernst C, Breuhahn K, James M, Jäger D, Halama N, Grabe N (2013). Wound healing revised: a novel reepithelialization mechanism revealed by in vitro and in silico models. *J Cell Biol* **203**(4):691-709.

Saito K, Fujimura-Kamada K, Hanamatsu H, Kato U, Umeda M, Kozminski KG, Tanaka K (2007a). Transbilayer phospholipid flipping regulates Cdc42p signaling during polarized cell growth via Rga GTPase-activating proteins. *Dev Cell* **13**(5):743-51.

Saito K, Tautz L, Mustelin T (2007b). The lipid-binding SEC14 domain. *Biochim Biophys Acta* **1771**(6):719-26.

Sandre O, Moreaux L, Brochard-Wyart F (1999). Dynamics of transient pores in stretched vesicles. *Proc Natl Acad Sci U S A* **96**(19):10591–10596.

Sandquist JC, Means AR (2008). The C-terminal tail region of nonmuscle myosin II directs isoform-specific distribution in migrating cells. *Mol Biol Cell* **19**(12):5156-67.

Sanny J, Chui V, Langmann C, Pereira C, Zahedi B, Harden N (2006). Drosophila RhoGAP68F is a putative GTPase activating protein for RhoA participating in gastrulation. *Dev Genes Evol* **216**(9):543-50.

Santaguida S, Amon A (2015). Short- and long-term effects of chromosome mis-segregation and aneuploidy. *Nat Rev Mol Cell Biol* **16**(8):473-85.

Scheffer LL, Sreetama SC, Sharma N, Medikayala S, Brown KJ, Defour A, Jaiswal JK (2014). Mechanism of $Ca^{2+}$-triggered ESCRT assembly and regulation of cell membrane repair. *Nat Commun* **5**:5646.

Schiel JA, Simon GC, Zaharris C, Weisz J, Castle D, Wu CC, Prekeris R (2012). FIP3-endosome-dependent formation of the secondary ingression mediates ESCRT-III recruitment during cytokinesis. *Nat Cell Biol* **14**(10):1068-78.

Schindelin J, Arganda-Carreras I, Frise E, Kaynig V, Longair M, Pietzsch T, Preibisch S, Rueden C, Saalfeld S, Schmid B, et al. (2012) Fiji: an open-source platform for biological-image analysis. *Nat Methods* **9**:676-82.

Schroeder TE (1970). The contractile ring. I. Fine structure of dividing mammalian (HeLa) cells and the effects of cytochalasin B. *Z Zellforsch Mikrosk Anat*. **1109**(4):431-49.

Sen CK, Gordillo GM, Roy S, Kirsner R, Lambert L, Hunt TK, Gottrup F, Gurtner GC, Longaker MT (2009). Human skin wounds: a major and snowballing threat to public health and the economy. *Wound Repair Regen* **17**(6):763-71.

Serriere-Lanneau V, Teixeira-Clerc F, Li L, Schippers M, de Wries W, Julien B, Tran-Van-Nhieu J, Manin S, Poelstra K, Chun J, Carpentier S, Levade T, Mallat A, Lotersztajn S (2007). The sphingosine 1-phosphate receptor S1P2 triggers hepatic wound healing. *FASEB J* **21**(9):2005-13.

Shang X, Zhou YT, Low BC (2003). Concerted regulation of cell dynamics by BNIP-2 and Cdc42GAP homology/Sec14p-like, proline-rich, and GTPase-activating protein domains of a novel Rho GTPase-activating protein, BPGAP1. *J Biol Chem* **278**(46):45903-14.

Sharei A, Poceviciute R, Jackson EL, Cho N, Mao S, Hartoularos GC, Jang DY, Jhunjhunwala S, Eyerman A, Schoettle T, *et al.* (2014). Plasma membrane recovery kinetics of a microfluidic intracellular delivery platform. *Integr Biol (Camb)*. **6**(4): 470–475.

Sharma N, Medikayala S, Defour A, Rayavarapu S, Brown KJ, Hathout Y, Jaiswal JK (2012). Use of Quantitative Membrane Proteomics Identifies a Novel Role of Mitochondria in Healing Injured Muscles. *J Biol Chem* **287**(36):30455–30467.

Shen SS, Tucker WC, Chapman ER, Steinhardt RA (2005). Molecular regulation of membrane resealing in 3T3 fibroblasts. *J Biol Chem* **280**(2):1652-60.

Shen Y, Li N, Wu S, Zhou Y, Shan Y, Zhang Q, Ding C, Yuan Q, Zhao F, Zeng R, Zhu X (2008). Nudel binds Cdc42GAP to modulate Cdc42 activity at the leading edge of migrating cells. *Dev Cell* **14**(3):342-53.

Shi R, Asano T, Vining N, Blight AR (2000). Control of Membrane Sealing in Injured Mammalian Spinal Cord Axons. *J Neurophysiol* **84**(4):1763-1769.

Schindelin J, Arganda-Carreras I, Frise E, Kaynig V, Longair M, Pietzsch T, Preibisch S, Rueden C, Saalfeld S, Schmid B, *et al.* (2012). Fiji: an open-source platform for biological-image analysis. *Nat Methods* **9**(7):676-82.

Shindo A, Hara Y, Yamamoto TS, Ohkura M, Nakai J, Ueno N (2010). Tissue-tissue interaction-triggered calcium elevation is required for cell polarization during Xenopus gastrulation. *PLoS One* **5**(2):e8897.

Simon CM, Vaughan EM, Bement WM, Edelstein-Keshet L (2013). Pattern formation of Rho GTPases in single cell wound healing. *Mol Biol Cell* **24**(3):421–432.

Singer AJ, Clark RA (1999). Cutaneous wound healing. *N Engl J Med* **341**(10):738-46.

Sirokmány G, Szidonya L, Káldi K, Gáborik Z, Ligeti E, Geiszt M (2006). Sec14 homology domain targets p50RhoGAP to endosomes and provides a link between Rab and Rho GTPases. *J Biol Chem* **281**(9):6096-105.

Slattum G, McGee KM, Rosenblatt J (2009). P115 RhoGEF and microtubules decide the direction apoptotic cells extrude from an epithelium. *J Cell Biol* **186**(5):693-702.

Smutny M, Cox HL, Leerberg JM, Kovacs EM, Conti MA, Ferguson C, Hamilton NA, Parton RG, Adelstein RS, Yap AS (2010). Myosin II isoforms identify distinct functional modules that support integrity of the epithelial zonula adherens. *Nat Cell Biol* **12**(7):696–702.

Sokac AM, Co C, Taunton J, Bement W (2003). Cdc42-dependent actin polymerization during compensatory endocytosis in Xenopus eggs. *Nat Cell Biol* **5**(8):727-32.

Solnica-Krezel L (2005). Conserved patterns of cell movements during vertebrate gastrulation. *Curr Biol* **15**(6):R213-28.

Somers WG, Saint R (2003). A RhoGEF and Rho family GTPase-activating protein complex links the contractile ring to cortical microtubules at the onset of cytokinesis. *Dev Cell* **4**:29–39.

Sonnemann KJ, Bement WM (2011). Wound repair: toward understanding and integration of single-cell and multicellular wound responses. *Annu Rev Cell Dev Biol* **27**:237–63.

Sönnichsen B, De Renzis S, Nielsen E, Rietdorf J, Zerial M (2000). Distinct membrane domains on endosomes in the recycling pathway visualized by multicolor imaging of Rab4, Rab5, and Rab11. *J Cell Biol* **149**(4):901-14.

Soto X, Li J, Lea R, Dubaissi E, Papalopulu N, Amaya E (2013). Inositol kinase and its product accelerate wound healing by modulating calcium levels, Rho GTPases, and F-actin assembly. *Proc Natl Acad Sci U S A* **110**(27):11029-34.

Stahelin RV (2009). Lipid binding domains: more than simple lipid effectors. *J Lipid Res* **50**:S299-304.

Stasia MJ, Jouan A, Bourmeyster N, Boquet P, Vignais PV (1991). ADP-ribosylation of a small size GTP-binding protein in bovine neutrophils by the C3 exoenzyme of Clostridium botulinum and effect on the cell motility. *Biochem Biophys Res Commun* **180**(2):615-22.

Steenblock C, Heckel T, Czupalla C, Espírito Santo AI, Niehage C, Sztacho M, Hoflack B (2014). The Cdc42 guanine nucleotide exchange factor FGD6 coordinates cell polarity and endosomal membrane recycling in osteoclasts. *J Biol Chem* **289**(26):18347-59.

Steinhardt RA, Bi G, Alderton JM (1994). Cell membrane resealing by a vesicular mechanism similar to neurotransmitter release. *Science* **263**(5145):390–3.

Straight AF, Cheung A, Limouze J, Chen I, Westwood NJ, Sellers JR, Mitchison TJ (2003). Dissecting temporal and spatial control of cytokinesis with a myosin II Inhibitor. *Science* **299**(5613):1743-7.

Stricker J, Falzone T, Gardel M (2010). Mechanics of the F-actin Cytoskeleton. *J Biomech* **43**(1):9-14.

Struhl G, Struhl K, Macdonald P (1989). The gradient morphogen bicoid is a concentration-dependent transcriptional activator. *Cell* **57**:1259–73.

Sud M, Fahy E, Cotter D, Brown A, Dennis EA, Glass CK, Merrill AH Jr, Murphy RC, Raetz CR, Russell DW, Subramaniam S (2007). LMSD: LIPID MAPS structure database *Nucleic Acids Res.* **35**:D527-32.

Suzuki J, Kanemaru K, Ishii K, Ohkura M, Okubo Y, Iino M (2014). Imaging intraorganellar Ca2+ at subcellular resolution using CEPIA. *Nat Commun* **5**:4153.

Swaggart KA, Demonbreun AR, Vo AH, Swanson KE, Kim EY, Fahrenbach JP, Holley-Cuthrell J, Eskin A, Chen Z, Squire K, *et al.* (2014). Annexin A6 modifies muscular dystrophy by mediating sarcolemmal repair. *Proc Natl Acad Sci U S A* **111**(16):6004–9.

Szubinska B (1971). "NEW MEMBRANE" FORMATION IN *AMOEBA PROTEUS* UPON INJURY OF INDIVIDUAL CELLS : Electron Microscope Observations. *J. Cell Biol*. **49**(3): 747–772.

Takada H, Furuya K, Sokabe M (2014). Mechanosensitive ATP release from hemichannels and $Ca^{2+}$ influx through TRPC6 accelerate wound closure in keratinocytes. *J Cell Sci* **127**(19): 4159-71.

Takaishi K, Sasaki T, Kameyama T, Tsukita S, Tsukita S, Takai Y (1995). Translocation of activated Rho from the cytoplasm to membrane ruffling area, cell-cell adhesion sites and cleavage furrows. *Oncogene* **11**(1):39-48.

Tatsumoto T, Xie X, Blumenthal R, Okamoto I, Miki T (1999). Human ECT2 is an exchange factor for Rho GTPases, phosphorylated in G2/M phases, and involved in cytokinesis. *J Cell Biol* **147**(5):921-8.

Tcherkezian J, Lamarche-Vane N (2007). Current knowledge of the large RhoGAP family of proteins. *Biol Cell* **99**(2):67-86.

Terasaki M, Miyake K, McNeil PL (1997). Large plasma membrane disruptions are rapidly resealed by Ca2+-dependent vesicle-vesicle fusion events. *J Cell Biol* **139**:63–74.

Theriot JA, Mitchison TJ (1991). Actin microfilament dynamics in locomoting cells. *Nature* **352**(6331):126-31.

Togo T (2006). Disruption of the plasma membrane stimulates rearrangement of microtubules and lipid traffic toward the wound site. *J Cell Sci* **119**(13):2780-6.

Togo T, Krasieva TB, Steinhardt RA (2000). A decrease in membrane tension precedes successful cell-membrane repair. *Mol Biol Cell* **11**(12):4339–46.

Turing AM (1952). The Chemical Basis of Morphogenesis. *Philos Trans R Soc Lond B Biol Sci* **237**(641):37-72.

Turner PR, Schultz R, Ganguly B, Steinhardt RA (1993). Proteolysis results in altered leak channel kinetics and elevated free calcium in mdx muscle. *J Membr Biol* **133**(3):243-51.

van Meer G, Voelker DR, Feigenson GW (2008). Membrane lipids: where they are and how they behave. *Nat Rev Mol Cell Biol* **9**:112-124.

Vaughan EM, Miller AL, Yu HY, Bement WM (2011). Control of local Rho GTPase crosstalk by Abr. *Curr Biol* **21**(4):270-7.

Vaughan EM, You J-S, Yu, H-YE, Lasek A, Vitale N, Hornberger TA, Bement WM (2014). Lipid domain–dependent regulation of single-cell wound repair. *Mol Biol Cell* **25**(12):1867–1876.

Vetter IR, Wittinghofer A (2001). The guanine nucleotide-binding switch in three dimensions. *Science* **294**(5545):1299-304.

Wang L, Yang L, Filippi MD, Williams DA, Zheng Y (2006). Genetic deletion of Cdc42GAP reveals a role of Cdc42 in erythropoiesis and hematopoietic stem/progenitor cell survival, adhesion, and engraftment. *Blood* **107**(1):98-105.

Wang L, Yang L, Debidda M, Witte D, Zheng Y (2007). Cdc42 GTPase-activating protein deficiency promotes genomic instability and premature aging-like phenotypes. *Proc Natl Acad Sci U S A* **104**(4):1248-53.

Watanabe N, Madaule P, Reid T, Ishizaki T, Watanabe G, Kakizuka A, Saito Y, Nakao K, Jockusch BM, Narumiya S (1997). p140mDia, a mammalian homolog of Drosophila diaphanous, is a target protein for Rho small GTPase and is a ligand for profilin. *EMBO J* **16**, 3044–3056.

Weber I, Gerisch G, Heizer C, Murphy J, Badelt K, Stock A, Schwartz JM, Faix J (1999). Cytokinesis mediated through the recruitment of cortexillins into the cleavage furrow. *EMBO J* **18**(3):586-94.

Williams CL (2003). The polybasic region of Ras and Rho family small GTPases: a regulator of protein interactions and membrane association and a site of nuclear localization signal sequences. *Cell Signal* **15**(12):1071-80.

Williams-Masson EM, Malik AN, Hardin J (1997). An actin-mediated two-step mechanism is required for ventral enclosure of the C. elegans hypodermis. *Development* **124**(15): 2889-901.

Wu J, Liu L, Matsuda T, Zhao Y, Rebane A, Drobizhev M, Chang YF, Araki S, Arai Y, March K, *et al.* (2013). Improved orange and red $Ca^{2+}$ indicators and photophysical considerations for optogenetic applications. *ACS Chem Neurosci* **4**(6):963-72.

Wühr M, Freeman RM, Presler M, Horb ME, Peshkin L, Gygi S, Kirschner MW (2014). Deep Proteomics of the *Xenopus laevis* Egg using an mRNA-derived Reference Database. *Curr Biol* **24**(13):1467–1475.

Xu S, Chisholm AD (2011). A Gαq-$Ca^{2+}$ signaling pathway promotes actin-mediated epidermal wound closure in C. elegans. *Curr Biol* **21**(23):1960-7.

Yan D, Lin X (2009). Shaping Morphogen Gradients by Proteoglycans. *Cold Spring Harb Perspect Biol* **3**:a002493.

Yang Y, Drossopoulou G, Chuang PT, Duprez D, Marti E, Bumcrot D, Vargesson N, Clarke J, Niswander L, McMahon A, *et al*. (1997). Relationship between dose, distance and time in Sonic Hedgehog–mediated regulation of anteroposterior polarity in the chick limb. *Development* **124**:4393–404.

Yang L, Wang L, Zheng Y (2006). Gene targeting of Cdc42 and Cdc42GAP affirms the critical involvement of Cdc42 in filopodia induction, directed migration, and proliferation in primary mouse embryonic fibroblasts. *Mol Biol Cell* **17**(11):4675-85.

Yatani A, Irie K, Otani T, Abdellatif M, Wei L (2005). RhoA GTPase regulates L-type Ca2+ currents in cardiac myocytes. *Am J Physiol Heart Circ Physiol*. **288**(2):H650-9.

Yawo H, Kuno M (1985). Calcium dependence of membrane sealing at the cut end of the cockroach giant axon. *J Neurosci* **5**(6):1626-32.

Yoo SK, Deng Q, Cavnar PJ, Wu YI, Hahn KM, Huttenlocher A (2010). Differential regulation of protrusion and polarity by PI(3)K during neutrophil motility in live zebrafish. *Dev Cell* **18**(2): 226–236.

Yoo SK, Freisinger CM, LeBert DC, Huttenlocher A (2012). Early redox, Src family kinase, and calcium signaling integrate wound responses and tissue regeneration in zebrafish. *J Cell Biol* **199**(2):225-34.

Yu H-YE, Bement WM (2007). Control of local actin assembly by membrane fusion-dependent compartment mixing. *Nat Cell Biol* **9**(2):149–159.

Yu QC, McNeil PL (1992). Transient disruptions of aortic endothelial cell plasma membranes. *Am J of Pathol* **141**(6):1349–1360.

Yumura S, Hashima S, Muranaka S (2014). Myosin II does not contribute to wound repair in Dictyostelium cells. *Biol Open* **3**(10):966-73.

Zhang B, Chernoff J, Zheng Y (1998). Interaction of Rac1 with GTPase-activating proteins and putative effectors. A comparison with Cdc42 and RhoA. *J Biol Chem* **273**(15):8776-82.

Zhang B, Zheng Y (1998). Regulation of RhoA GTP hydrolysis by the GTPase-activating proteins p190, p50RhoGAP, Bcr, and 3BP-1. *Biochemistry* **37**(15):5249-57.

Zhou YT, Chew LL, Lin SC, Low BC (2010). The BNIP-2 and Cdc42GAP homology (BCH) domain of p50RhoGAP/Cdc42GAP sequesters RhoA from inactivation by the adjacent GTPase-activating protein domain. *Mol Biol Cell* **21**(18):3232-46

Zick ML, Stroupe C, Orr A, Douville D, Wickner WT (2014). Membranes linked by trans-SNARE complexes require lipids prone to non-bilayer structure for progression to fusion. Elife **3**: e01879.

Ziv NE, Spira ME (1993). Spatiotemporal distribution of Ca2+ following axotomy and throughout the recovery process of cultured Aplysia neurons. Eur J *Neurosci* **5**(6):657-68.

Ziv NE, Spira ME. (1995). Axotomy induces a transient and localized elevation of the free intracellular calcium concentration to the millimolar range. *J Neurophysiol* **74**(6):2625-37.